An Assessment of a Regional Turboprop Featuring Wingtip-Mounted Propellers

Design Integration Coupling Propeller-Wing Aerodynamics and Structural Wing Weight

Quinty van der Leer

Technische Universiteit Delft

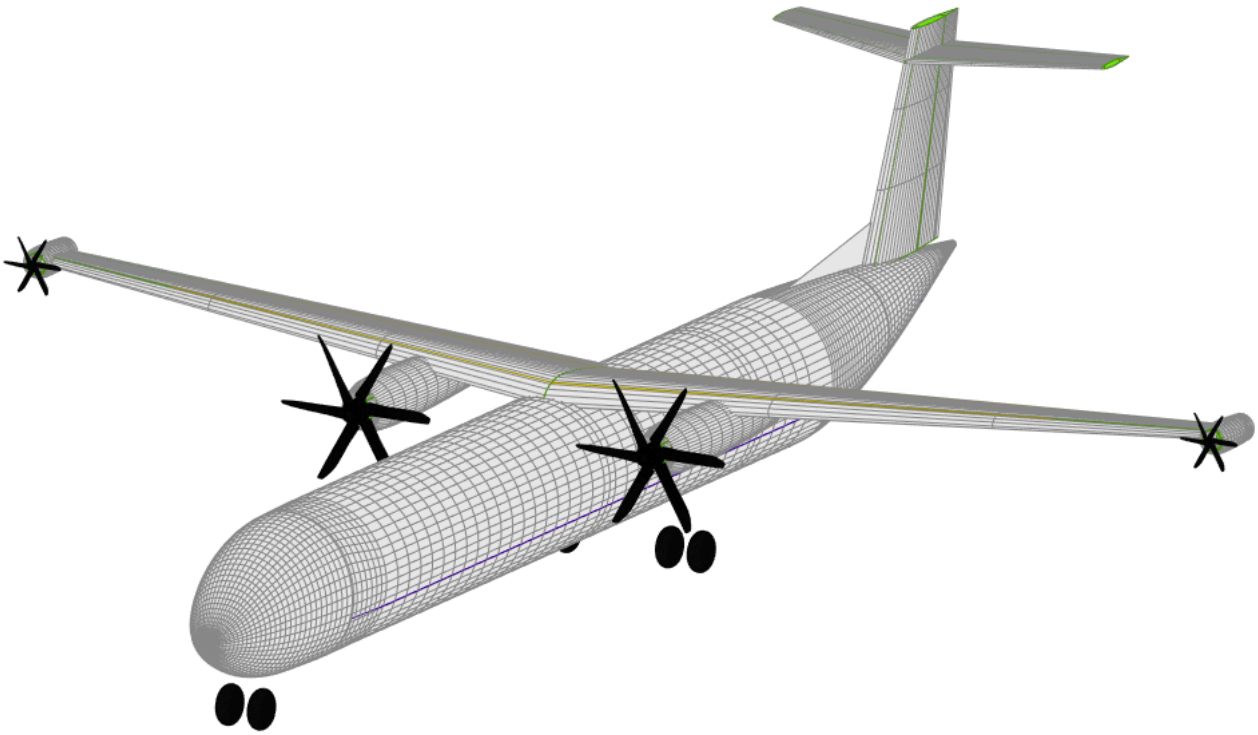

TU Delft Delft University of Technology

Challenge the future

An Assessment of a Regional Turboprop Featuring Wingtip-Mounted Propellers

Design Integration Coupling Propeller-Wing Aerodynamics and Structural Wing Weight

by

Quinty van der Leer

January 2021

in partial fulfillment of the requirements for the degree of

Master of Science
in Aerospace engineering

at the Delft University of Technology,
to be defended publicly on Friday January 29, 2021 at 9:00 AM.

Student number:	4435931	
Project duration:	April 2020 – January 2021	
Thesis committee:	Dr. ir. M. F. M. Hoogreef	TU Delft, supervisor
	Prof. dr. ir. L. L. M. Veldhuis	TU Delft, chairman
	Dr. ir. B. F. Santos	TU Delft

TU Delft Delft University of Technology

PREFACE

The last 5.5 years at the TU Delft have been challenging, exciting and moreover a lot of fun. I have really felt at home at the faculty of Aerospace Engineering. With this thesis, my time as a student has come to an end.

I am thankful to my daily supersivor Maurice Hoogreef who has given me the opportunity to work on a topic that connect well with the objective of the Flight Performance Master profile; integrating the knowledge and expertise of various aeronautical subdisciplines. Although we have not been able to meet each other in person due to the current pandemic, our collaboration went very well and organised. I appreciate your advice, useful feedback and how you walk the talk.

Moreover, I would like to thank my parents for always supporting me in my life. You bring me joy, and make sure I am not pushing myself too hard. There are many things which I am thankful for in my life, but you are at the top of the list.

Quinty van der Leer
Spijkenisse, January 2021

SUMMARY

Due to the rising concern about climate change, the aviation industry is forced to look into more environmental friendly solutions and design concepts. A shift towards more fuel-efficient designs is required. The introduction of hybrid electric propulsion could contribute to lowering emissions and offering more design freedom. This type of propulsion system makes the use of distributed propulsion more attractive. Simultaneously, propellers are an attractive way of providing propulsion since they have a relatively high propulsive efficiency compared to jets. Moreover, when correctly integrated with the wing, their mutual interaction offers aerodynamics benefits.

When mounted in tractor configuration to the wingtip, the propeller can be used as a tip-vortex attenuating device, reducing the wing induced drag. The wingtip-mounted propeller configuration is believed to offer a significant aircraft performance benefit from an aerodynamic perspective. So far, studies on wingtip-mounted propellers mainly concentrated on the aerodynamic interaction effects, disregarding the integration with the airframe and wing-structural mass. This thesis presents a methodology to integrate aerodynamic, aero-propulsive, and aero-structural effects of tip-mounted propellers in the context of a typical turboprop featuring partial turbo-electric propulsion. The concept comprises two turboprops on the primary shaft and two elektroprops on the secondary shaft. The shaft power ratio, a measure of the power share between the shafts, is constant throughout the different flight phases. Subsequently, a number of case studies are performed to investigate the sensitivity to modifications of the propulsion system on both wing and aircraft level.

The methodology consists of two parts; an aero-propulsive model and an aero-structural model. The aero-propulsive model analysis the aerodynamics of the propeller-wing system. The main building blocks of this numerical model consist of a vortex lattice method, blade element method, slipstream model and jet correction method. Both the vortex lattice method and blade element method allow for non-uniform inflow. The slipstream model comprises methods to account for deflection, contraction and azimuthal circulation distribution. The finite height of the propeller slipstream is taken into account by the jet correction. The major assumption used in the model states that the individual propellers do not interfere with each other and their induced velocity fields can simply be superimposed. The aerodynamic behaviour of the propeller and wing are dependent on each other. The propeller model is dependent on the wing induced velocities and at the same time the wing model is dependent on the propeller induced velocities. The aero-propulsive model uses an iterative approach to capture the two-way interaction. Data from windtunnel experiments were used to validate the aero-propulsive model. It was found that the numerical model predicts the experimentally observed trends well.

The aero-structural model performs an estimation of the wing weight based on physical phenomena rather than statistics. For a given wing geometry, it calculates the minimal structure required by using a boom discretization method. An optimisation problem is formulated for the wing box design in order to get the minimum amount of primary structure

required while the box can withstand the critical loadcase without exceeding the maximum allowable mechanical stress in the structural members, including a 1.5 safety factor. Typically, a clean aerodynamic wing loading is used for such an approach. However, by including the aero-propulsive model in the structural weight estimation, an aero-structural model is obtained that is sensitive to a change in aero-propulsive load. It also takes the weight of the engines into account by treating them as discrete loads on the wing. If the propulsive design is changed, this does effect the structural wing weight estimation by both a change in aerodynamic and inertia load.

The sensitivity of the aircraft performance and/or weight has been tested against a change in propulsive design in the form of shaft power ratio, disk loading and inboard propeller location. First a study on wing level has been performed that focused on the effect of the aero-propulsive load on the weight of the wing. For this study, no feedback loop in terms of weight or performance is included to greater aircraft level. Moreover, it does not include the potential aerodynamic benefits of the system throughout the different flight phases. It was found that the inclusion of the aero-propulsive load prediction only has a minor effect on the estimated wing weight compared to a clean aerodynamic wing assumption. Furthermore, increasing the shaft power ratio from 0.1 to 0.3 leads to a slight (1%) decrease in wing weight. This weight benefit is easily overshadowed by the corresponding increase in propulsion system mass which is increased by 20%. Combined this leads to a propulsion-wing system weight increase of 8%. From a purely aero-structural point of view, the mass penalty introduced by the partial turbo-electric propulsion system modification cannot be compensated by the reduction in wing weight.

On aircraft level both aero-structural and aero-propulsive effects are considered. Contrary to the wing level study, the aero-propulsive benefits for the different flight phases are included and a design convergence study is performed by use of the TU Delft in-house build Aircraft Design Initiator. Within the initiator, the aerodynamic performance of the aircraft is updated by including the aero-propulsive benefits. The aero-propulsive benefits are partly estimated by use of an already build-in simplified surrogate model and the developed aero-propulsive model. In addition, the structural wing weight estimation is replaced by the aero-structural wing weight estimation.

The different initiated designs stressed the importance of the size of the wingtip-mounted propeller. A system with a larger tip-mounted propeller, so a smaller disk loading, greatly enhances the aero-propulsive benefits in terms of lift enhancement and induced drag reduction. For a shaft power ratio of φ=0.1 a span fraction of $\Delta Y \approx$0.2 occupied by the distributed propulsors results in a similar performance to a conventional aircraft with the same top-level requirements. With increasing shaft power ratio, the required tip-mounted propeller size also increases. This is because a higher shaft power ratio will result in a heavier propulsion system and consequently a heavier aircraft. The higher this mass penalty, the larger the aero-propulsive benefits required to overcome this mass penalty. For this reason, the highest potential for the wingtip-mounted propeller configuration is expected to be found for a configuration with a low shaft power ratio and large wingtip-mounted propeller size. The lower the shaft power ratio, the easier to overcome the partial turbo-electric weight penalty by use of aero-propulsive interaction benefits.

CONTENTS

List of Figures

List of Tables

1

INTRODUCTION

Until the end of the second world war propellers have been the standard propulsors for aircraft. Due to the drop in fuel prices and the trend for faster aircraft, higher altitude and extended range, the jet era arouse. The current focus in the aviation industry for more sustainable propulsion could mean the revive of propeller propulsion as propellers offer a higher propulsion efficiency than jets. In addition, the emerge of Hybrid Electric Propulsion (HEP) aircraft offers more design freedom in terms of distributed propulsion. This enables the use of more novel-designs in which new propeller-wing configurations are studied to further utilize the benefits offered by propellers.

One of these propeller-wing configurations that is currently under interest, is the use of wingtip-mounted propellers in tractor configuration. This research focuses on the multidisciplinary potential of such an aircraft. This chapter will give an introduction to the wingtip-mounted propeller configuration and elaborate on the research objectives. Section 1.1 provides background information on wingtip-mounted propellers including history, relevant disciplines and integration studies. This information is used to establish the research objective which is presented in Section 1.2 together with the research scope. The outline of the thesis is given in Section 1.3.

1.1. BACKGROUND INFORMATION ON WINGTIP-MOUNTED PROPELLERS

The wingtip-mounted propeller configuration is believed to offer significant aerodynamic benefits. This section will first give a brief overview of the origin of this configuration including the physical explanation for the expected aerodynamic benefits. Of course, aerodynamics is not the only discipline playing a role in the overall aircraft performance. This section also discusses other disciplines playing a role in the conceptual design phase of an aircraft featuring wingtip-mounted propulsion. Moreover, it discusses the integration studies that have been performed and their major findings.

1.1.1. HISTORY

The idea of wingtip-mounted propellers has been around for a while. It was already put into practise in the 1930's as Zimmerman designed the Vought V-173 [1], shown in Figure 1.1. This aircraft, also known as the flying pancake, featured two large propellers at its wingtips.

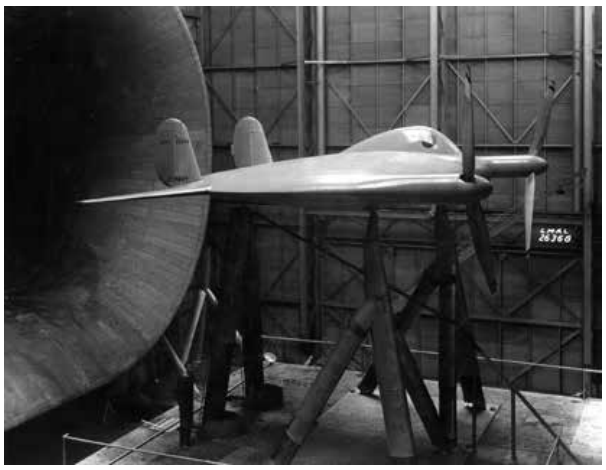

Figure 1.1: Zimmermans' Vought V-173 scale model during a wind tunnel experiment [1].

Zimmerman purposely designed these propellers to rotate inboard up, as he argued that opposing the rotational direction of the tip vortex helps to decrease tip losses and induced drag. The V-173 was a remarkable aircraft design that was capable of short landings and takeoff. Its prototype showed the prove of Zimmermans' concept and was later designated to be further developed as the XF5U-1. This aircraft, however, never entered production as the navy lost interest in the program due to the emerge of the jet fighter.

The thoughts of Zimmerman on wingtip-mounted propellers were later confirmed by Snyder [2]. He conducted wing tunnel test and showed that a decrease in induced drag results from of a propeller that rotates in the opposite direction to that of the wing tip vortex. In the 1980's Miranda [3] analytically confirmed the potential performance benefits of a wingtip mounted propeller. Again, the sense of rotation was emphasized and it was concluded that the propeller rotation should indeed oppose the tip vortex as shown in Figure 1.2. Miranda performed a similar but improved study as Loth and Loth [4] and the developed model was validated using wind tunnel data that was obtained by Patterson [5]. Miranda studied two different ways to achieve the tip vortex attenuation: a pusher propeller and a tractor propeller. It was found that both configurations lead to a reduction in required power. The performance benefit of a pusher propeller occurred in the form of an increased propeller efficiency whereas the tractor propeller resulted in a decrease in wing induced drag as summarised in Figure 1.3.

Currently the aviation industry is leaning towards more sustainable propulsive solutions. With the emerge of HEP aircraft, more design space is offered giving room to more novel-designs. This is due to the fact that electric propulsion is a relative scale independent technology enabling the distribution of propulsion across the airframe penalty free [6]. The introduction of this new propulsive architecture combined with the interest in more efficient designs, makes the wingtip-mounted propeller configuration a compelling design option.

1.1.2. RELEVANT DISCIPLINES

The wingtip-mounted propeller configuration comprises at least two powertrains. One powertrain is responsible to deliver the main propulsion of the aircraft, where a secondary powertrain drives the wingtip-mounted propellers. These tip-mounted propellers are used

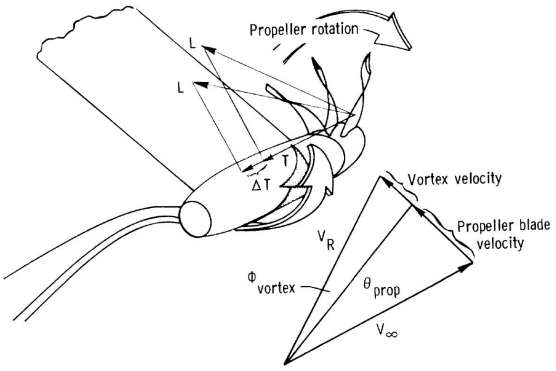

Figure 1.2: Wingtip-mounted propeller sense of rotation [5].

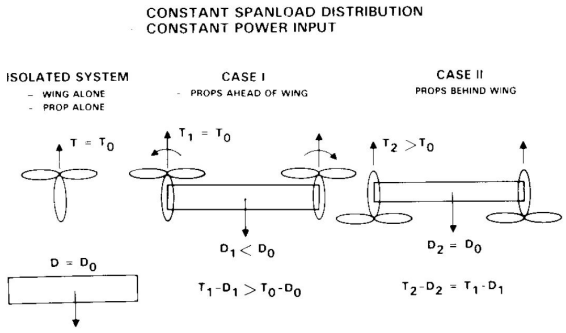

Figure 1.3: Effect of tractor and pusher configuration [3].

as tip-vortex attenuating devices but also provide thrust as a byproduct. This additional trust generation and reduction of tip-losses, requires a re-scaling of the propulsion unit. The challenge for a wingtip-mounted propeller design is much more complex than this re-sizing. It comprises the design of the optimal power split between the shafts, sizing of the propeller and establishing an arrangement for optimal propeller-wing aerodynamic interaction. These design considerations do of course affect the combined aerodynamics of the wing and propeller. The modified loading distribution, the additional mass at the tip and the resizing of the propulsor unit, likely affect the structural design requirements of the wing, which in turn affect the overall performance.

Although the idea of wingtip-mounted propellers arose because of aerodynamic benefits, this is not the only discipline playing an important role, like with any aircraft design consideration. The disciplines that are deemed most important in the early design stage of a wingtip-mounted propeller configuration are discussed below.

AERODYNAMICS

The isolated wing and propeller aerodynamics and the interaction between the two are extensively be discussed in Chapter 2. Here, the most important aerodynamic aspects of a wingtip-mounted propeller are summarised. Furthermore, aerodynamic studies and their findings on the wingtip-mounted propeller configuration are discussed.

Wingtip-mounted propellers are believed to reduce the wing induced drag significantly, this was derived from both experimental [2][7] and numerical studies [3][8]. All of these studies stress the importance of the sense of rotation of the propeller which has to counteract the wingtip vortex, resulting in an inboard-up rotation. In this manner, the propeller swirl attenuates the tip vortex and reduces the corresponding tip-losses. The wingtip-mounted propeller is expected to realise an induced drag reduction of 15% [7].

Considering a single way interaction, the most pronounced effects of the propeller on the wing are due to the slipstream induced velocities. These affect the loading distribution on the wing as the axial induced velocity increases the dynamic pressure on the wing part immersed in the slipstream. In addition, the tangential induced velocity causes a variation in angle of attack seen by the wing, resulting in a propeller induced upwash for a wingtip-mounted inboard-up propeller. The effects of the slipstream wash can easily be analysed by superimposing an isolated propeller flow on a wing. Nevertheless, the interaction effects

of the propeller are more complex than this. Due to the increasing dynamic pressure in the slipstream, the slipstream needs to contract. This contraction further affects the wing loading and also alters the viscous effects [8]. Additionally considering the wing effects on the upstream propeller, results in a two-way or full interaction model. The presence of the wing will also cause the slipstream to deflect due tot the asymmetric propeller loading that is introduced by the wing induced upwash. An overview of the aerodynamic interaction effects is presented in Table 1.1.

Table 1.1: Summary of propeller wing aerodynamic interaction effects for an inboard-up rotating wingtip-mounted tractor propeller.

Source	Effect	Consequence
Propeller induced axial velocity	Increased dynamic pressure	Lift enhancement
	Slipstream contraction	Angle of attack change on wing
Propeller induced tangential velocity (swirl)	Propeller induced upwash	Swirl recovery
	Partial cancellation of tip vortex	Reduced induced drag
Wing induced upwash	Asymmetric propeller load	Slipstream deflection

A number of methods have been developed to assess the aerodynamic performance of a propeller, wing, and combination of the two. These methods range from low-fidelity to high-fidelity models. The latter involve studies that have been performed using CFD to gain a deeper understanding of the propeller-wing aerodynamic interactions [9][10]. These methods are computationally too expensive and the results are not generic enough to be applied in the conceptual design phase of an aircraft. Low-fidelity models usually comprise an Actuator Disk (AD) model or Blade Element Method (BEM) for the propeller. The induced velocities found by the propeller model are superimposed to the freestream velocity, this process is visualised in Figure 1.4. It can be seen that the velocity experienced by the wing sections outside the slipstream are unaltered. For the wing section immersed in the slipstream, the propeller induced velocities are added to the freestream velocity.

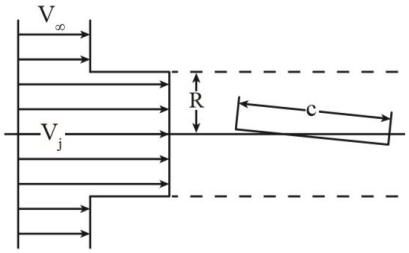

Figure 1.4: Superposition of propeller induced axial velocity and freestream [11].

As will be further explained in Section 2.2.3, the AD theory only considers axial momentum variations. This means that the AD theory only yields the axial velocity increase

and is not capable of providing the swirl velocity in the slipstream. If the resulting induced velocities from the AD theory are superimposed on the freestream velocity, the potential flow method used for the wing will only take into account the effect of the increased dynamic pressure in the slipstream which is moreover assumed to be homogeneous in radial direction.

Effects of the slipstream swirl and radial varying axial velocity can be incorporated when a BEM is used. This model also yields the tangential induced velocity in the slipstream and provides insight in the radial variation of the axial velocity. Although the BEM provides a good indication of the performance of a propeller, it fails to predict the development of the slipstream. The analysis results in the flow characteristics far downstream of the propeller plane. Direct superposition of these results thus assumes that the propeller is located at an infinite distance. In reality the slipstream develops downstream in terms of velocity distribution and contraction. It is assumed that the tangential velocity instantaneously develops in full directly after the propeller. The axial velocity, however, gradually develops downstream. A model that can be used to model the development of the axial velocity was derived by Conway [12]. This model has for instance been implemented by Alba [13]. To determine the contraction ratio of the slipstream, momentum theory can be used as explained by Veldhuis [8].

A propeller in the presence of a downstream lifting surface experiences an induced upwash. This induction has similar consequences as a propeller under an non-zero angle of attack. The increased effective angle of attack will cause the resultant force to tilt, producing a force in the propeller plane and causing the slipstream to deflect. De Young [14] proposed a method to determine the strength of the normal force and slipstream deflection based on momentum theory. This method has been implemented by Veldhuis[8] and more recently by Alba[15] and Epema[16].

Besides the wing causing an upwash on the propeller, it also reduces part of the propeller induced swirl. This means that the wing experiences a lower tangential velocity than is induced by the propeller. Ultimately, the tangential velocity produced by the propeller needs to be corrected in order to match the tangential velocity experienced by the wing. Veldhuis[8] introduces a Swirl Recovery Factor (SRF) for this. In his approach he uses a constant factor of 0.5 in order to better match the desired results which is not based on any physical phenomena. Alba [13] comes up with a formulation of the SRF which is based on the swirl energy. According to Epema [16] experimental results show that the swirl recovery varies over the wing span and should be modelled as such.

Moreover, superposition as shown in Figure 1.4 assumes a infinite slipstream height. However, research has shown that an airfoil immersed in a slipstream with a finite radius R and jet velocity V_j produces less lift than an airfoil experiencing a freestream velocity of V_j [17][18][19]. It was concluded that neglecting the finite height of the slipstream results in an over prediction of the lift coefficient. This becomes especially relevant for cases where the slipstream height is in the same (or smaller) order of magnitude as the wing sectional chord [17] which could well be the case for a wingtip-mounted propeller.

Nederhof [20] investigated a number of suitable methods to correct for the finite slipstream height. His approach used potential flow theory, in particular a lifting-line method. He discovered that the implementation of a Full 3D correction method based on the work of Rethorst [21] greatly improves the prediction of the spanwise lift distribution as can be

seen in Figure 1.5. Nevertheless, it must be noted that this correction method has a number of limitations. It assumes a constant axial velocity throughout the slipstream and the method was developed for a single symmetric propeller use case. Moreover, the correction method only accounts for the axial velocity and does not include the propeller swirl. After all, the model still seems to give reasonable results for non-symmetric propeller slipstream cases and when propeller swirl is included.

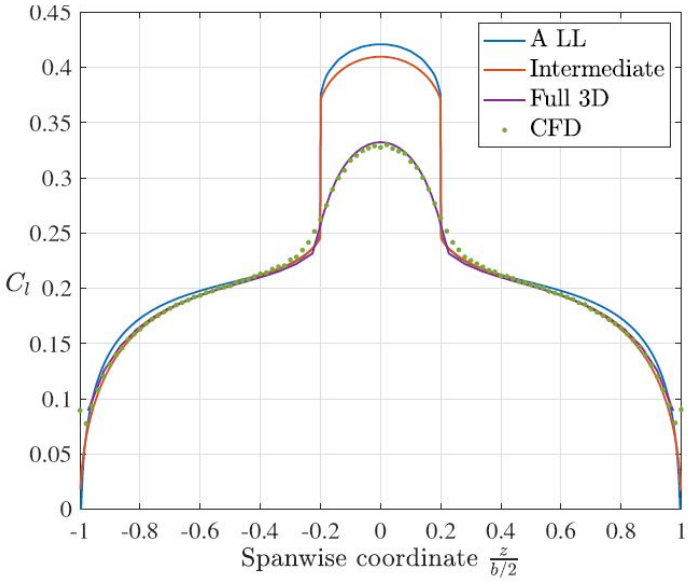

Figure 1.5: Comparison of different potential flow correction methods with CFD data for $V_j = 1.5V_\infty$ [20].

PRELIMINARY SIZING

Part of the conceptual aircraft design involves the preliminary sizing, comprising Class I weight estimation. Traditional aircraft preliminary sizing methods such as explained by Torenbeek [22] Roskam[23] or Raymer [24] can only be used for commonly used aircraft configurations as they rely on statistics. Based on high level mission and design requirements, similar aircraft are selected. The data of these reference aircraft are then used to make an estimation of the different weight fractions of the to-be-designed aircraft. For new aircraft configurations, like the wingtip-mounted propeller HEP aircraft, another approach has to be taken to conduct a preliminary weight estimation as no database on similar aircraft exist.

A number of studies have analysed HEP aircraft preliminary sizing but use a predefined aircraft [25] and often keep the takeoff weight constant [26]. Other studies are lacking aero-propulsive effects in the method [27]. A preliminary sizing method for Hybrid Electric Propulsion has been developed by de Vries [28] to overcome these shortcomings. He expanded traditional sizing methods to make them suitable for HEP aircraft. Moreover, the aircraft configuration can feature multiple propulsion systems. A detailed discussion on the method is given in [28].

Besides top-level aircraft requirements, the model only requires a limited amount of input parameters that are known in the preliminary design phase. The required inputs are

listed in Table 1.2. The first four parameters are straightforward and belong to the wing geometry whereas the last 5 parameters describe the propulsion system. In case of a typical wingtip-mounted propeller configuration, the number of primary and secondary propulsors will be equal to two. The Distributed Propulsion (DP) span fraction describes what fraction of the wingspan is covered by the DP system. The spacing between the propulsors will be determined by the position of the primary propeller. And the axial position describes the spacing between the propulsors and the wing in spanwise direction.

Table 1.2: Inputs of the preliminary sizing tool developed by de Vries [28].

Parameter	Symbol
Aspect ratio	A
Half chord sweep	$\Lambda_{c/2}$
Taper ratio	λ
Root thickness over chord	t/c_r
Number of primary propulsors	N1
Number of secondary propulsors	N2
DP span fraction	ΔY
Spacing between DP propulsors	Δy
Axial position of DP propulsors	x_p/c

Moreover the designer must specify two power control parameters that define the power shares of the system along the mission. The control parameters that need to be specified are the supplied power ratio (Equation 1.1) and shaft power ratio (Equation 1.2).

$$\Phi = \frac{P_{bat}}{P_{bat} + P_f} \tag{1.1}$$

$$\varphi = \frac{P_{s2}}{P_{s2} + P_{s1}} \tag{1.2}$$

Using the specified design parameters, control parameters and top level design requirements, the wing area, installed power and aircraft weight are computed. This is done in four main steps. First, a modified propulsive power- loading diagram is produced accounting for the aerodynamic interactions between the propulsors and airframe. Next, the formulated powertrain model is used and the power-loading diagram is transformed into a series of power-loading diagrams. Each diagram corresponds to one of the powertrain components. As usual, the loading diagrams are a summary the performance constraints and indicate the feasible design space region. Based on this information the designer is required to select a design point within the indicated region. This is then followed by the estimation of battery and fuel energy required. For this process, a mission analyses is performed with a assumed Takeoff Weight (TOW) which is later updated. Combining the obtained power and energy requirements, an adjusted Class I weight estimation is conducted. The resulting TOW is used to update the assumed value used for the mission analyses. This is repeated until the TOW is found to converge. The preliminary sizing tool eventually yields a

wing surface area, wing loading, power loading and mass breakdown of the different components.

WING WEIGHT ESTIMATION

In terms of wing structure, the application of wingtip-mounted propellers can either have a positive or negative effect. The wingtip-mounted propeller will be responsible for part of the total thrust provided by the propulsors, resulting in the requirement to re-scale the propulsion unit. This re-scaling, possible re-positioning and application of the wingtip propeller will all influence the lift distribution and change the inertia loads on the wing. The exact consequence on the wing weight will depend on the specific design.

In commonly preliminary sizing methods [23] [24], [22], the aircraft weight and corresponding component weight are estimated using statistics in Class I and Class II weight estimations respectively. However, for a configuration with wingtip-mounted propellers, these methods are not design sensitive enough to accurately perform a weight estimation. Higher class methods exists where the approach is more physical-based such as Class III weight estimation methods by Droegkamp [29] and Bindolino [30]. These methods typically use Finite Element Analysis (FEA) and are more design-sensitive, provide weight estimations with higher accuracy. On the contrary, these methods requires too detailed geometry information and the computational cost are high which makes this an unattractive approach. Hybrid methods exist which combines the benefits of Class II and Class III weight estimation into a Class II.V [31][32] weight estimation method. The resulting method is quasi-analytical and makes use of both statistical methods and elementary structural wing box analyses. Such sizing method is highly desirable for a wingtip-mounted propeller configuration.

OTHER

Of course, there are also other disciplines that play a role in the design of a wingtip-mounted propeller configuration. A non-exhaustive list of other disciplines that might have important influences, but are deemed out of scope for this research, is provided here together with references to previous research.

First of all, aero-elastic effects can dictate the design of wingtip-mounted propeller configurations. The application of a propeller at the tip changes the loading distribution and adds inertia loads to the structure. Moreover, additional forces and moments are introduced by the rotating blades. Aeroelastic analysis might find that instabilities occur within the flight envelope. A phenomena that might need more attention than usual is for example propeller-wing whirl flutter [33].

Propellers are an effective means of propulsion but are also great noise sources. The optimum aerodynamic propeller design, might be far from the ideal propeller design for noise reduction. The effects of the propeller design on the noise production and aerodynamic performance has been studied simultaneously by Sinnige [34].

As the propellers mounted at the tip have a larger moment arm, the idea has aroused to use these features for stability and control of the aircraft. If the propellers are used to enhance directional stability and control, the size of the vertical tailplane can be reduced. On the other hand, an one-engine-inoperative situation might result in a yawing moment that is to large to be correct by the rudder. Van der Meer [35] studied the contribution of tip-mounted (pusher) propellers to static stability, dynamic stability, and control.

1.1.3. INTEGRATION STUDIES

A number of researches have been conducted, studying the integration of wingtip-mounted propellers with the airframe. NASA is one of the institutes that dedicated research to the wingtip-mounted propeller configuration. They came up the Parallel Electric-Gas Architecture with Synergistic Utilization Scheme (PEGASUS) concept [36]. This concept features both hybrid electric and electric propulsors and is based on the ATR-42-500. Two hybrid electric propellers are mounted to the wingtip and two additional electric propellers are mounted further inboard. The inboard propulsors are only used to provide additional thrust during the takeoff and climb phase. During cruise, these propulsors are folded. Moreover, the concept features an additional propulsor mounted to the rear of the aircraft as suggested by Weldstead [37] in order to decrease the required propulsive power by Boundary Layer Ingestion (BLI). Figure 1.6 and 1.7 shows the PEGASUS concept in takeoff and cruise respectively. A number of PEGASUS studies were performed by NASA. The configuration, methodology and relevant results are summarised in Table A.1.

Figure 1.6: The Pegasus concept [36].

Figure 1.7: The Pegasus concept in cruise [38].

Antcliff [36] (Study A, Table A.1) investigated the potential of the PEGASUS configuration. It used two different approaches to quantify the benefits (or disadvantages) of the configuration in terms of gross weight and propulsive efficiency. A related research, by Blaesser [38] (Study B, Table A.1), uses higher fidelity tools to asses the concept. However, it still only considers a one-way interaction and does not account for the weight variation due to the propeller design and corresponding wing loading effects. Moreover, the propeller design is limited to the radius, as an actuator disk model is used. It was concluded that using the inboard propellers in addition to the wingtip-mounted propellers gives the best results in this particular study. A ~50-50 thrust distribution between the propeller classes reduced the system power consumption by ~ 5% compared to a single propeller class operating.

Capristan [39] performed an updated analyses of the PEGASUS concept. It incorporated an approach which can handle multiple propulsors and aero-propulsive interactions ignored previously. The FLOPS-based methodology used in study A was not developed for unconventional aircraft configurations. On the other hand, SUAVE was specially developed for unconventional aircraft configurations but lacks the capability of handling multiple propellers correctly. That is why the Layered and Extensible Aircraft Performance System (LEAPS) mission analysis tool was used. In addition, a scaled version of the ATR-72-500 was used to account for the expected takeoff weight increase due to the electrification. This study assumed values for the benefits of BLI and wingtip-mounted propellers and analysed the sensitivities of different performance parameters to these assumptions. Again,

the main conclusions can be found in Table A.1 (Study C).

NASA also runs a similar study on a light General Aviation (GA) aircraft which are characterised by relative low wing loadings. This project is known as the Scalable Convergent Electric Propulsion Technology Operations Research (SCEPTOR) [40]. The X-57 "Maxwell" shown in Figure 1.8 is part of the project and uses the Tecnam P2006T as baseline aircraft, featuring a number of high-lift distributed propellers and two wingtip-mounted propellers providing the majority of the required thrust. In a study by Borer [40], low-order tools are used to assess the potential performance benefits of this configuration. Aerodynamic effects were studied using tools such as XROTOR and AVL. Although a simple mass property estimation was included based on Raymer's [24] method, no structural analysis was conducted. A summary of this study is shown in Table A.2, study D. Cole [41] investigated the potential cruise efficiency benefits of a propeller wing system variant based on the X-57 and the effects of propeller design and positioning. The approach and findings of the study are presented in Table A.2 (Study E).

Also DLR has conducted a conceptual design study in which different HEP aircraft concepts were identified [42]. After careful selection the number of concepts had been reduced and these remaining concepts were studied more closely. A high aspect ratio wing with wingtip-mounted propellers was identified as the most promising concept. This configuration in shown in Figure 1.9. The configuration and findings are summarised in Table A.2, study F.

Figure 1.8: Wingtip-mounted propeller concept by NASA; X-57[43].

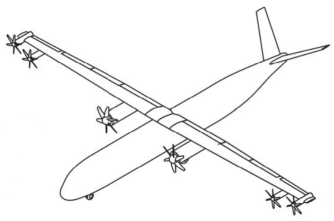

Figure 1.9: Wingtip-mounted propeller concept studied by DLR [42].

TU Delft also studied a wingtip-mounted propeller concept [44]. The baseline aircraft was generated using an in-house developed design tool, the Initiator[45], which generates feasible designs rather than optimum designs. The baseline aircraft was synthesized for different future technology scenarios, shaft power ratios and also the effect of the aircraft range was analysed. The configuration studied is shown in Figure 1.10. Findings on this wingtip-mounted configuration are summarised in Study G in Table A.2.

An even more recent paper, by Habermann [46], explores the effect of the integration of the propeller and wing design on the wing weight. The effect of the position, loading and size of the propellers has been studied. Although an empirical relation was used to quantify the induced drag reduction of the wingtip-mounted propellers, this study lacks a more sophisticated aerodynamic interaction analysis. The general idea, approach and background in presented in study H, Table A.2.

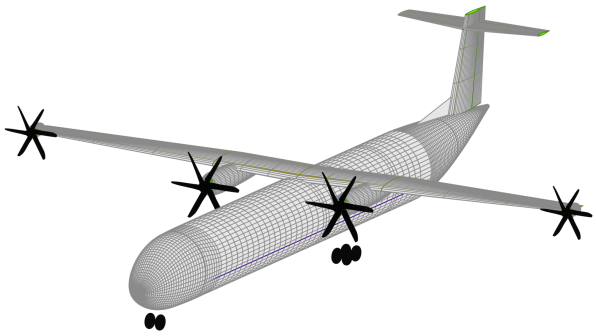

Figure 1.10: Wingtip-mounted propeller concept studied by TU Delft [44].

1.2. RESEARCH OBJECTIVE AND SCOPE

Aircraft design is by all means a multidisciplinary challenge. Yet, the aerodynamic interaction effects is what makes the wingtip-mounted propeller design so appealing at first. Wingtip-mounted propellers in tractor configuration are believed to reduce the wing induced drag significantly, this was derived from both experimental [2][7] and numerical studies [3][8]. All of these studies stress the importance of the sense of rotation of the propeller which has to counteract the wingtip vortex, resulting in an inboard-up rotation. In this manner, the propeller swirl attenuates the tip vortex and reduces the corresponding tip-losses.

The introduction of Hybrid Electric Propulsion offers more design freedom and makes the use of distributed propulsion more atractive [6]. This could enable the use of a wingtip-mounted propeller next to an inboard situated propeller in a hybrid electric power train. The wingtip-mounted propeller will provide an induced drag reduction and simultaneously be responsible for part of the total thrust provided by the propulsors. This results in a required resizing of the propulsion system. This re-scaling, possible re-positioning and application of the wingtip propeller will all influence the lift distribution and change the inertia loads on the wing. The wingtip-mounted propeller configuration both impacts the aerodynamics and structures of the system.

Ultimately, these disciplines need to be coupled in order to assess the wingtip-mounted propeller potential on a higher level. Numerous integration studies have been performed on (variations of) wingtip-mounted propeller configurations. Some studies have mainly investigated the aerodynamic effects [36][38][40][41]. Some studied the effect on the aircraft weight by assuming aerodynamic benefits [39] or by ignoring mutual interference [46]. Others integrated both aerodynamic and structural disciplines but used simplified surrogate models for aero-propulsive effects and assumed a clean wing for the aerodynamic load used for the structural wing weight estimation [44].

The inclusion of the wingtip-mounted propeller has an effect on the aerodynamic load distribution and alters the distribution of the inertia loads on the wing. So far, none of the studies performed a complete integration of aerodynamic, propulsive and structural effects of a wingtip-mounted propeller configuration. In this thesis, a methodology is presented to investigate the potential of the wingtip-mounted configuration when aero-propulsive and (aero-)structural effects are accounted for. This methodology is used to assess whether performance benefits of a wingtip-mounted propeller configuration are still substantial when not only looking at aero-propulsive but also at structural effects.

The thesis focuses on a typical turboprop aircraft with two additional wingtip-mounted

propellers. The aircraft features a Partial Turbo Electric (PTE) power train in which the wingtip-mounted propellers are driven by an electric motor. This type of powertrain is used because it is believed to result in the lightest HEP concept due to the fact that no batteries are used. The resulting configuration is shown in Figure 1.11. The study is performed with a level of detail similar to a conceptual design phase. The effect of the integrated aerodynamic, propulsive and structural effects of the wingtip-mounted propellers on aircraft performance is investigated on both wing and aircraft level by coupling the different disciplines. Other potential relevant disciplines like aeroelasticity, aero-acoustics, control and stability are not considered.

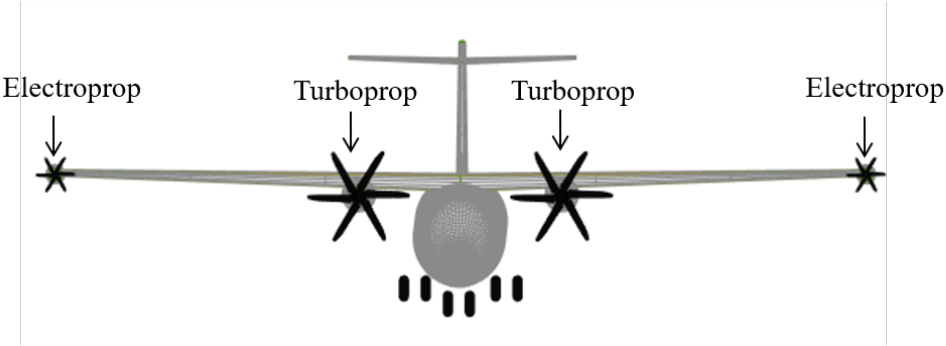

Figure 1.11: Front view of a wingtip-mounted propeller configuration as studied in this thesis.

1.3. THESIS OUTLINE

The wing and propeller aerodynamics and the main interaction effects between the two are treated in Chapter 2. An aero-propulsive model is developed to analyse the combined propeller-wing aerodynamics as presented in Chapter 3. Next, Chapter 4 presents an aero-structural model which couples the aerodynamics of the system to a wing weight estimation. The developed models are applied in the sensitivity studies performed on wing and aircraft level presented in Chapter 5 and Chapter 6 respectively. Bases on the performed analyses, a number of conclusions and recommendations are made, which are presented in Chapter 7.

2

Wing and Propeller Aerodynamic Theoretical Background

To get a good understanding of why wingtip-mounted propellers could result in an aerodynamic performance increase, it is important to first discuss their basic aerodynamic characteristics. This discussion will furthermore review the existing approaches and challenges that are faced when modelling the aerodynamics of a propeller-wing system. This chapter will focus on the steady aerodynamic effects as these thrive the overall performance. Before exploring the interaction effects between the propeller and wing, the isolated wing and propeller aerodynamics are discussed independently in Section 2.1 and 2.2 respectively. Section 2.3 will elaborate on the aerodynamic mutual interference effects between the propeller and lifting surface.

2.1. Wing Theory

This section discusses the wing aerodynamics, first the aerodynamic forces acting on a wing and their origin are discussed based on the information provided in Anderson's Introduction to Flight [47]. Secondly, commonly used calculation methods are described.

2.1.1. Aerodynamic Forces

Essentially, a wing is a device used to generate lift. This is done by using a cross sectional shape that results in a higher pressure at the bottom surface than the upper surface. Lift is defined as the force perpendicular to the freestream velocity. The force parallel to the freestream velocity is called drag. The lift (L) and drag (D) forces on an airfoil are shown in Figure 2.1. Additionally, N and A are the normal and tangential forces and R is the resultant force. The airfoil has a chord of length c and is depicted to be under an angle of attack α.

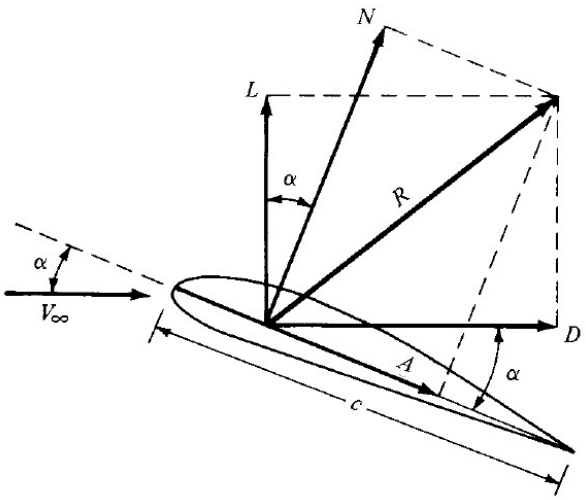

Figure 2.1: Forces on an airfoil [48].

All aerodynamics forces have two simple sources: pressure distribution on a surface and shear stress (friction) on a surface. Pressure exerted by a fluid on the surface always acts in normal direction. Shear is due to frictional effects of the fluid and the surface and always acts tangential to the surface.

The presence of friction in a flow produces two sources of drag. Shear stress at the wall causes skin friction drag. And there is pressure drag due to flow separation, this is sometimes also referred to as form drag. Together they form the profile drag, which is the total drag due to viscous effects. Another source of drag is induced drag, this is drag that is present due to the finite span of the wing. Due to the higher pressure at the bottom surface and the lower pressure at the upper surface, the flow will have the tendency to 'leak' in case of a finite wing. The air will flow from the higher pressure side to the lower pressure side over the wingtips. This will result in a circulatory motion of the flow downstream of the wing, this motion is known as a vortex. This phenomena is visualised in Figure 2.2.

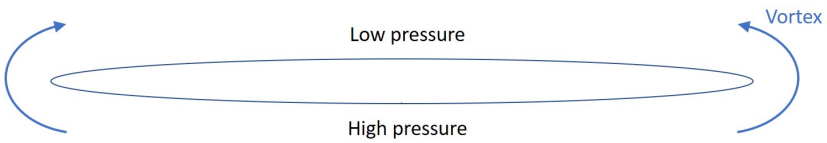

Figure 2.2: Front view of wing showing origin of wingtip vortices on finite wing.

The trailing vortex induces a downward velocity component on the wing, this is called downwash. The downwash results in a canted downward local velocity compared to the freestream velocity as can be seen from Figure 2.3. This reduces the angle of attack (AoA) that is seen by the wing. Furthermore, there is an increase in drag which is called induced drag. The downwards canted velocity changes the pressure distribution over the surface making the lift vector to tilt backwards. This introduces an additional force parallel to the freestream velocity, a drag force as shown in Figure 2.4.

The drag experienced by a wing thus is a summation of the profile drag, consisting of skin friction drag and pressure drag due to flow separation, and the induced drag. The con-

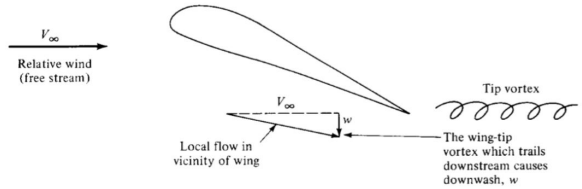

Figure 2.3: The origin of downwash [48].

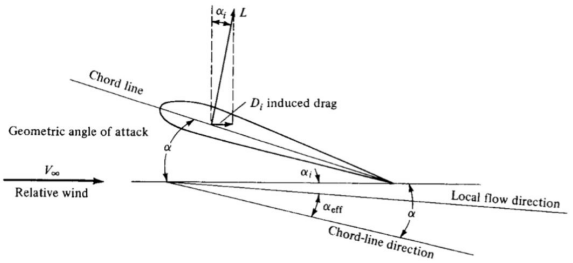

Figure 2.4: The origin of induced drag [48].

tribution of the induced drag is dependent on the vortex strength and is a type of pressure drag.

2.1.2. CALCULATION METHODS

In order to predict the aerodynamic performance of lifting surfaces, a number of simulation methods were developed. These methods range from simple and fast models to more complex and computational expensive methods. An overview of the most commonly used lower-order methods is presented, summarising the basic principles.

LIFTING LINE

The lifting line method developed by Prandtl [49] was the first practical theory to predict the aerodynamic properties of a finite wing. In this method the wing is represented by a number of bounded horseshoe vortices. A horseshoe vortex consist of a bound vortex and 2 free-trailing vortices as shown in Figure 2.5. If a number of these horseshoe vortices are placed along a line, a lifting line is formed [47]. In Figure 2.6 a superposition of a finite number of horseshoe vortices along the lifting line is shown. In this example the lifting line consists of three horseshoe vortices. The first horseshoe is made up of a bound vortex spanning from $-\frac{b}{2}$ to $\frac{b}{2}$ and free trailing vortices with strength $d\Gamma_1$. The bound vortex of the second horseshoe spans from B to E and the third spans from C to D. This superposition results in a variation of circulation along the lifting line. From A-B and E-F only one vortex is present with strength $d\Gamma_1$. Along the lifting line section B-C and E-D two vortices are superimposed, resulting in a circulation with strength $d\Gamma_1 + d\Gamma_2$. Along section C-D three vortices are superimposed and the circulation strength becomes $d\Gamma_1 + d\Gamma_2 + d\Gamma_3$. The strength of the trailing vortices correspond to the change in circulation along the lifting line. If the number of horseshoe vortices is increased to an infinite number, the circulation along the lifting line will be a continuous distribution along the lifting line given by $\Gamma(y)$ and a vortex sheet trailing downstream will occur. This method can be used to determine the lift distribution. If the lift distribution is integrated along the span, the total lift is obtained. Moreover, the induced angle of attack can be determined, which, together with the lift distribution and Figure 2.4 is used to determine the induced drag and total induced drag. This method is however limited to high aspect ratios and the evaluation of wings with complex geometry is difficult [50]. Moreover, it does not take into account viscous effects since it uses potential flow theory.

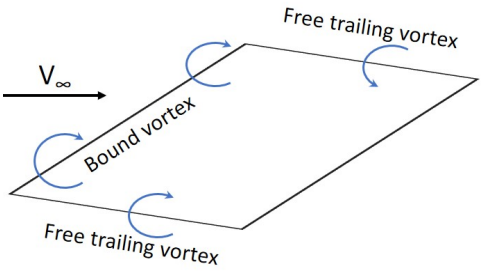

Figure 2.5: Horse shoe vortex.

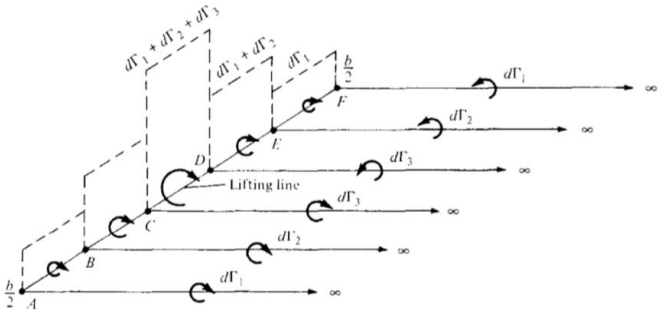

Figure 2.6: Superposition of a finite number of horseshoe vortices along a lifting line [47].

LIFTING SURFACE

Another potential flow method is the lifting surface method. This method is an extension of the Prandtl lifting line model that makes it possible to also analyse more complicated planforms. It places a number of lifting lines on the wing at different chord wise locations. Increasing the number of lines to infinity, results in a vortex sheet build up of infinitesimal strengths with vortex lines running parallel to the y-axis. The strength of the sheet, γ, varies in y direction and each lifting line will have a different strength. That makes γ dependent on both x and y. A horseshoe vortex also comprises trailing vortices. Each lifting line has its own system of trailing vortices. In case of the lifting surface method, the systems of trailing vortices are superimposed parallel to the x-axis. These vortices form another vortex sheet with strength δ. When moving along the x axis from the leading edge towards the trailing edge of the wing, additional trailing vortices are added to the strength of the trailing vortex sheet. From this it is clear that γ varies with x. The two vortex sheets form a lifting surface that is distributed over the wing. At any point at this surface the spanwise vortex strength is given by $\gamma(x, y)$ and the chord wise strength is given by $\delta(x, y)$. As shown in Figure 2.7 , downstream of the wing there are no spanwise vortex lines but only trailing vortices. Thus, the wing wake only consists of chord wise vortices. As the downstream trailing vortices do not cross any lifting lines, the strength of each of these vortices is constant. The trailing vortex strength in the wake is only dependent on the spanwise direction, given by $\delta_w(y)$ and equals the trailing edge value of $\delta(x, y)$. A flow tangency condition is imposed at all points on the wing to solve the system.

VORTEX LATTICE METHOD

An approach that is related to the lifting surface method is the Vortex Lattice Method (VLM). This method superimposes a finite number of horseshoe vortices on the wing. These horseshoe vortices vary in strength which is denoted by Γ_n. The wing surface is divided into a number of panels which do not have to be the same size. The length of a panel in stream wise direction is given by l. At every panel a horseshoe vortex is placed at a distance $\frac{1}{4}l$ from the front of the panel. Simultaneously, a control point, P, is placed at $\frac{3}{4}l$ measured from the front of the panel. A visual representation is shown in Figure 2.8. At any control point, the normal induced velocity by all the horseshoes placed on the wing can be obtained from the Biot-Savart law. When the flow tendency condition is applied at all control points simultaneously, the system can be solved.

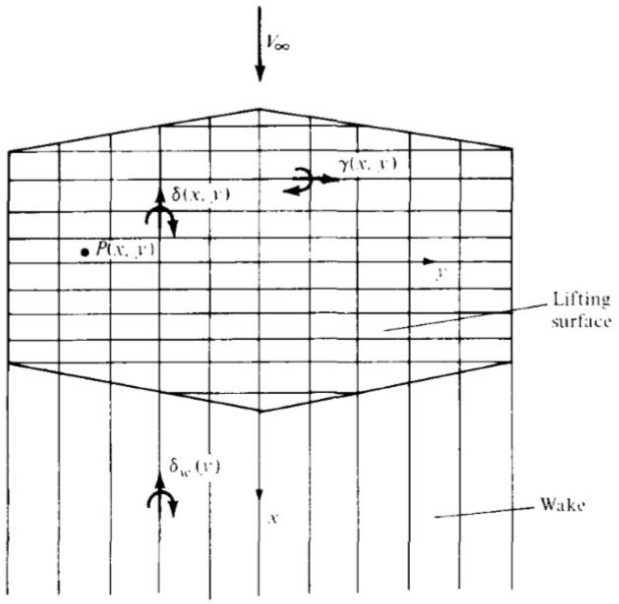

Figure 2.7: Schematic representation of the lifting surface [48].

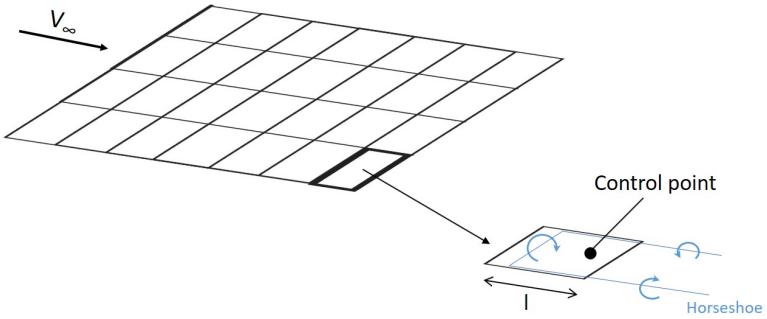

Figure 2.8: Vortex lattice system.

2.2. ISOLATED PROPELLER THEORY

A propeller is essentially a rotating wing that generates thrust by accelerating an amount of air. The invention of the rotor dates back to approximately 200 BC when the Archimedes screw was a machine used to raise water [51]. In the 19th century, propellers were first applied to ships and Rankine [52] and Froude [53] developed fundamental momentum equations. Although their work was meant for the marine industry, these fundamental principles could also be applied to air propellers. A summarising article on the aerodynamics of propellers has been written by Wald [54]. This section discusses the aerodynamic performance of a propeller as well as its slipstream characteristics and commonly used computational methods.

The propeller geometry is defined by different parameters. The propeller is divided into a number of identical blades (B). Main parameters that describe the geometry of these blades are the radius (R), chord distribution (c/r), twist distribution (β/r), blade pitch (Θ), and the airfoil used. A visual representation of the blade geometry is shown in Figure 2.9.

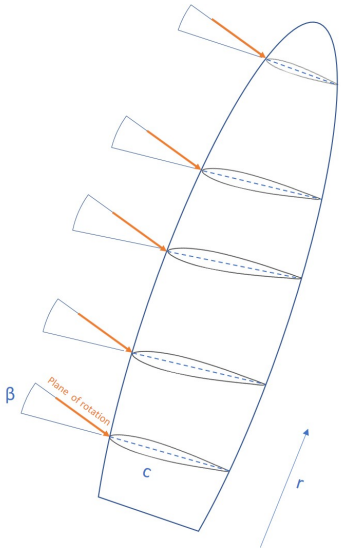

Figure 2.9: Blade geometry.

2.2.1. AERODYNAMIC PERFORMANCE

The propeller adds axial and angular momentum to the flow. The axial momentum increase contributes to the thrust whereas the angular momentum imparts a swirl to the flow. The most important forces acting on a propeller are shown in Figure 2.10. The thrust produced is a function of the mass flow and velocity increase as shown in Equation 2.1.

$$T = \dot{m}\Delta V \tag{2.1}$$

The propulsive efficiency is defined as the efficiency with which the propulsive jet power is utilized to generate thrust power. With $\dot{W}_{prop_{jet}} = \frac{1}{2}\dot{m}(V_j^2 - V_0^2)$ and $\dot{W}_{thrust} = \dot{m}(V_j - V_0)V_0$ the expression for propulsive efficiency can be written as shown in Equation 2.2.

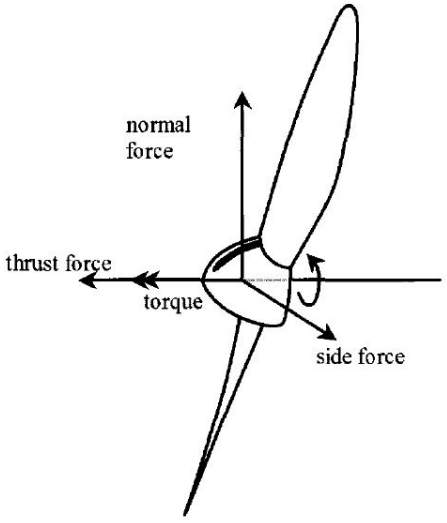

Figure 2.10: The most important forces and moments acting on a propeller [8].

$$\eta_p = \frac{2}{1 + \frac{V_j}{V_0}} \tag{2.2}$$

From this equation it becomes clear that a higher propulsive efficiency is achieved when a large mass flow is accelerated by a small velocity increment instead of accelerating a small mass flow by a larger velocity increment. This is why propellers are an efficient means of propulsion compared to jets.

A number of dimensionless parameters are defined in order to quantify propeller performance in a dimensionless way [55]. The thrust coefficient, torque coefficient and power coefficient are given by Equation 2.3a-2.3c.

$$C_T = \frac{T}{\rho n^2 D^4} \tag{2.3a}$$

$$C_Q = \frac{Q}{\rho n^2 D^5} \tag{2.3b}$$

$$C_P = \frac{P_t}{\rho n^3 D^5} \tag{2.3c}$$

The advance ratio, or speed coefficient, is given by Equation 2.4. The dimensionless parameters can be used to calculate the propulsive efficiency by use of Equation 2.5.

$$J = \frac{V}{nD} \tag{2.4}$$

$$\eta_p = \frac{C_T J}{C_P} \tag{2.5}$$

The propeller loading is given by the disk loading and blade loading, these define the thrust per unit disk area and thrust per unit blade radius.

2.2.2. PROPELLER SLIPSTREAM

The presence of the propeller alters the flow downstream of the propeller, forming a helical vortex system downstream as shown in Figure 2.11, which is called the slipstream. The propeller adds axial and tangential momentum to the flow changing its velocity compared to the freestream. The velocity of the slipstream has three components: the axial, tangential and radial velocity.

The axial velocity is the main component of interest. This component runs parallel to the freestream and is responsible for the thrust generation of the propeller. The propeller adds axial momentum to the flow, meaning it causes an increase in axial velocity. This axial velocity varies over the blade radius [8]. Due to the increase in axial velocity, the slipstream contracts such that the mass flow is preserved. This results in a radial velocity component. Theodorsen [56] showed that the contraction of the slipstream is small for lightly loaded propellers. The contraction behind a heavily loaded propeller, thus high radial velocity component, can however not be neglected [8].

The rotation velocity of the propeller causes an increase in angular momentum in the flow and is responsible for the helical shape of the propeller slipstream, introducing a tan-

gential velocity component in the slipstream, also referred to as swirl [8]. The swirl of a propeller is generally seen as loss as it does not contribute to the production of thrust.

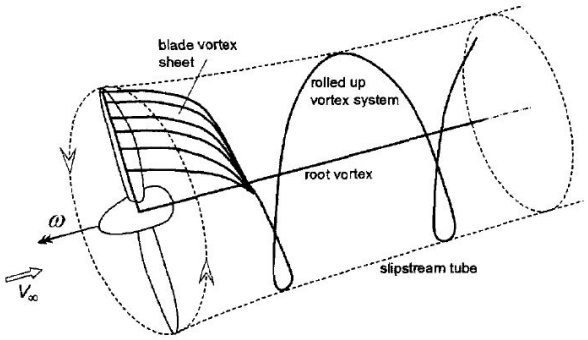

Figure 2.11: Helical vortex system generated by a propeller [8].

2.2.3. COMPUTATIONAL METHODS

Both high- and low-fidelity tools exist to model the propeller aerodynamics. High-fidelity analyses can be performed by for example CFD simulations. Although they offer more reliable results, these tools are computational expensive and not desirable within a conceptual design phase. A number of low-fidelity methods is described here.

ACTUATOR DISK THEORY

One way to get an initial idea on the propeller performance, is by using the Actuator Disk Theory (AD) [55]. This theory models the propeller as an infinite thin plate that is placed perpendicular on the thrust direction which is called an actuator disk. This disk introduces a momentum increase to the fluid passing through it. This leads to an increase in axial velocity and momentum. This theory assumes that the flow is steady, inviscid, incompressible, irrotational and one dimensional. A schematic representation of the Actuator Disk Model is shown in Figure 2.12. Station 1 is far upstream of the propeller, station 2 is just in front of the propeller, station 3 is just after the propeller, and station 4 is far downstream. Moreover, the distance between station 2 and 3 is infinitely small.

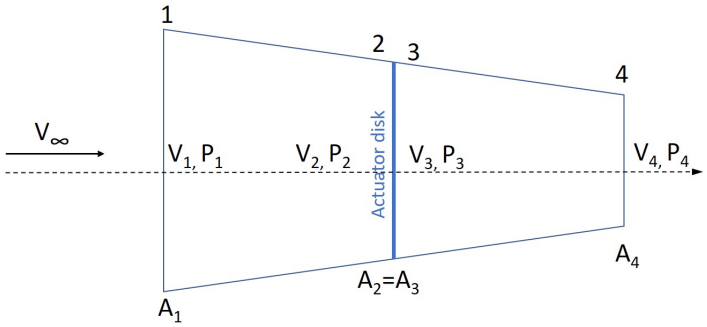

Figure 2.12: Actuator disk stream tube model.

The pressure is assumed to experience an instantaneous jump over the actuator disk whereas the velocity varies in a continuous matter. At station 1 and 4, the static pressure

equals the ambient pressure ($P_1 = P_4 = P_a$). For the velocity holds that the velocity at station 2 equals the velocity at station 3 ($V_2 = V_3$). The velocity just in front of the disk is given by $V_2 = V_1(1+a)$ where a is the axial inflow factor and V_1 is equal to the free stream velocity (V_∞). The velocity far downstream is given by $V_4 = V_1(1+b)$ where b is the slipstream factor.

As shown by Equation 2.1 the propeller thrust is simply given by the rate of increase in momentum of the airflow. For the actuator disk theory this results in Equation 2.6.

$$T = \dot{m}(V_4 - V_1) \tag{2.6}$$

Rewriting leads to Equation 2.7.

$$T = \dot{m}[V_\infty(1+b) - V] = \dot{m}bV_\infty \tag{2.7}$$

The mass flow is given by $\dot{m} = \rho A V_2 = \rho A V_\infty(1+a)$, where A is the actuator disk area and ρ the freestream density. Substituting the mass flow expression results in Equation 2.8

$$T = \rho A V_\infty^2(1+a)b \tag{2.8}$$

Force equilibrium over the disk requires $T = A\Delta P$. Combining this with Equation 2.8 yields Equation 2.9.

$$\Delta P = \rho V_\infty^2(1+a)b \tag{2.9}$$

Using Bernoulli's equation between stations 1 and 2, and stations 3 and 4, one will find that $b = 2a$. This results in Equation 2.10 which states that the axial velocity at the disk is the average of the freestream velocity and the jet velocity.

$$V_2 = \frac{V_\infty + V_4}{2} \tag{2.10}$$

From the velocity expressions at the different stations and the knowledge that $b = 2a$ the trust equation can be derived as shown in Equation 2.11. Additionally, the ideal actuator disk efficiency, also known as Froude efficiency which represent the theoretical upper limit for aircraft performance, can be derived resulting in Equation 2.12 [55].

$$T = \rho A V_\infty^2(1+a)2a \tag{2.11}$$

$$\eta_F = \frac{1}{1+a} \tag{2.12}$$

This simplified model of a propeller has a number of limitations. It only incorporates axial momentum changes, neglecting the angular velocity component introduced by the rotation of the propeller. Moreover, it does not take into account any propeller design parameters except for the radius. This means that the predicted performance is independent on for instance blade geometry or the number of blades.

BLADE ELEMENT THEORY

To overcome the shortcoming of the AD theory another theory can be used such as the Blade Element Momentum Theory (BEM) [55]. This theory is visualised in Figure 2.13. The BEM theory has similarities to wing theory as the blades are divided into small sections along the radial direction. These sections all have their own characteristics and the forces on each section are calculated individually. These forces are integrated over the propeller radius to predict the propeller thrust, torque and power.

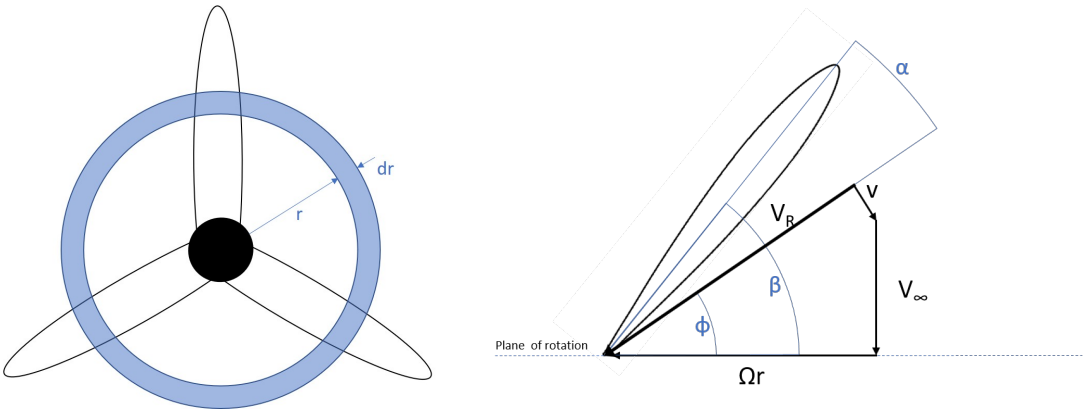

Figure 2.13: Blade Element Momentum Theory.

The axial and tangential velocities at the propeller disk are given by Equations 2.13 and 2.14. The axial velocity can be written in terms of the freestream velocity and the axial induction factor (a), or as the sum of the freestream velocity and the induced velocity (v_a). Similarly, the tangential velocity can be written in terms of the rotational speed times the radius (Ωr) and the tangential induction factor (a') or as the rotational speed times the radius minus the tangential induced velocity (v_t).

$$\begin{aligned} V_a &= V_\infty(1+a) \\ &= V_\infty + V_\infty a \\ &= V_\infty + v_a \end{aligned} \tag{2.13}$$

$$\begin{aligned} V_t &= \Omega r(1-a') \\ &= \Omega r - \Omega r a' \\ &= \Omega r - v_t \end{aligned} \tag{2.14}$$

The expression for the advance angle (ϕ) is easily derived from Figure 2.13 and is shown in Equation 2.15. The blade angle, or geometric pitch angle, is also easily derived and given by Equation 2.16.

$$\phi = \tan^{-1}\left(\frac{V_a}{V_t}\right) \tag{2.15}$$

$$\beta = \alpha + \phi \tag{2.16}$$

The axial loading, resulting in thrust and the tangential loading, resulting in torque, are calculated by decomposing the lift and drag forces on the blade section as shown in Equation 2.17, where the sectional lift and drag and dynamic pressure are defined as presented in Equation 2.18. The lift and drag coefficients (C_l, C_d) must be taken from the airfoil lift and drag polar at an angle of attack α. Furthermore the resulting velocity (V_r) can be written as shown in Equation 2.19

$$\begin{aligned} \delta T &= \delta L\cos\phi - \delta D\sin\phi = \left(l\cos\phi - d\sin\phi\right)\delta r \\ \frac{\delta Q}{r} &= \delta L\sin\phi + \delta D\cos\phi = \left(l\sin\phi + d\cos\phi\right)\delta r \end{aligned} \tag{2.17}$$

$$l = C_l\frac{1}{2}\rho V_R^2 c \quad d = C_d\frac{1}{2}\rho V_R^2 c \quad q = \frac{1}{2}\rho V_R^2 \tag{2.18}$$

$$V_R = \frac{V_\infty(1+a)}{\sin\phi} \tag{2.19}$$

The trust and torque gradients can now be written as presented in Equation 2.20, assuming the number of blades to be equal to B.

$$\begin{aligned} \frac{\delta T}{\delta r} &= Bcq(1+a)^2\frac{c_l\cos\phi - c_d\sin\phi}{\sin^2\phi} \\ \frac{\delta Q}{\delta r} &= Brcq(1+a)^2\frac{c_l\sin\phi + c_d\cos\phi}{\sin^2\phi} \end{aligned} \tag{2.20}$$

Using Newton's second law the thrust is simply written as the mass flow times the change in axial velocity. The change in axial velocity is the difference between the free stream velocity and the axial velocity in the slipstream. As found in Subsection 2.2.3, the slipstream factor is twice the axial inducting factor. Using this knowledge, rewriting the thrust equation results in Equation 2.21. Using $\dot{m} = \rho A V_a$ and $\delta A = 2\pi r\delta r$ this equation can further be rewritten to obtain the trust gradient as shown in Equation 2.22.

$$\delta T = \delta\dot{m}\Delta V_{axial} = \delta\dot{m}V_\infty(1+a)2a \tag{2.21}$$

$$\frac{\delta T}{\delta r} = \rho 2\pi r V_\infty^2(1+a)2a \tag{2.22}$$

Similar reasoning can be used for the angular direction. The torque is given by the mass flow times the change in tangential velocity times the radius as shown in Equation 2.23. The change in tangential velocity is the difference between the freesteam tangential velocity, which is zero, and the tangential velocity in the slipstream. A similar approach as presented previously can be applied in tangential direction to shown that the angular velocity in the slipstream is twice the induced angular velocity at the propeller disk ($V_{t_{slipsteam}} = 2v_t = 2a'\Omega r$). Again applying the expressions for the mass flow and disk area, Equation 2.23 can be rewritten resulting in the expression for the torque gradient as shown in Equation 2.24.

$$\delta Q = \dot{m}\Delta V_{angular} \times r \tag{2.23}$$

$$\frac{\delta Q}{\delta r} = \rho 2\pi r V_\infty(1+a)2a'\Omega r^2 \tag{2.24}$$

The application of the Blade Element Momentum theory is an iterative procedure. Eventually the trust and torque gradients calculated from Equation 2.20 should equal the values obtained from Equations 2.22 and 2.24. This can for example be achieved by starting with initial assumed values for the induction factors (a, a'). These values can then be used to obtain values for the trust and torque gradients by use of Equation 2.20. The gradients in turn, can be used in Equations 2.21 and 2.23 to find updated values for the induction factors that can be used for the next iteration. Once the induction factors have converged the total trust and torque produced by the propeller can be obtained from the integration of the force gradients over the propeller span. The propulsive efficiency can be calculated by use of Equation 2.25.

$$\eta_p = \eta = \frac{TV_\infty}{P} = \frac{TV_\infty}{\Omega Q} \tag{2.25}$$

2.3. PROPELLER WING INTERACTION

Already in 1921 Ludwig Prandtl [57] acknowledged the strong interaction between the propeller and wing. There exists a two-way interaction where the propeller affects the wing, which in turn, affects the propeller. The two ways of interaction in case of a tractor propeller configuration are discussed here. This section is split into two parts, first discussing the propeller effect on the wing, followed by the wing effect on the propeller. Again, note that only the steady effects are discussed.

2.3.1. PROPELLER SLIPSTREAM EFFECT ON THE WING

In a tractor configuration, the propeller is installed upstream of the wing. This means that a part of the wing is immersed in the propeller slipstream. Several studies have shown that the integration of the propeller with the wing can result in both drag reduction and lift augmentation [3][58][59]. The aerodynamic effects of the propeller induced slipstream on the wing are discussed below.

SLIPSTREAM WASH

As discussed in Section 2.2, the propeller wake comprises both a tangential and axial induced velocity. The axial induced velocity is responsible for an increase in dynamic pressure in the propeller slipstream. This means that the part of the wing immersed in the slipstream of the propeller experiences a higher local dynamic pressure. This increased dynamic pressure enhances the local lift. As stated in Section 2.2, the dynamic pressure is not uniform in the propeller slipstream but depends on the radial position. The effect of the axial velocity increase due to a neutral positioned propeller on the immersed wing section can be depicted as shown in Figure 2.14.

The effect of the axial propeller induced velocity is symmetric with respect to the propeller rotational axis. Contrary, the effect of the tangential induced velocity (swirl) shows anti-symmetric behaviour. The slipstream swirl causes a change in local angle of attack. The wing fraction where the blades make an upward motion, experience a propeller induced upwash, resulting in an increased angle of attack and lift enhancement. The other part experiences a downwash responsible for an angle of attack decrease [34]. This effect of the propeller swirl on the lift distribution can be seen in Figure 2.15.

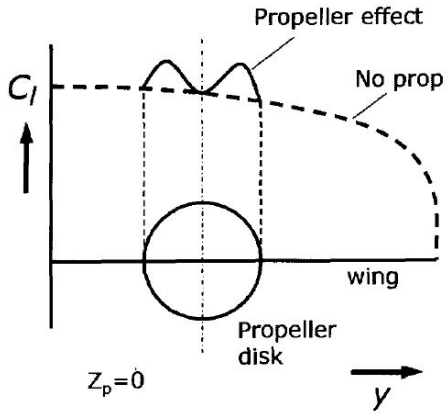

Figure 2.14: Effect on local lift distribution due to the axial induced velocity in the slipstream [8]

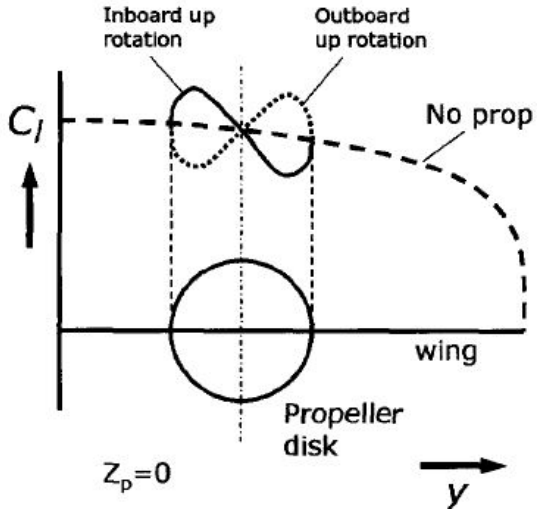

Figure 2.15: Effect of propeller slipstream on wing list distribution [8].

Combining the axial and tangential propeller induced velocity effects is more complicated than just superimposing the effects to the isolated wing aerodynamics. The wing region that is immersed in the slipstream is directly affected by the slipstream wash but also the other wing sections are influenced by the slipstream [34]. The change in spanwise lift distribution on the immersed wing part causes large gradients near the propeller slipstream edge. This in turn, causes the shed of vorticity, affecting the loading distribution on the complete wing. The vorticity shedding also causes a spanwise velocity component to occur. This velocity results in a distortion of the slipstream after interaction with the wing [60]. At the advancing blade side the slipstream moves away from the propeller axis, whereas the slipstream flows towards the propeller axis at the retreating blade side. This is depicted in Figure 2.16. The spanwise velocity introduces a spanwise shearing which modifies the wing performance locally [34].

The effects of the slipstream wash on the wing spanwise sections is summarised in Figure 2.17 and 2.18. These effects increase with propeller size and loading [8].

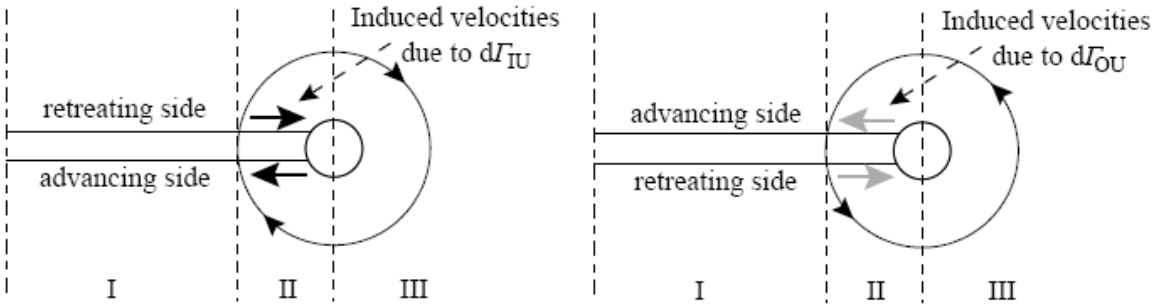

Figure 2.16: Spanwise flow for inboard-up and out-board up propeller [34].

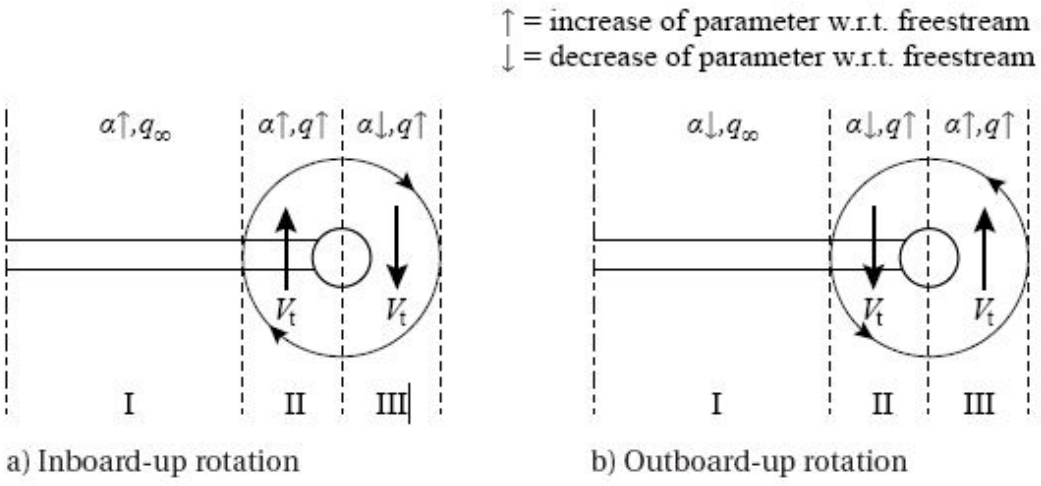

Figure 2.17: Aerodynamic effects of propeller slipstream on wing [34].

SWIRL RECOVERY

The slipstream modifies the loading distribution in amplitude as well as in orientation. The propeller wash on the wing changes the effective angle of attack. This means that the sectional resultant force is tilted. Because of a propeller induced upwash, the lift force will be tilted forward. If the propeller induces a downwash this effect is reversed. The effect of the propeller wash on the tilting of the local force is presented in Figure 2.19. In case of a propeller induced upwash, the forward tilt of the resultant force will make it to have a component that has a negative contribution to the induced drag. This component can be considered to enhance the propeller performance. Alternatively, it can be regarded as a reduction in swirl loss, known as swirl recovery [8].

TIP VORTEX ATTENUATION

If the propeller rotates in the opposite direction as the wingtip vortex, the tip vortex tangential velocities can partially be cancelled by the propeller swirl. This leads to a decrease in induced drag and is mostly apparent in case of a wingtip-mounted propeller[8].

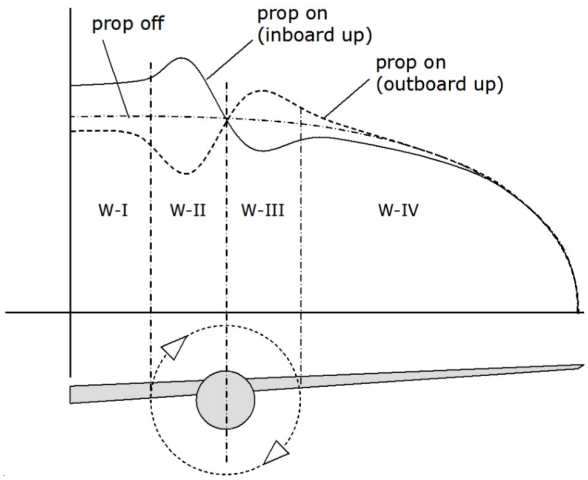

Figure 2.18: Aerodynamic effects of propeller slipstream on wing lift distribution [8].

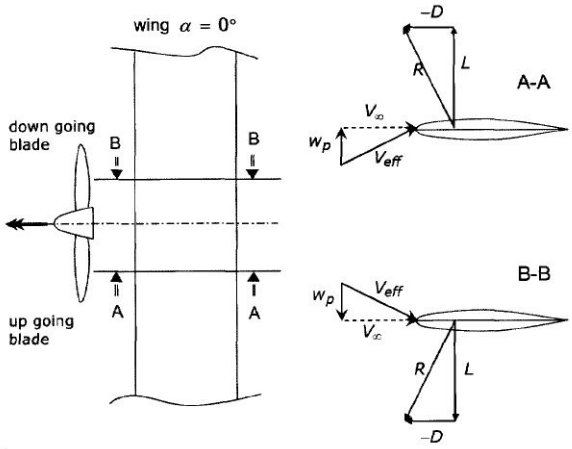

Figure 2.19: Swirl effect of propeller on local wing forces [8].

2.3.2. WING EFFECT ON PROPELLER

In a wing mounted tractor propeller configuration also upstream aerodynamic effects are present. The downstream lifting surface, the wing, introduces an upwash on the propeller. This upwash causes an unsymmetrical loading of the propeller blades [8]. This is due to the fact that the up-going blade is moving along the upwash whereas the down-going blade is moving against it. This results in a decreased angle of attack for the up-going blade and an increased angle of attack for the down-going blade [58]. This means that the up-going blade will experience a decrease in tangential velocity, decreasing the thrust produced by the blade. For the down-going blade the opposite happens and the thrust is increased. This effect is illustrated in Figure 2.20.

The load on the blade depends on its position in the rotational cycle, the azimuthal position. This effect is similar to the effect of an incidence angle on an uninstalled propeller and causes an asymmetry in the propeller slipstream [8].

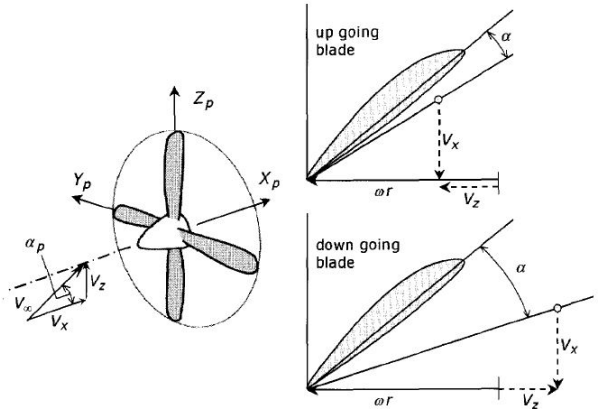

Figure 2.20: Upwash effect of wing on propeller [8].

2.3.3. EFFECTS OF PROPELLER POSITIONING

The previous discussion on the propeller slipstream wash effect and the tip vortex attenuation, reveals that inboard-up rotating propellers are more favourable than outboard-up rotating propellers, as they offer a reduction of induced drag, this was also argued by Witkowsi [58]. Besides the sense of rotation of the propeller, the positioning with respect to the wing influences the aerodynamic interaction effects to a great extend as explained by Veldhuis [8].

The vertical position of the propeller affects the dynamic pressure seen by the slipstream immersed wing section. Recalling that the dynamic pressure varies radially, having its maximum at the propeller thrust axis, a vertical shift of the propeller away from the axis will always result in a decrease of dynamic pressure on the slipstream immersed wing section. Moreover, the vertical position of the propeller will influence the effective angle of attack seen by the wing. Due to the increase of dynamic pressure in the slipstream, the slipstream tube will contract in order to sustain the same amount of mass flow. This results in radial velocities within the streamtube and alters the wing effective angle of attack. This can visually be explained by the use of Figure 2.21.

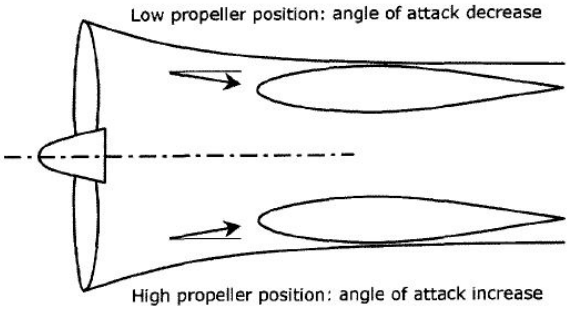

Figure 2.21: Effect of vertical propeller position on local angle of attack [8].

In case of a high propeller position the slipstream immersed wing section will experience a contraction induced increase in angle of attack, which tilts the force vector forward, reducing the induced drag. For a low propeller position the exact opposite happens and the contraction of the slipstream causes an increase in induced drag. The vertical position of the propeller also has an influence on the axial inflow velocity of the propeller. In a high

propeller configuration, the propeller is situated on the suction side of the wing, increasing the inflow velocity and consequently reducing the propeller efficiency.

The spanwise positioning of the propeller influences the extent of tip vortex attenuation, which becomes more pronounced when the propeller is placed further outboard. The highest attenuation occurs is case of a tip-mounted propeller. Moreover, if an inboard-up rotating propeller is mounted to the wingtip, the downwash effect on the wing vanishes. This is because there is no wing section situated behind the down-going blade side.

As one can imagine, the interaction effects between propeller and wing become more prominent if they are positioned in close proximity to each other. The streamwise position of the propeller influences the propeller efficiency. A slight increase in propulsive efficiency is obtained when the propeller is placed further upstream because of the rise in the axial flow velocity and because the upstream effects of the wing will vanish [8].

3

AERO-PROPULSIVE MODEL

An aerodynamic model was developed to predict the aerodynamic performance of the combined propeller-wing system. In particular, this model is applicable to a propeller-wing configuration featuring both a pair of wingtip propellers and inboard propellers, both installed in tractor configuration. The developed aerodynamic model is built upon the propeller-wing model developed by Willemsen [61]. His model is only applicable to a wing system with two propellers mounted to the tip. The model has been extended in order to be applicable to a wing with both an inboard and tip-mounted propeller. This chapter discusses the foundation of the model as well as the extensions made. The tool consists of a propeller and wing module. These modules are discussed in Section 3.1 and Section 3.2. The integration of the two modules is presented in Section 3.3.

3.1. PROPELLER MODEL

The propeller model predicts the aerodynamic performance of the propeller based on its geometry and operating conditions. Figure 3.1 shows the process flow of the propeller model. The velocity field in which the propeller operates is obtained iteratively. When the propeller model is evaluated for the first time, this velocity field is uniform and equals the freestream velocity in magnitude. As the propeller-wing model is capturing a two-way interaction between propeller and wing, this velocity field will eventually be modified by the wing induced velocities. The propeller model used by Willemsen consists of a BEM and accounts for non-uniform inflow, slipstream contraction and deflection which will be further elaborated in this section. The model eventually yields the propeller performance and induced velocities by the propeller.

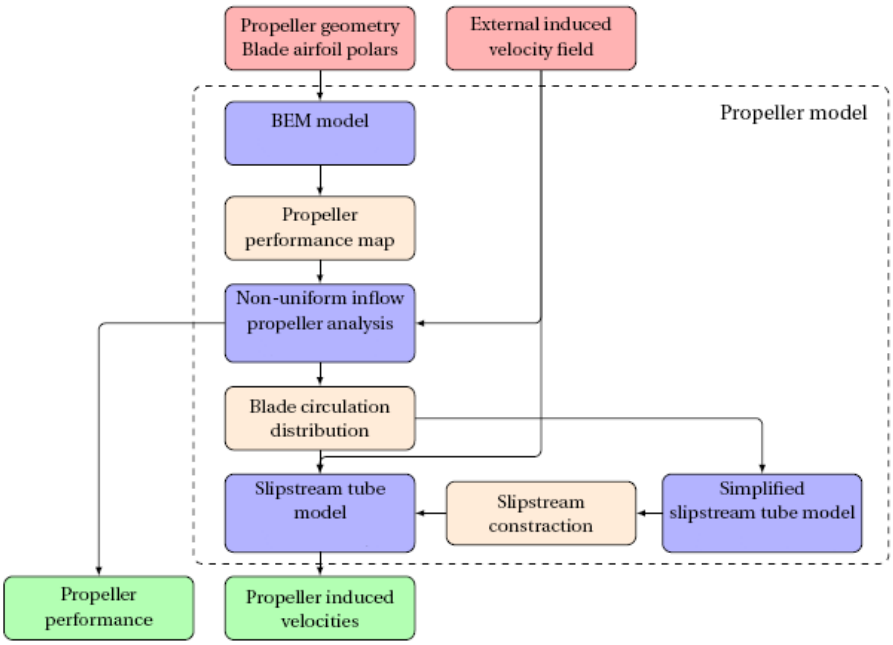

Figure 3.1: Flow chart of numerical propeller model [61].

BLADE ELEMENT METHOD

A BEM is used to analyse the isolated propeller performance. The formulation used is based on the *graded momentum* formulation. This formulation is also used in existing codes such as XROTOR and QPROP [62]. XROTOR has been used widely at the TU Delft and shows good agreement with CFD data [63][64]. The fact that XROTOR cannot take in direct airfoil polars was identified by Willemsen as a weakness of the model. That is why he developed his own BEM model based on XROTOR that is able to take in airfoil polars. As explained in Subsection 2.2.3, the solution of a BEM must be obtained iteratively. The model of Willemsen performs an iterative procedure until convergence for the circulation on the bade is reached. He introduces a dummy variable Ψ to speed up the calculation which is defined as shown in Figure 3.2. From the induced velocities and induction factors, the circulation can be obtained by use of Equation 3.1 [65]. The Prandtl tip loss factor is given by F and no root loss factor is applied.

$$\Gamma = v_t \frac{4\pi r}{B} F \sqrt{1 + \left(\frac{4V_a}{\pi B V_t}\right)^2} \tag{3.1}$$

The aerodynamics behaviour of the blade also depends on the angle of attack, Mach number and Reynolds number experienced. With the obtained (induced) velocities from the BEM formulation, these properties can be determined. Blade airfoil polars are a required input for the BEM model and are used to determine the aerodynamic response of the blade based on the previously mentioned parameters. The provided airfoil polars must yield lift and drag coefficients as a function of angle of attack, Mach number and Reynolds number. The airfoil polars need to be provided for a Mach number of zero as a Prandtl-Glauert compressibility correction is applied inside the BEM model. These required 2D

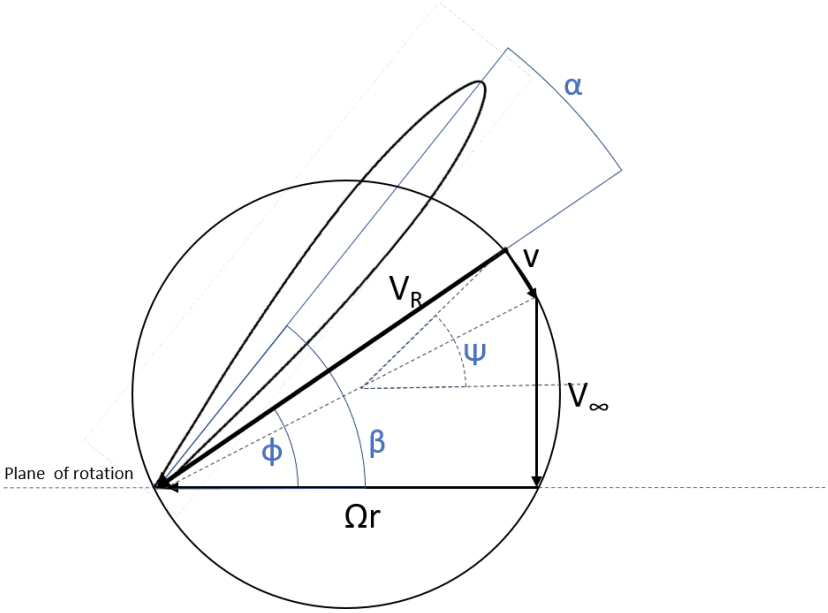

Figure 3.2: Definition of dummy variable Ψ.

airfoil polars can for instance be obtained by XFOIL [1]. This will yield a second equation for the circulation as shown in Equation 3.2.

$$\Gamma = \frac{1}{2} V_R c C_l(\alpha, Re) \frac{1}{\sqrt{1-M^2}} \tag{3.2}$$

With Equation 3.1 and Equation 3.2, the dummy variable is updated and eventually the residual between the two equations will be less than 10^{-12} once convergence has been reached.

The BEM formulation assumes that the induced velocity v is perpendicular to the total velocity vector V_R. Willemsen evaluated that this is a valid assumption to make if the circulation distribution follows the Goldstein optimal circulation distribution. Nevertheless, a propeller with an arbitrary circulation distribution shows a relatively large deviation for the axial velocity distribution while the predicted tangential velocity distribution is very close to the expected. Since the solution is relatively insensitive to errors in the axial velocity distribution but is mainly driven by the tangential velocity, the assumption is still usable for arbitrary propellers.

The goal of the developed BEM model is to resemble a propeller analysis tool like XROTOR but with the ability to directly incorporate airfoil polars. As such, the operating Mach and Reynolds number can be determined instead of assumed as a priori. The performance of the BEM model has been validated against XROTOR. It was found that the results match well over a broad range of advance ratios. Due to the direct inputt of airfoil polars it is even expected that the BEM provides more accurate results.

NON-UNIFORM INFLOW

For a propeller mounted to the wing in tractor configuration, the inflow field will be modified by the wash of the wing, resulting in a non-uniform inflow field. Van Arnhem et al. [66]

1

developed an engineering method to analyse a propeller in a non-uniform flow field. This method was included in the propeller model of Willemsen.

The method first performs a quasi-steady analysis. It determines the load on the blade for an assumed constant advance ratio J_∞ across the blade. However, locally the advance ratio deviates from the freestream advance ratio due to the induced velocities by the wing. To determine the effect of this local advance ratio, the load across the blade is calculated assuming this local advance ratio, J_{eff}, is experienced across the complete blade. The difference between the loading due to J_∞ and J_{eff} is used to determine the effect of the local change in advance ratio on the trust and torque coefficient: dC_T and dC_Q. This procedure is depicted in Figure 3.3 and is performed for both axial and tangential direction. The loading is determined by use of a so-called propeller performance map that relates the rotational and axial velocity to the propeller loading. The total load is obtained by superposition of the axial and tangential changes in load. Nonetheless, unsteady effects also play a role. If an airfoil experiences a change in inflow, the change in load in not instantaneous. To account for this unsteady effect, the Sears function is applied to the quasi-steady results. More details on this engineering method for a propeller in a non-uniform inflow can be found in Van Arnhem et al. [66].

The method was validated using CFD data and the integral thrust and torque force shows good agreement. Yet, the in-plane forces showed larger differences. Although these deviations are increasing with angle of attack, it is assumed that the contribution to the overall forces of the propeller-wing system is small.This means that these error only have a minor effect.

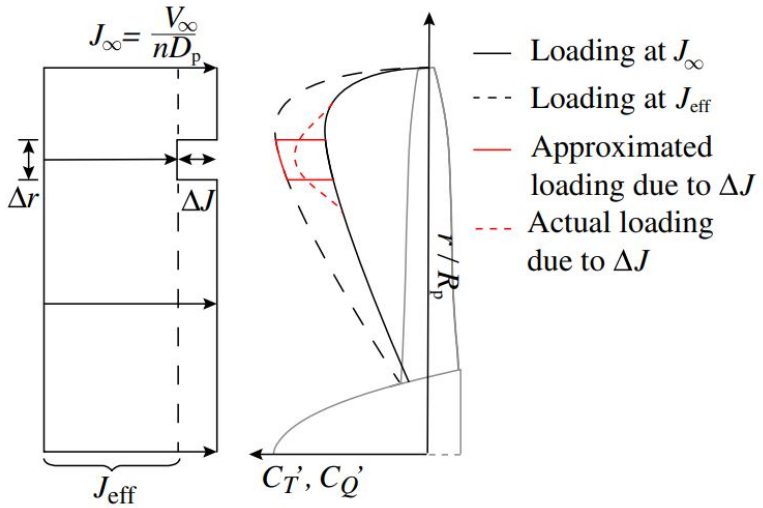

Figure 3.3: Relationship between local effective advance ratio and change in blade loading [66].

SLIPSTREAM MODEL

The slipstream model used by Willemsen is based on the slipstream tube model [3][8]. The slipstream is discretised in axial, radial and azimuthal direction. The induced velocity at a point P is affected by three sources of vorticity; the axial (γ_a) , tangential (γ_t) and propeller disk vorticity (γ_p). Each element has a corresponding vorticity γ. This model was enhanced to include the azimuthal circulation distribution, slipstream contraction and slip-

stream deflection. The radius of the slipstream decreases in streamwise direction due to the slipstream contraction. In addition, the centreline of the slipstream tube shifts when the slipstream travels downstream. Moreover, the circulation strength varies in azimuth direction due to the non-uniform inflow.

The azimuthal circulation distribution is provided by the non-uniform inflow propeller analysis. This circulation distribution is propagated downstream and rotation is accounted for. The rotation angle at each x-coordinate is given by $x_i\omega/U_\infty$ and is schematically presented in Figure 3.4. On purpose U_∞ is used instead of U_∞ plus the axial wake velocity such that the rotation angle for all radial stations is the same. Similarly, ω has been used without the tangential velocity component. Including the induced wake velocities will result in different azimuthal positions but the effect is deemed negligible for short distances between propeller and wing.

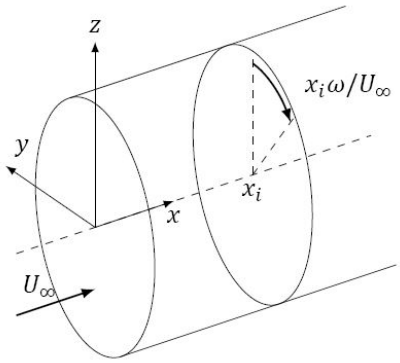

Figure 3.4: Propeller slipstream [61].

Due to the increase of dynamic pressure in the slipstream, the slipstream tube contracts in order to sustain the same amount of mass flow. Using this conservation of mass, and assuming a constant density, Equation 3.3 can be used to determine the radius at the an arbitrary axial position. However, it is computational expensive to compute this for every single position in the propeller wake. For this reason Conway's [12] analytical solution is used. The analytical solutions can be superimposed to form an analytical expression for the induced velocities for an arbitrary radial distribution.This expression is shown in Equation 3.4. The axial velocity at the propeller disk needs to be represented using an even number of polynomial functions. Willemsen determined that eight polynomials must be used to approximate the axial velocity distribution. By a least squares method the coefficients $U_{a0,\mu}$ can be determined. Good agreement between the slipstream tube model and Conway's model prediction for axial induced velocity was found. Conway's expression with eight polynomials can be used followed by Equation 3.3 to determine the slipstream contraction. With this slipsteam model some back flow near the root was observed, resulting in a slipstream expansion in this radial region. The largest contraction is observed near the tip of the propeller. This phenomena is shown in Figure 3.5. Moreover, the method was compared to the slipstream contraction method used by Veldhuis [8]. The 'mean' slipstream contraction predicted by Conway's method follows the solution by Veldhuis well in terms of magnitude and shape, indicating that this method is valid to use for the contraction of different radial stations. Also comparison with a frozen wake method [61] shows good agreement.

$$\frac{r}{r_0} = \sqrt{\frac{U_\infty + u_{a,0}}{U_\infty + u_a}} \tag{3.3}$$

$$U_a(r,0) = \sum_{\mu=1}^{N} U_{a0,\mu}\left(1-(r/R)^2\right)^{\mu} \tag{3.4}$$

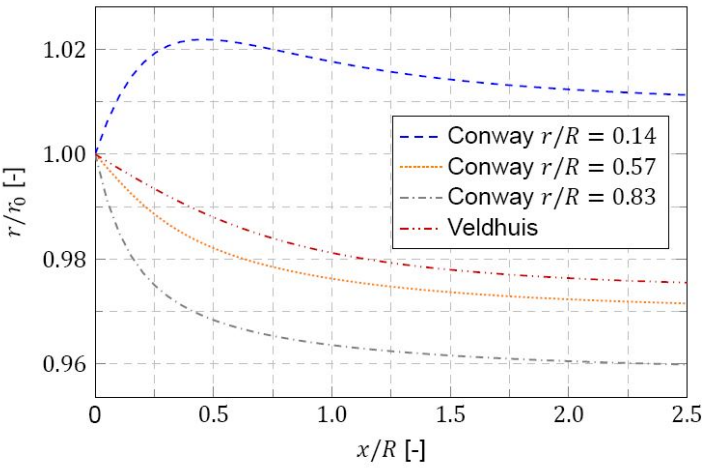

Figure 3.5: Slipstream contraction for different radial stations and comparison with method by Veldhuis[8][61].

Besides contracting, the slipstream will also deflect. This deflection is caused by the external induced velocities in vertical direction. The deflection angle and deflection of the slipstream centre line can be determined as shown in Figure 3.6 and yields $\frac{\Delta z}{\Delta x} = \frac{u_{z,i}}{U_\infty}$. For the axial velocity U_∞ is used instead of $U_\infty + U_{x,i}$ because this gives a different axial velocity for each radial position and results in a different deflection angle. Instead, using U_∞ will result in a single deflection angle for each x-coordinate and not over-complicate the slipstream geometry. This results in an over prediction in deflection angle. Since the distance between the propeller and wing will be relatively small, this is expected to not have a major effect. Moreover, an overestimation of the slipstream deflecting angle behind the wing will also have a minor effect on the induced velocities on the wing since the effect of vorticity decreases with distance.

In short, the slipstream model discretises the slipstream and numerically computes its shape and induced velocities based on vorticity and the Biot-Savart law. It accounts for azimuthal circulation distribution, slipstream contraction and slipstream deflection. It computes the induced velocities at the control points of the discretised geometry and uses an interpolation function to determine the induced velocity at all other locations.

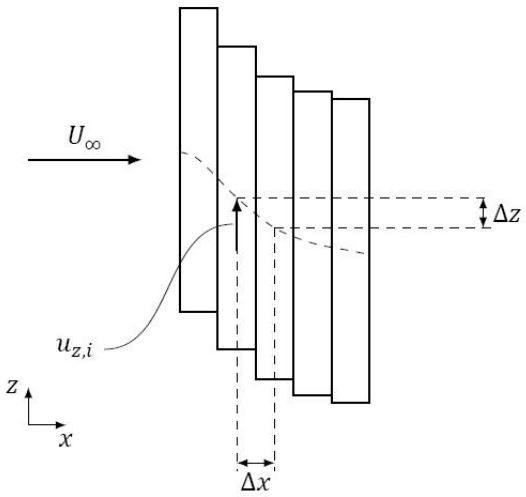

Figure 3.6: Slipstream deflection calculation method [61].

3.2. WING MODEL

The wing model analyses the wing aerodynamics. It requires the wing geometry and the flight conditions. If viscous effects need to be included, it also requires the polars of the used airfoil(s). In order to include the effects of the propeller on the wing, the propeller induced velocities on the wing also need to be present as an input. A flowchart of the wing model is shown in Figure 3.7. The model will yield the wing performance in terms of lift and drag and a loading distribution. It will also provide the wing induced velocities, which in turn, can be used as an input for the propeller model. This section will elaborate on the wing model. For a more in-depth explanation the reader is referred to [61].

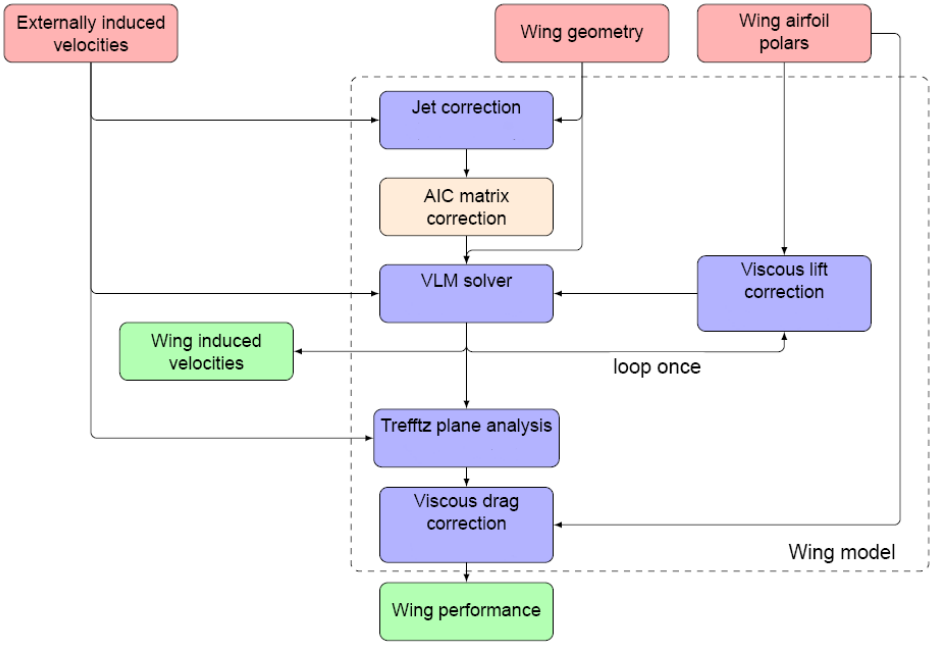

Figure 3.7: Flow chart of numerical wing model [61].

3.2.1. FOUNDATION

The wing model is primarily based on a VLM model. A comparison between different numerical models has been performed by Epema [16]. The VLM method was preferred in the model of Willemsen because a lifting like method would not give an accurate prediction of the wing load distribution. Moreover, a panel method would require more complexity. Besides a VLM model, the wing model includes a jet correction, Trefftz plane analysis and viscous correction.

The VLM method discretises the wing by dividing it in a number of panels. These panels are distributed in chordwise and spanwise direction and are placed in the x-y plane such that they reflect the 2D wing planform. This also applies to asymmetric airfoils, their chamber is introduced as a camberline slope in the boundary conditions.

A horseshoe vortex extending to infinity is associated with each panel and its bound vortex is placed at the quarter-chord line of the panel. At the centre of the 3/4-chord line, a control point is situated. The VLM geometry used is shown in Figure 3.8. Having all the geometry situated in one plane, simplifies the calculations. It must be noted that this simplification leads to modest errors if the model is used at high angles of attack and with cambered airfoils [50].

The normal velocity on the ith panel is given by Equation 3.5. Note the inclusion of the airfoil camber by $\frac{\partial g}{\partial x}$. The last term is obtained by the Biot-Savart law and represents the influence of horseshoe vortex j on control point i. By combining the different coefficients C, the Aerodynamic Influence Coefficient matrix ($\overline{\overline{AIC}}$) can be formed and Equation 3.5 can be rewritten to the system shown in Equation 3.6. The symbol $\overline{U_n}$ consists of the first three terms shown in Equation 3.5. This system can be solved for the circulation strength vector Γ. From this vector the lift can be calculated using the Kutta-Joukowski theorem. The validity of the VLM model was checked against other existing VLM codes and showed satisfying agreement.

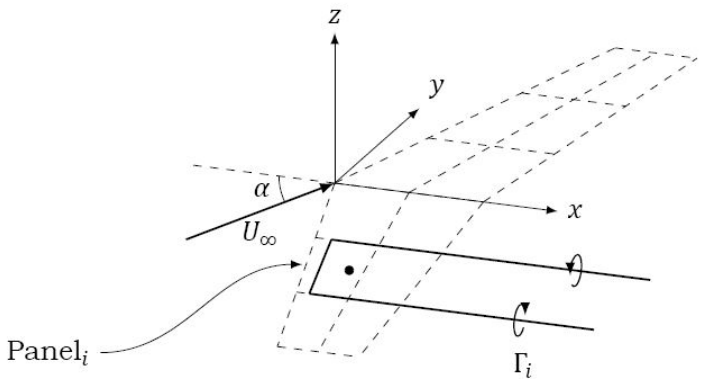

Figure 3.8: VLM geometry used [61].

$$U_{n,i} = U_\infty \left(\frac{\partial g}{\partial x} - a \right) + u_x \frac{\partial g}{\partial x} - u_z - \sum_j C_{j,i} \Gamma_j = 0 \tag{3.5}$$

$$\overline{\overline{AIC}} \times \Gamma = \overline{U_n} \tag{3.6}$$

The induced drag of the wing is calculated using a Tefftz plane analysis and is based on

derivations by Katz and Plotkin [50] and Veldhuis and Heyma [67]. For a detailed distribution the reader is referred to Willemsen [61]. Lift estimation comparison with XFLR5 and AVL showed good agreement. Furthermore, the predicted drag distribution matches well with the prediction of XFLR5. In general, the VLM Tefftz plane drag analysis is in agreement with existing codes.

An important feature of the wing model is that it includes a correction for the finite height of the propeller slipstream. The effect of a finite slipstream height is depicted in Figure 3.9. An airfoil immersed in a slipstream with jet velocity U_j and a finite radius R, produces less lift than an airfoil experiencing a freestream velocity of U_j. This effect is mainly present for the axial velocity direction and can be neglected for the tangential direction [20]. Rethorst [21] developed a 3D method to account for the effect of the finite height of the slipstream. He introduced a correction matrix G to be applied to the Aerodynamic Influence Coefficient matrix as show in Equation 3.7. The correction is based on pressure and slipstream continuity on the jet boundary for a geometry as shown in Figure 3.10. The correction matrix gives the correction to be applied to each of the coefficients in the AIC. The derivation and formulation of the correction method is explained in detail in Rethorst [21].

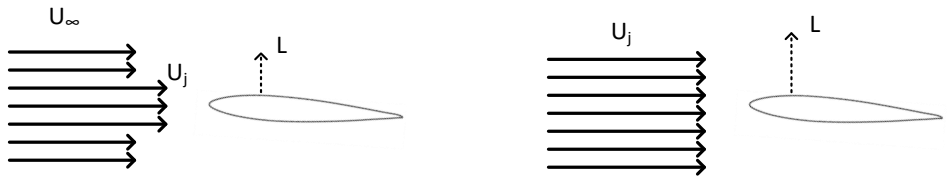

(a) Lift on an airfoil in a slipstream with finite radius. (b) Lift on an airfoil in a freestream.

Figure 3.9: Comparison of lift on an airfoil in a slipstream with finite height and freestream.

$$\left(\overline{\overline{AIC}} + \overline{\overline{G}}\right)\overline{\Gamma} = \overline{U_n} \tag{3.7}$$

The method was developed for a symmetrical case in which the jet is located at half span. Figure 3.11 presents a simple geometry consisting of five vortex pairs for such a case. The symmetry around the jet centre means that $\Gamma_1 = \Gamma_5$, $\Gamma_2 = \Gamma_4$ and Equation 3.7 yields Equation 3.8.

$$\left(\begin{bmatrix} C_{11}+C_{15} & C_{12}+C_{14} & C_{13} \\ C_{21}+C_{25} & C_{22}+C_{24} & C_{23} \\ C_{31}+C_{35} & C_{32}+C_{34} & C_{33} \end{bmatrix} + \begin{bmatrix} G_{11} & G_{12} & G_{13} \\ G_{21} & G_{22} & G_{23} \\ G_{31} & G_{32} & G_{33} \end{bmatrix}\right) \begin{bmatrix} \Gamma_1 \\ \Gamma_2 \\ \Gamma_3 \end{bmatrix} = \begin{bmatrix} U_{n,1} \\ U_{n,2} \\ U_{n,3} \end{bmatrix} \tag{3.8}$$

Although the method was developed for a propeller on the wing symmetry axis, it can also be applied to an asymmetrical configuration since the correction is most noticeable around the jet boundary [20]. In order to apply it to an asymmetric case, an imaginary wing part needs to be introduced. This imaginary wing part ensures the propeller to be in the centre of the wing as shown in Figure 3.12 and will disregard the correction on this imaginary part. For this example, Equation 3.8 is rewritten to Equation 3.9 and is described

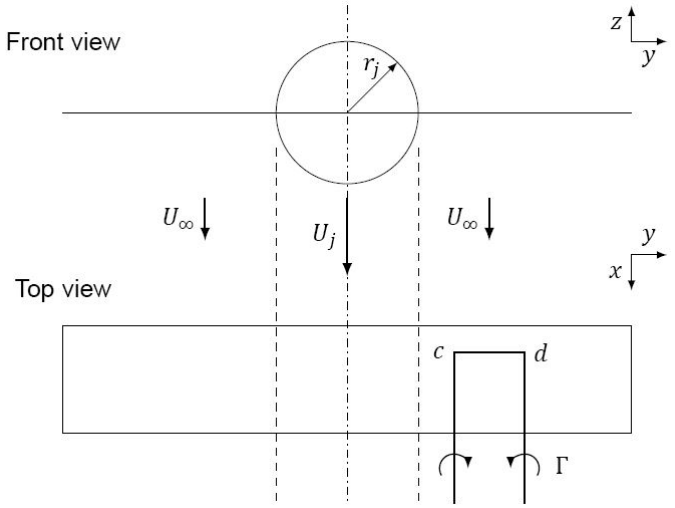

Figure 3.10: Jet correction geometry used by Rethorst [21].

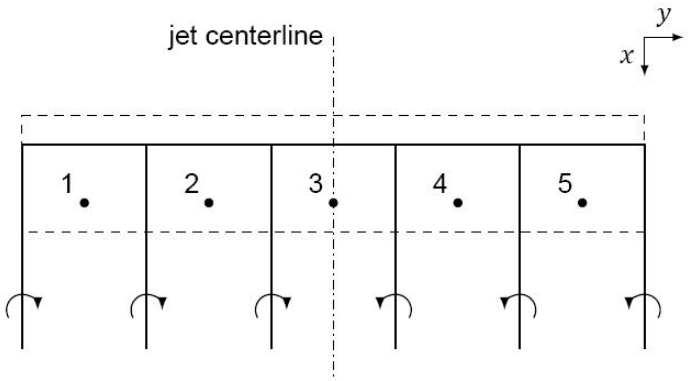

Figure 3.11: Simple geometry for jet correction calculation for symmetrical case [61].

by Willemsen as the *equally divided correction*. Alternatively, the jet correction can be calculated for section I and the correction for sections II and III can be obtained by mirroring the correction matrix of section I. The correction obtained for section III will be disregarded because this is only an imaginary wing section. This formulation is shown in Equation 3.10 and is described by Willemsen as the *symmetry correction*. Both methods provide good results.

It must be noted that the correction method imposes a number of conditions for the VLM mesh used. First of all, the jet centerline must be in the center of one the vlm strips and the jet boundary must coincide with one of the strip boundaries. Moreover, the distribution of the vortex strips should be symmetric about the propeller axis. For the wingtip-mounted propeller this does not impose any problems as the symmetry section only consists of a virtual wing part and will be disregarded.

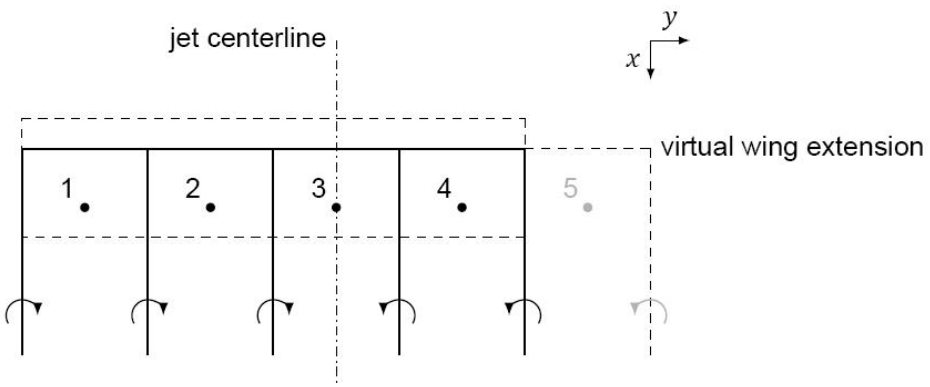

Figure 3.12: Simple geometry for jet correction calculation for asymmetrical case [61].

$$\left(\begin{bmatrix} C_{11} & C_{12} & C_{13} & C_{14} & C_{15} \\ C_{21} & C_{22} & C_{23} & C_{24} & C_{25} \\ C_{31} & C_{32} & C_{33} & C_{34} & C_{35} \\ C_{41} & C_{42} & C_{43} & C_{44} & C_{45} \\ \cancel{C_{51}} & \cancel{C_{52}} & \cancel{C_{53}} & \cancel{C_{54}} & \cancel{C_{55}} \end{bmatrix} + \begin{bmatrix} G_{11}/2 & G_{12}/2 & G_{13} & G_{12}/2 & G_{11}/2 \\ G_{21}/2 & G_{22}/2 & G_{23} & G_{22}/2 & G_{21}/2 \\ G_{31}/2 & G_{32}/2 & G_{33} & G_{32}/2 & G_{31}/2 \\ G_{21}/2 & G_{22}/2 & G_{23} & G_{22}/2 & G_{21}/2 \\ \cancel{G_{11}/2} & \cancel{G_{12}/2} & \cancel{G_{13}} & \cancel{G_{12}/2} & \cancel{G_{11}/2} \end{bmatrix} \right) \begin{bmatrix} \Gamma_1 \\ \Gamma_2 \\ \Gamma_3 \\ \Gamma_4 \\ \Gamma_5 \end{bmatrix} = \begin{bmatrix} U_{n,1} \\ U_{n,2} \\ U_{n,3} \\ U_{n,4} \\ \cancel{U_{n,5}} \end{bmatrix} \tag{3.9}$$

$$\left(\begin{bmatrix} C_{11} & C_{12} & C_{13} & C_{14} & C_{15} \\ C_{21} & C_{22} & C_{23} & C_{24} & C_{25} \\ C_{31} & C_{32} & C_{33} & C_{34} & C_{35} \\ C_{41} & C_{42} & C_{43} & C_{44} & C_{45} \\ \cancel{C_{51}} & \cancel{C_{52}} & \cancel{C_{53}} & \cancel{C_{54}} & \cancel{C_{55}} \end{bmatrix} + \begin{bmatrix} G_{11} & G_{12} & G_{13} & 0 & 0 \\ G_{21} & G_{22} & G_{23} & 0 & 0 \\ G_{31} & G_{32} & G_{33} & 0 & 0 \\ 0 & 0 & G_{23} & G_{22} & G_{21} \\ \cancel{0} & \cancel{0} & \cancel{G_{13}} & \cancel{G_{12}} & \cancel{G_{11}} \end{bmatrix} \right) \begin{bmatrix} \Gamma_1 \\ \Gamma_2 \\ \Gamma_3 \\ \Gamma_4 \\ \Gamma_5 \end{bmatrix} = \begin{bmatrix} U_{n,1} \\ U_{n,2} \\ U_{n,3} \\ U_{n,4} \\ \cancel{U_{n,5}} \end{bmatrix} \tag{3.10}$$

The jet correction as described by Rethorst assumed the propeller slipstream to be uniform in axial direction. In reality, a propeller introduces a distribution in axial velocity in the slipstream. The assumption has been revised and modified by Willemsen to the assumption of a radially symmetric axial velocity distribution. The jet velocity is discretized and for every significant step in velocity μ_i, a correction matrix G_i is calculated as if a jet with of radius r_i and axial induced velocity u_i is present. Summing all the correction matrices results in the total jet correction to be applied. This approach is visualised in Figure 3.13.

The wing model also features a way to correct for viscous effects on the lift and drag. In order to do this, airfoil polars are required that provide the 2D lift and drag coefficient for a range of angles of attack for different Mach numbers and Reynolds numbers. For the viscous lift correction, the correction is determined by comparison of thin airfoil theory used in the VLM with the airfoil polars. The way the viscous lift correction is determined is visualized in Figure 3.14 and Equation 3.11. The viscous polars can be obtained by Xfoil [2] for example. These polars are also used to determine the skin friction coefficient.

[2] https://web.mit.edu/drela/Public/web/xfoil

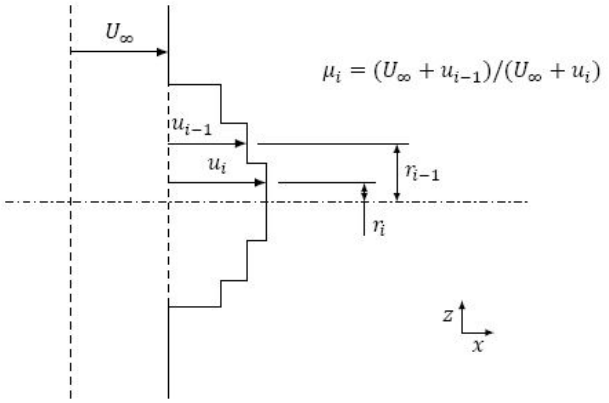

Figure 3.13: Discretization of a jet velocity profile for the calculation of the jet correction [61].

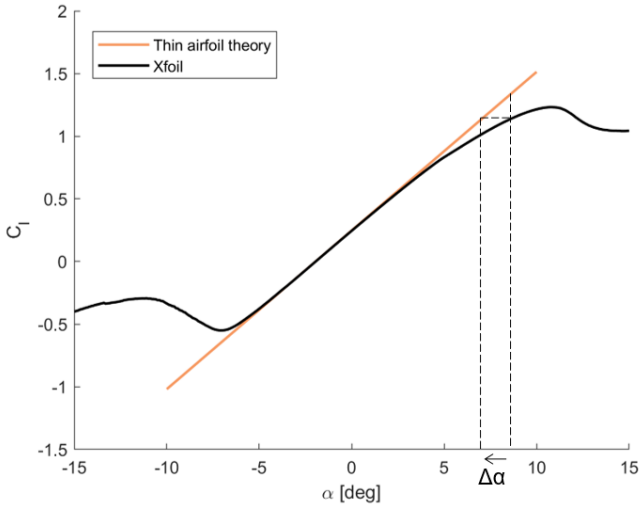

Figure 3.14: Visualisation of the way the viscous lift correction is determined.

$$d\alpha_{corr} = \frac{C_{l,visc} - C_{l,inv}}{2\pi} \tag{3.11}$$

3.2.2. ADJUSTMENTS

As the original model has been developed for a wing with wingtip-mounted propeller only, the main adaption that had to be made to the model was incorporating the ability of analysing a wing with an additional inboard propeller.

The aforementioned model has been adapted such that it could analyse a propeller-wing system of interest for this study. This means its adapted version is able to analyse a wing with a wingtip-mounted propeller and a main propeller in tractor configuration. Moreover, it is suitable for a regional turboprop in terms of aircraft dimensions and flight conditions.

JET CORRECTION FORMULATION

The original jet correction was only valid for a wingtip-mounted propeller. Its formulation has been modified to make it applicable to a propeller at an arbitrary spanwise location.

As mentioned before, the jet correction assumes the propeller to be located at a (virtual) symmetry axis of the wing. It requires the VLM strips to be distributed symmetrically about the propeller axis. Naturally, the wing root also needs to be an axis of symmetry since the propulsion system is symmetrically spaced with respect to this axis. Figure 3.15 shows the symmetry axes required for a propeller wing system with two main propellers.

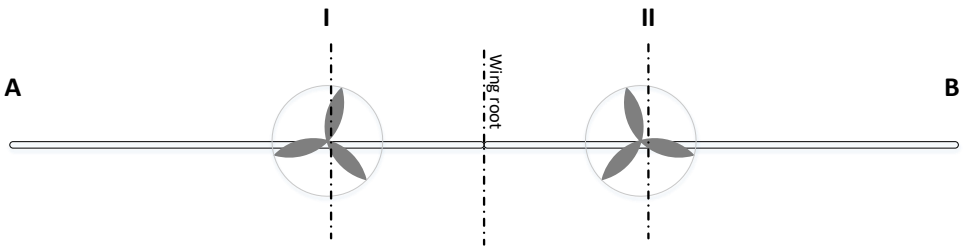

Figure 3.15: Symmetry axes required for jet correction due to main wing.

Obeying these symmetry requirements, the jet correction matrix can be generated in two different ways. The correction can be calculated for one wing half first. This means calculating the correction for section I-A, mirroring about I with the other wing side as imaginary. Subsequently, the correction matrix can be mirrored to obtain the correction for the other wing half. This process is demonstrated in Figure 3.16. Alternatively, the correction can be calculated for the complete wing (section A-B) with one propeller first and its inverse can be added to the matrix to obtain the correction for a complete wing with two main propellers. This is shown in Figure 3.17. Again, these tricks can be applied because the correction is most present around the jet boundary. This also enables the superposition of the obtained correction matrices for the inboard and wingtip-mounted propeller.

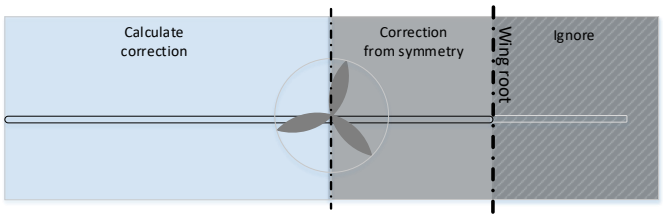

(a) Step 1: calculate jet correction for one wing half.

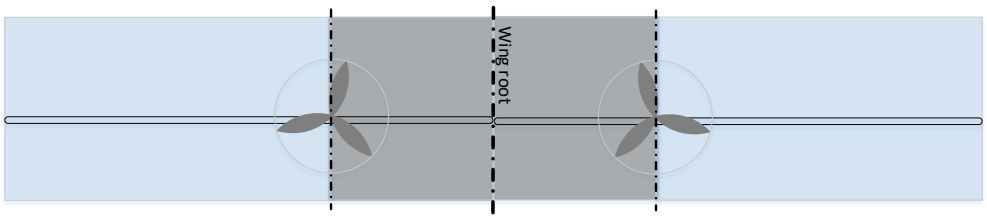

(b) Step 2: mirror jet correction matrix about wing root.

Figure 3.16: Jet correction determination, option 1.

(a) Step 1: calculate jet correction for complete wing with one propeller.

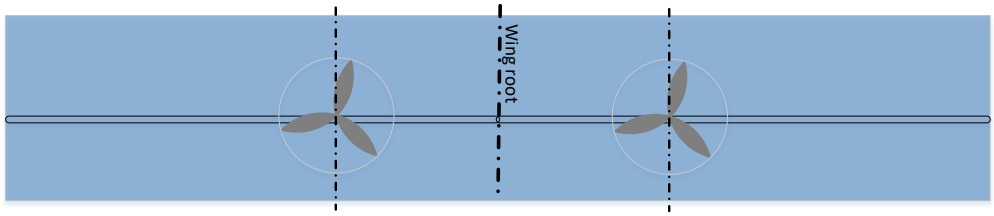

(b) Step 2: add inverse of correction matrix.

Figure 3.17: Jet correction determination, option 2.

The two methods are compared for a simple wing geometry with a uniform panel distribution across the span and an assumed axial induced velocity distribution like presented in Figure 3.21 with μ=0.87 and a propeller radius of r=0.1b at 0.2 y/b. Figure 3.18 shows the effect of a jet correction on the lift distribution. The two correction methods produce similar results. For an inboard propeller, the first method is preferred because the second method can only be applied if a uniform strip distribution is used which is far from desired.

Consequently, for a wing with a wingtip-mounted propeller and inboard propeller, the wing mesh will need to be divided into five sections as shown in Figure 3.19. Section I and III need to have the same amount of strips and a similar, but opposite, spacing (eg. inverse sine vs sine). Section II needs an uneven number of strips and a symmetric spacing about its centre. The type of spacing used per section is shown in Table 3.1. A convergence study has been performed to determine the optimum number of panels regarding computational time and accuracy.

Table 3.1: Type of spacing used per section.

Section	I	II	III	IV	V
Spacing	Inverse sine	Uniform	Sine	Inverse sine	Uniform

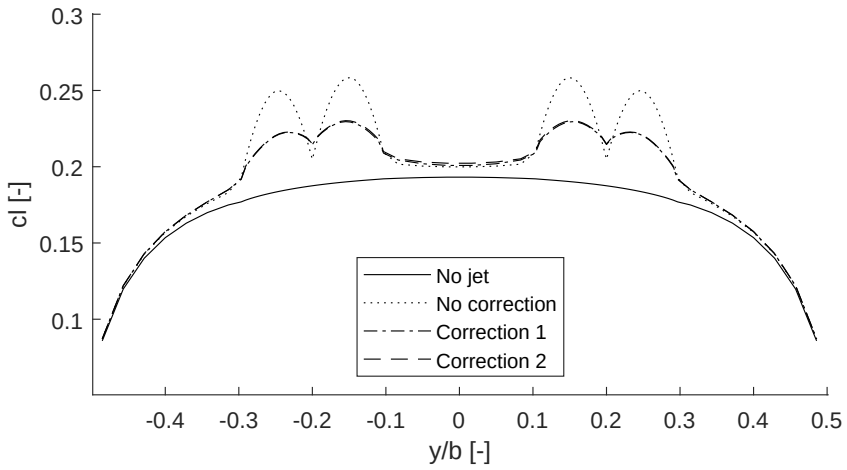

Figure 3.18: Comparison of lift distribution for various jet-correction approaches.

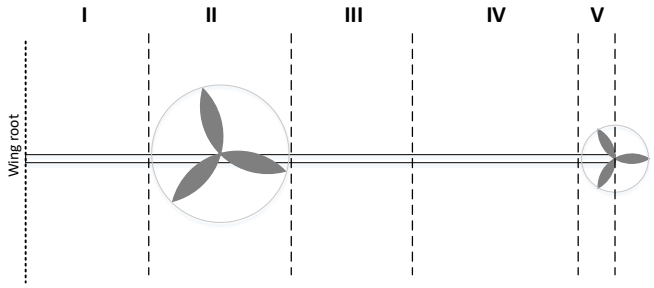

Figure 3.19: Division of wing sections.

COMPRESSIBILITY EFFECTS

The original aero-propulsive model was only used for low flight speeds and no mach number correction was included in the wing model. As a turboprop aircraft is to be studied at cruise conditions (M_{cr}=0.5-0.6), compressibility effect will become more significant. That is why a Prandtl Glauert compressibility correction has been applied to the vortex strength at each panel. This means that the corrected circulation is given by $\Gamma_c = \frac{1}{\sqrt{1-M^2}}\Gamma_i$ [68].

LOADING DISTRIBUTION

In addition, the model only provided the aerodynamic loading distribution in terms of lift and drag. From a structural perspective, the pitching moment distribution is also desired. The moment distribution due to lift was added and is easily obtained from the sum of the lift of the individual panels multiplied by their distance to the quarter chord line.

To check whether the compressibility correction and pitching moment calculation are correctly implemented, the results obtained for the modified method are compared to analyses by AVL. A clean wing (no propellers) was used. Furthermore, the wing is tapered, swept and uses an asymmetric airfoil. The geometry used is representable for a wing of interest in this study. The results are shown in Figure 3.20. It can be seen that the lift distribution matches quite well while the moment distribution shows some discrepancies. A constant offset between the AVL and VLM predicted moment is observed across the span. This is caused by the fact that the wing model only accounts for the pitching moment caused the lift and disregards the moment introduced by the airfoil camber. The effect of this discrep-

ancy has been investigated in combination with the structural model presented in Chapter 4. It was found that the structural model is relatively insensitive to the magnitude of the pitching moment distribution. The wing weight was determined for various designs both using the pitching moments distribution computed by AVL and the wing model. The results showed that the difference in pitching moment leads to a difference of wing mass of 2kg maximum, which is insignificant.

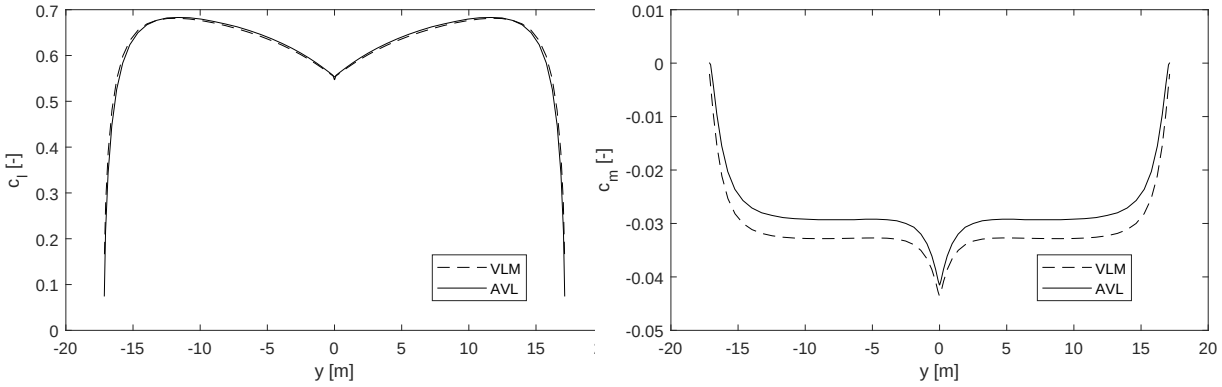

(a) Lift distribution.

(b) Pitching moment distribution.

Figure 3.20: Comparison of the load distribution computed by AVL and the wing model for a clean aerodynamic wing.

PROPELLER INDUCED VELOCITIES

The major modification is the addition of an additional propeller. To combine two propellers on one wing-half, it is assumed that the propellers do not have an effect on each other. It was found that both the axial and tangential propeller induced velocity rapidly approaches zero once the distance to propeller axis is larger than its radius, as sketched in Figure 3.21. Since the distance between the two propellers will be much larger than the radius, the assumption of no mutual propeller interaction can be applied. This also means that the induced velocities by the propeller can simply be superimposed onto the wing velocity field.

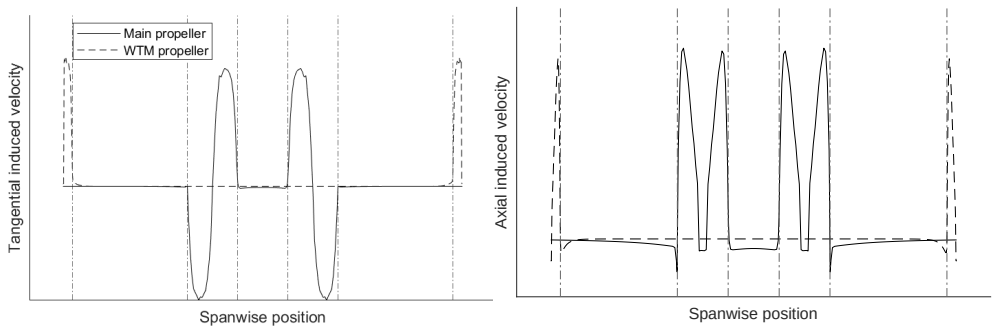

Figure 3.21: Illustration of typical tangential and axial induced velocity distribution over the wing with inboard and tip-mounted propeller.

3.3. PROPELLER-WING MODEL INTEGRATION

There is a mutual interaction between the wing and the propeller. The performance of the wing depends on the propeller induced velocities, while the propeller itself depends on the wing induced velocities. For this reason, the propeller-wing system aerodynamic analyses requires an iterative procedure. An updated process flow is depicted in Figure 3.22. The iterative process continues until the results have converged. This state is reached once the residuals between the previous and current solution fall below the convergence threshold specified in Table 3.2.

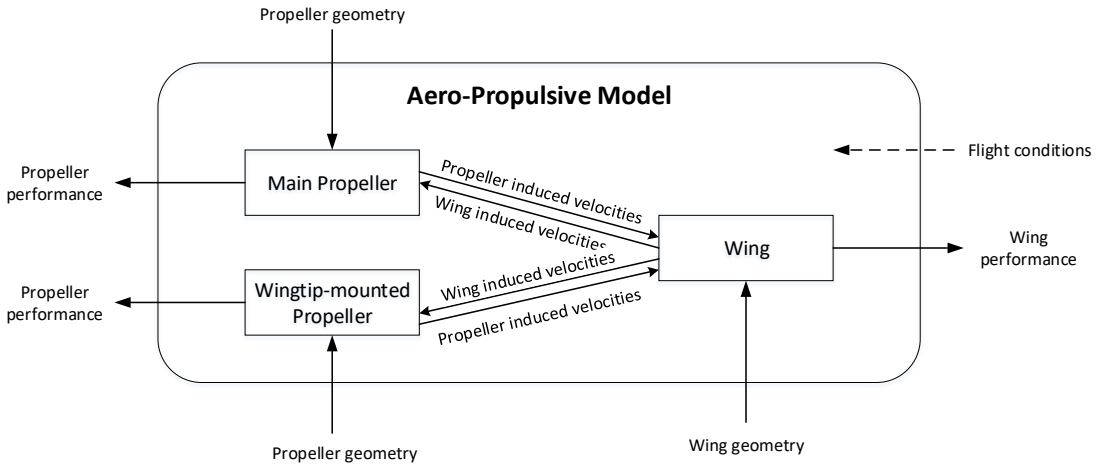

Figure 3.22: Flow chart of modified aero-propulsive model.

Table 3.2: Convergence thresholds for the propeller-wing system.

Parameter	Threshold
ΔC_T	1e-4
ΔC_L	1e-3
ΔC_Q	1e-4
ΔC_D	1e-4

The converged solution of the system is sensitive to a number of settings. It depends on the number of spanwise and chord wise panels used as well as the density of the discetised propeller grid and slipstream stations. A convergence study has been performed to study the influence of the grid densities on the solution. The convergence study has been conducted for a propeller-wing system representable for the design and flight conditions under consideration in this study. More on such a design can be found in Chapter 5. The conditions used are the most extreme flight condition that will be considered in this study: a 2.5g load. A default value is used for all of the important convergence variables and these have been varied to study the effect of a coarser or denser grid on the final solution. The convergence study showed that the density of the propeller grid has an insignificant effect on the obtained performance coefficients of the system and only shows a large effect on the computational time. A twice as dense propeller grid will result in a difference in lift coefficient

of less than ($1.0 \cdot 10^{-7}$) while doubling the computational time. For this reason, the propeller has been discretised with a relative coarse grid. Changing the number of slipstream stations used, barely effects the results and also the computational time is not drastically affected. If the number of slipstream stations is doubled the system lift coefficient changes by 0.1% and the computational time increases by roughly 20%.

For the wing mesh, the size of the panels did show to have a significant influence on the obtained solution. The results for the lift coefficient of the convergence study performed for the spanwise and chordwise panels is shown in Figure 3.23 and 3.24 respectively. Note that also the thrust, drag and torque coefficient have been studied but the lift coefficient showed to be the most sensitive. The panel factors of 1.5 and 2.0 were chosen such that the deltas are less than 0.5%. With this new number of panels, the convergence study has been re-performed and confirmed that the combination of both panel distributions show satisfying results.

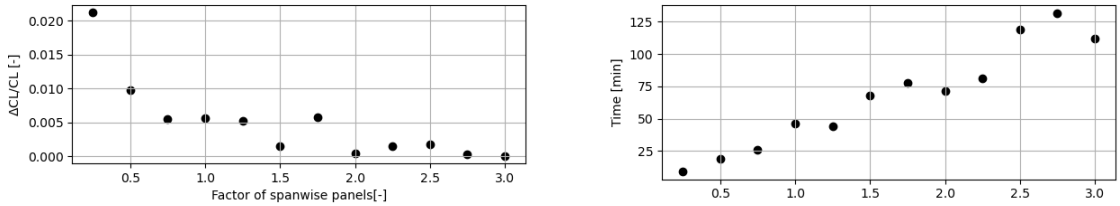

(a) Difference in lift coefficient with varying number of panels. (b) Effect on computational time.

Figure 3.23: Convergence study results spanwise panels.

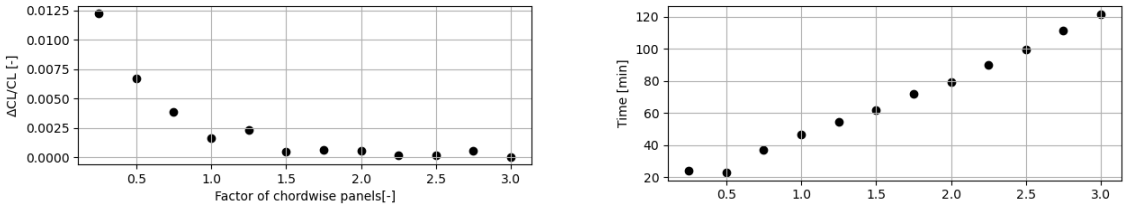

(a) Difference in lift coefficient with varying number of panels. (b) Effect on computational time.

Figure 3.24: Convergence study results chordwise panels.

3.4. VALIDATION

The original aero-propulsive method was built for a wing with a wingtip-mounted propeller only. Willemsen [61] checked its validity by comparing the method's results against experimental data collected by Sinnige et al. [7]. The experimental set up of this experiment is shown in Figure 3.25. For completeness, the comparison of the predicted aerodynamic polars for the wing with a wingtip-mounted propeller are shown in Figure 3.26a and 3.26c.

The same experiment was performed for an inboard propeller. This data has been used to validate the correct implementation of the inboard propeller in the aero-propulsive model. The results are shown in Figure 3.26b and 3.26d. Both numerical and experimental data show that the lift increases with a decrease in advance ratio (which equals a thrust increase). Moreover, the validation data shows an increase in lift curve slope for increasing thrust. This trend is also predicted by the numerical model. The two configurations also

show similar behaviour in terms of the numerical predicted lift-drag polar compared to the experimental data. The discrepancies in both lift curve slope and lift drag polar are supposed to be caused by not modelling the nacelle. In general, the aero-propulsive model is able to model the major trends of the interfering propeller-wing system.

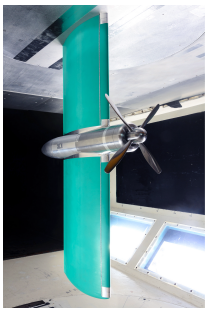

(a) Conventional configuration.

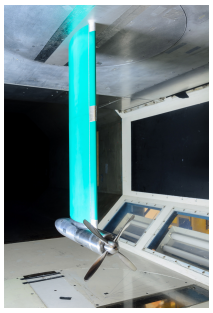

(b) Wingtip-mounted configuration.

Figure 3.25: Experimental set up by Sinnige et al. [7].

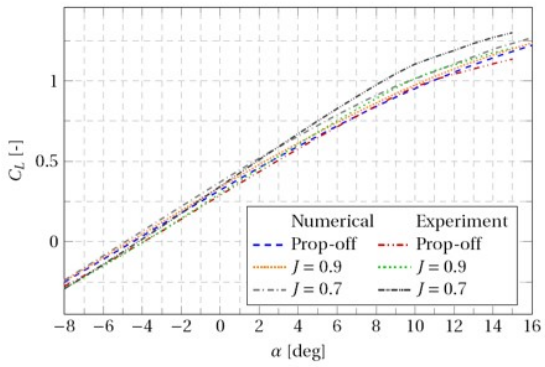

(a) Lift polar- Wingtip propeller only [61].

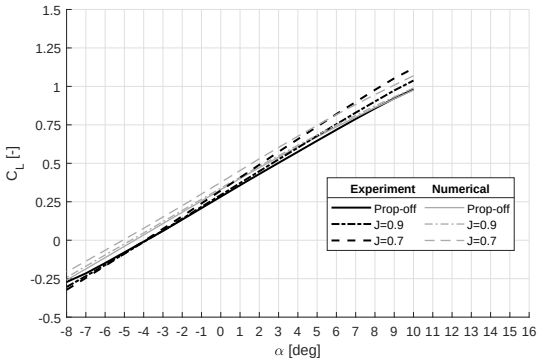

(b) Lift polar - inboard propeller only.

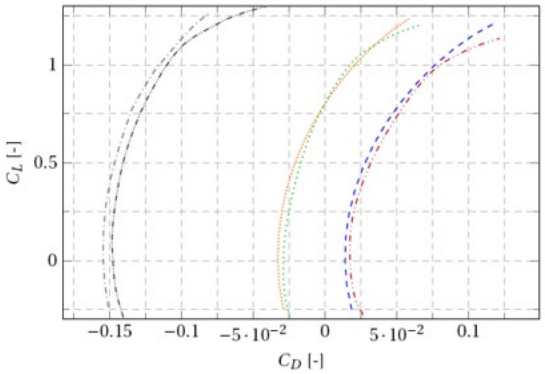

(c) Lift drag polar - wingtip propeller only [61].

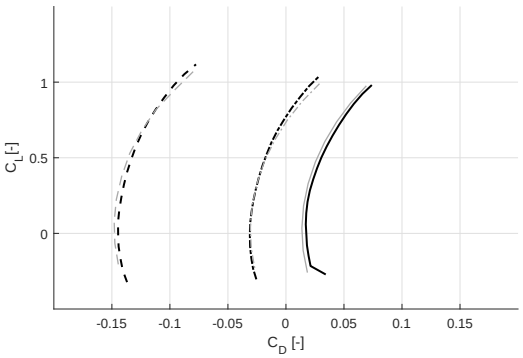

(d) Lift drag polar - inboard propeller only.

Figure 3.26: Comparison of numerical results of the aero-propulsive model with experimental results [7].

3.5. APPLICATION

The model presented in this chapter is now usable for a propeller wing system featuring an inboard and tip-mounted propeller. The model is capable of analysing and identifying

major aerodynamic behaviour and basic geometry. Nevertheless, the model does have a number of limitations. First of all, its formulation and assumptions used make it only applicable to a wing with a continuous leading and trailing edge, this means a wing with a kink cannot be analysed. Moreover, in its current formulation only constant airfoil with constant thickness can be used throughout the span. It can feature a taper ratio different to one, but it cannot cope with dihedral or large sweep angles. The propeller design can be specified in terms of number of blades, chord-distribution, twist-distribution, radius and rotation velocity.

4

AERO- STRUCTURAL MODEL

The purpose of the structural model is to estimate the wing weight of the design under consideration. It is important that the model is sensitive to the loading distribution such that the aero-propulsive effects on the wing weight can be studied. Moreover, a modification of the design such as a different power share between the shafts will affect the respective weight of both power trains. Similarly, changing the position the engines will make the weight act at a different position on the wing. In short, a modification in propulsive design will have an effect on both aerodynamic and discrete loads acting on the wing. In order to study the effects of a wingtip-mounted propeller configuration on the wing weight, the structural model needs to be sensitive to these two kinds of loads. Section 4.1 gives an overview of a number of existing wing weight estimation methods that are commonly used within the conceptual design phase of an aircraft whereafter Section 4.2 discusses the specific method used in this research. Section 4.3 explains how the aero-propulsive model and structural model are integrated.

4.1. OVERVIEW OF DIFFERENT METHODS

In commonly preliminary sizing methods [22][23][24], the aircraft weight and corresponding component weight are estimated using statistics in Class I and Class II weight estimations respectively. However, for a configuration with wingtip-mounted propellers, these methods are not design sensitive enough to accurately perform a weight estimation. Higher class methods exists where the approach is more physical-based such as Class III weight estimation methods by Droegkamp [29] and Bindolino [30]. These methods typically use Finite Element Analysis (FEA) and are more design-sensitive, providing weight estimations with higher accuracy. On the contrary, these methods require too detailed geometry information and the computational cost are high which makes this an unattractive approach. Hybrid methods exist which combines the benefits of Class II and Class III weight estimation into a Class II.V weight estimation method. The resulting method is quasi-analytical and makes use of both statistical methods and elementary structural wing box analyses. Elham [31] reviewed the existing Class II.V methods and concluded that the accuracy of the weight prediction varies considerably. He identified the weaknesses of these methods and developed an improved Class II.V method which is explained in [31]. This software was implemented in the Aircraft Design Initiator, which is a design synthesise tool developed by the TU Delft and is discusses in more detail in Section 6.1. Elmendorp [45] later replaced

this by another Class II.V method which was needed in order to analyse more unconventional wing designs such as a box-wing. This model is currently used within the Initiator, and was chosen as the best suitable option for the aero-propulsive integration thanks to its low computational time, accuracy and easy integration of the aerodynamic loads.

4.2. FINITE ELEMENT METHOD

The structural model used is a so-called Finite Element Method (FEM). The FEM used has been coded by Elmendorp [32]. It discretises the wing and uses an idealised boom representation to model the wing sections. This idealisation method models the wingbox by use of booms and skin only. The stringers and spar flanges are replaced by concentrations of area, called booms. The direct stresses are carried by these booms while the skin is effective only in shear. This method in explained by Megson [69]. The idealisation method is depicted in Figure 4.1.

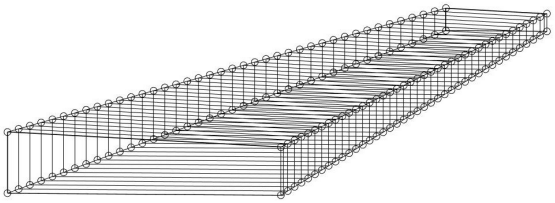

Figure 4.1: Idealised wing representation as used in the structural model.

Using this approach, the internal stresses are determined for each element. Because the stresses are depended on the section properties, like boom areas and skin thicknesses, a sizing method is required. An optimisation problem is formulated for the wing box design in order to get the minimum amount of primary structure required while the box can withstand the critical loadcase without exceeding the maximum allowable mechanical stress in the structural members, with a 1.5 safety factor included. The optimisation problem is shown in Equation 4.1 and a flowchart is presented in Figure 4.2.

$$\begin{aligned} &\text{Minimize:} && f(\bar{x}) \\ &\text{Subject to:} && \sigma(\bar{x}) \leq \sigma_{max}, \\ & && \delta(\bar{x}) \leq \delta_{max} \\ &\text{Where:} && (A_1, \ldots, A_n, t_1, \ldots, t_n) \end{aligned} \tag{4.1}$$

The structural wingbox weight estimation is sensitive to the aerodynamic load acquired by the aero-propulsive module, consisting of lift, drag and moment distribution. It also takes the weight of the engines into account. These are included as discrete loads on the wing as if there were point masses. Straightforwardly, the wing also has to be able to carry its own weight. The different aerodynamic and inertial forces on the nodes are shown in Figure 4.3.

The weight of the secondary elements is based on the weight of the wingbox and is estimated using Torenbeek [22]. A breakdown of the total wing structural weight is shown in Figure 4.4.

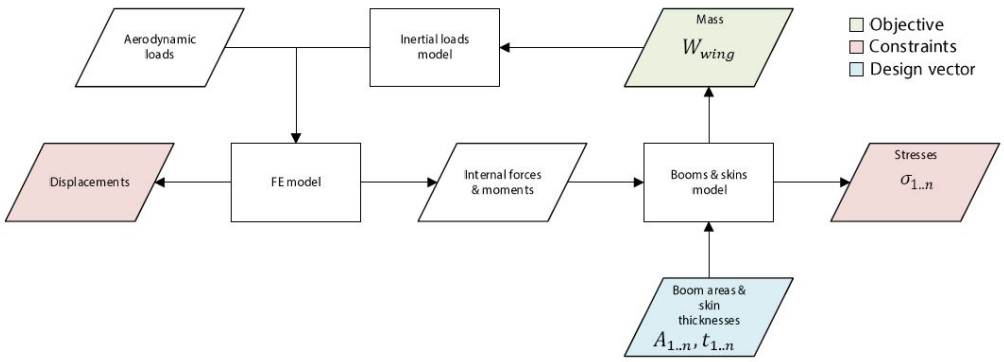

Figure 4.2: Optimisation flow of the structural wing weight estimation model [32].

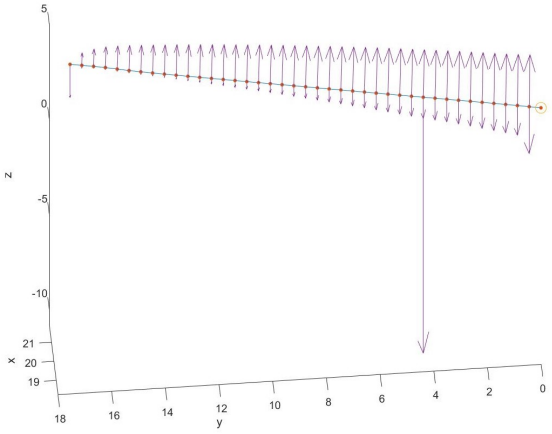

Figure 4.3: Loading distribution over the wing including aerodynamic and inertia loads.

4.3. INTEGRATION WITH AERO-PROPULSIVE MODEL

The wing of the aircraft needs to be designed for critical conditions. For this, a 2.5g load is used at which the structural model will be evaluated to estimate the wing weight with both Maximum Take-Off Mass (MTOM) and Zero Fuel Mass (ZFM). This load condition is often used for wing weight sizing conditions [31][22]. The aerodynamic load for this condition is acquired by the aero-propulsive model which yields the aerodynamic load distribution consisting of lift, induced drag and pitching moment. It is assumed that the 2.5g load has to be withstand at a flight altitude of 3000ft above cruising altitude. Simultaneously, the cruise Mach number is increased by 0.04. For this flight condition the required lift coefficient can simply be determined by use of the lift formula and the value from MTOW from previous Class I and Class II analyses. As explained in Chapter 3, the aero-propulsive model requires an angle of attack input and generates the corresponding lift coefficient. As the aero-propulsive model is computationally expensive, sweeping the angle of attack to match the required lift coefficient is not an option. Moreover, the aero-propulsive module only analyses the wing and no other lifting surfaces. This is why AVL[1] is used to predict the required angle of attack at which the aero-propulsive module is evaluated as well as the division of lift provided by wing and tail.

[1] http://web.mit.edu/drela/Public/web/avl/

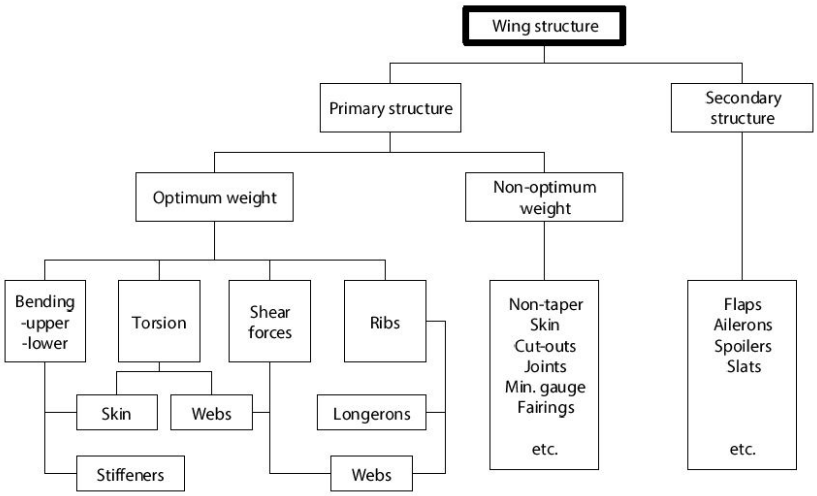

Figure 4.4: Mass breakdown of wing structural weight [32].

The inviscid propeller-wing model is analysed at this angle of attack with propeller power at cruise settings and yields the aerodynamic load distribution over the wing for the critical condition. This loading distribution is scaled to match the required wing lift coefficient of the wing and is forwarded to the structural model together with the known wing geometry and engine specifications. An overview of the process flow of the aero-structural model is shown in Figure 4.5.

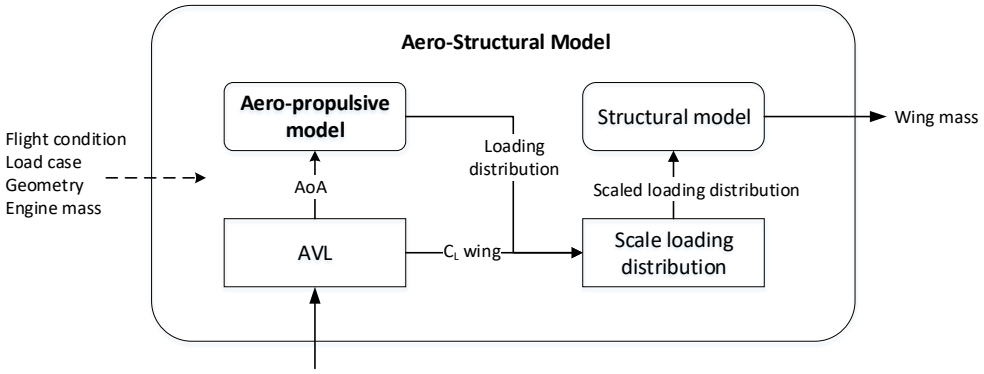

Figure 4.5: Overview of aero-structural process flow.

4.4. VERIFICATION

Elmendorp integrated his structural model within the Aircraft Design Initiator (more details on the Initiator can be found in Section 6.1). Because of close coupling and interdependency of different disciplines, the design tool was verified as an integrated system. Converged designs synthesised by the Initiator were compared to reference data of the existing airplanes and showed satisfying results.

Within the Initiator, the FEM model is directly dependent on AVL for the loading distribution at critical conditions. In the aero-structural model, the FEM model depends on the aero-propulsive model and AVL. To verify the correct integration between the aerodynamic and the structural model, results obtained by the aero-structural model are compared to the FEM model coupled with AVL for the aerodynamic load as in the original situation. To make a fair comparison between the two, the same (aerodynamic) wing system and flight conditions are used. Since AVL does not account for aero-propulsive effects, the aerodynamic analysis in the aero-propulsive model was also limited to a clean aerodynamic wing. The aerodynamic analysis for the verification study thus assumes that there are no propellers on the wing. Nevertheless, the structural model still includes the inertial loads of the propellers. So only the aerodynamic effects of the propeller are neglected in this verification study. This will not affect the purpose of this verification method as it focuses on the integration between the aerodynamic and structural model only. A number of different designs have been evaluated based on the design modifications and baseline designs presented in Section 5.2.1. Figure 4.6a presents that both methods show the same sensitivity of the wing mass to a design modification. For the same design modification, both methods predict an equally large change in wingmass compared to the baseline design. The absolute difference between the wingmass obtained by both methods is in the order of 0.5% as shown in Figure 4.6b. This difference is expected to be caused by a slight difference in predicted loading distribution between AVL and the VLM model used in the aero-propulsive model and not due to any integration issues. Overall, the integration of the aero-propulsive model within the structural analyses performs as desired.

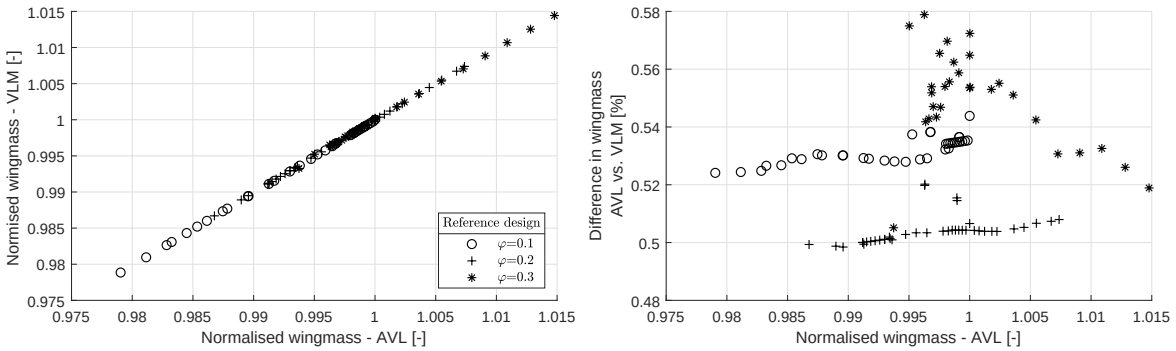

(a) Normalised wingmass

(b) Difference in wingmass

Figure 4.6: Wingmass comparison for different design by using AVL and VLM predicted loading distributions for a clean aerodynamic wing.

5

WING WEIGHT SENSITIVITY STUDY

One of the objectives is to study the effect of the propeller-wing aerodynamics on the wing weight for a wingtip-mounted propeller configuration. In order to do this, a number of different designs have been analysed varying the propulsion system while assuming a constant wing design. The design modification procedure, including its assumptions are presented in Section 5.1. The configurations studied are presented in Section 5.2. The results from the analyses are presented in Section 5.3 and are further discussed in Section 5.4.

5.1. METHODOLOGY

To study the effect of the wingtip-mounted propeller configuration on the wing-weight, the wing-propulsive system design has been varied based on different baseline designs which are presented in Section 5.2.1. To purely investigate the effect of a change in propulsive design on wing weight, the baseline wing planform is unmodified. The only adaptations that can be made are in terms of shaft power ratio, propeller diameter and engine location, see also Section 5.2 for more details. The effect of these design modifications are only studied at wing level. This means that there is no feedback to the broader aircraft level. Furthermore, only the aero-structural effects and aero-propulsive effect at the sizing condition are incorporated. The aerodynamic benefits of a wingtip-mounted propeller in cruise conditions are for instance not included. Consequently, it is assumed that, irrespective of the modifications made to the baseline design, the MTOM, thrust and drag of the system remain unaltered. This is the most important assumption used in the wing weight sensitivity study and is essentially the main difference with the aircraft level study presented in Chapter 6. An overview of the assumptions used for the wing weight study is given in Section 5.1.1.

To study the effects of the design modifications on the wing weight, the aero-structural model discussed in Chapter 4 is used. The structural wing weight analysis is mainly driven by the lift distribution and the discrete loads of the engines. By changing the propulsive design, the loading distribution over the wing will change due to the aero-propulsive interaction effects. The changed propulsive design will also influence the weight of the propulsive system. So, a change in propulsive design influences the wing weight analysis in two ways. It alters the aerodynamic loading distribution on the wing and it changes the distribution of the engine masses over the wing. The aerodynamic effect is accounted for by the aero-propulsive analysis module which is evaluated at a load case of 2.5g. For the weight

of the propulsion system, a sizing methodology has been developed which is presented in Section 5.1.2. Additionally, this sizing method estimates the required propeller RPM which is in turn needed for the aero-propulsive analysis.

5.1.1. ASSUMPTIONS

To purely investigate the effect of the propulsive design modifications on the structural wing weight, the wing planform is unmodified. In addition, the propeller design is kept constant and can only be scaled. The effect of the design modifications on the wing weight are only evaluated on wing level. This means that there is no feedback loop for the aircraft weight or aerodynamic performance. The aircraft weight and required trust are assumed from the used baseline design.

The propeller thrust equals the produced power divided by the velocity. The propeller produced power is given by the applied power times the efficiency of the propeller. It is assumed that the efficiency of the propellers are insignificantly influenced by the design modifications because they are operated around the same advance ratio. This results in the assumption of an unaltered total shaft power. Simultaneously, this makes it possible to say that the shaft power split between the two shafts equals the thrust split between the two. So, this would mean that for a shaft power ratio of 0.2, 20% of the power is delivered by the secondary shaft resulting in 20% of the total thrust. The total disk area, which is the total area of the propellers combined, is also kept constant. This makes it possible to vary the individual disk loading of the propellers while maintaining a constant total disk loading.

Furthermore, the side effects of changed axial and vertical propeller placement have to be minimised to prevent invalid comparison between designs. This has been done by freezing the vertical and axial location of the propeller with respect to the wing. The local distance in axial direction between the propeller and the leading edge of the wing remains constant. This means that the propeller can be placed along a line that follows the leading edge sweep of the wing with a constant offset. The vertical position of the propeller is a fixed fraction of the propeller radius. This is implemented to make sure that the ratio of disk area above and below the wing is insensitive to the propeller size.

In short, the method uses the following assumptions:

- MTOM is unaffected
- The total required thrust is not affected by the design modifications
- The total shaft power remains constant
- The shaft power ratio equals the thrust split
- The total disk area remains constant
- The axial distance between the wing leading edge and propeller remains constant
- The propeller offset in vertical direction is normalised by the radius and remains constant

5.1.2. SIZING METHOD

The changes in engine mass are estimated by an engine sizing procedure. This also determines the individual propeller rotational velocity to produce the required thrust. An overview of the propulsion system sizing procedure is shown in Figure 5.1.

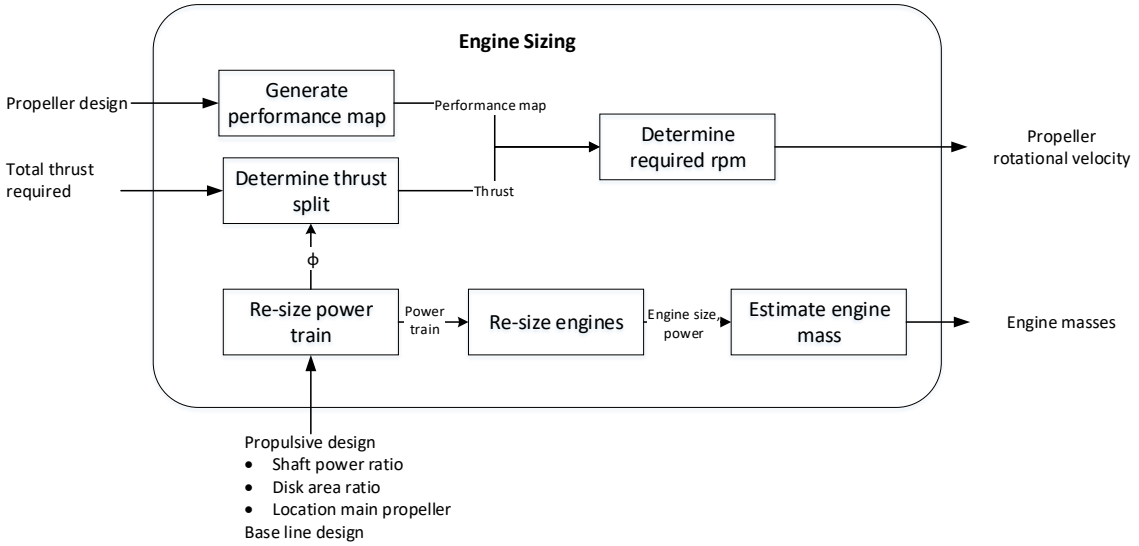

Figure 5.1: Overview of engine sizing process flow.

PROPELLER RPM

A change in shaft power ratio means an alternation of the thrust split between the inboard and wingtip-mounted propeller which will require the propellers to operate at a different rotational velocity to deliver the required thrust. Moreover, a change in propeller size will also require a change in propeller rotational velocity to maintain the thrust deliverance required. So, when the size of the propellers and/or shaft power ratio is changed, the propellers need to operate at a different rotational velocity to deliver the prescribed thrust.

With the total thrust and thrust split specified, it is easily determined how much thrust needs to be delivered by the individual propellers. For the propeller design used (N250), a performance map is produced to determine the rotational velocity at which the propeller needs to operate in order to produce the required thrust. This is done by sweeping the rotational velocities for the required flight conditions and propeller design. The generation of the performance map has been validated by comparison to a shoptest performed by NLR (Netherlands Aerospace Centre) [70] on the N250 propeller. These results can be seen in Figure 5.2 and are generated for 10,000 rpm at sea-level conditions.

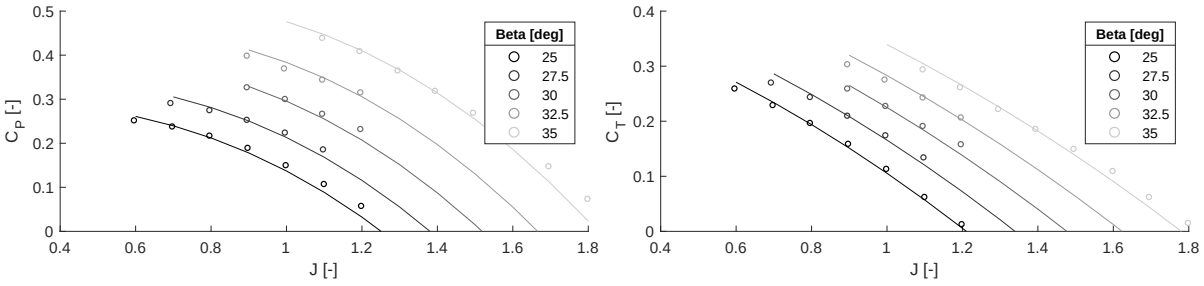

(a) Power coefficient.

(b) Thrust coefficient.

Figure 5.2: Validation with N250 propeller shop test [70].

ENGINE MASS

Besides the effect of the propulsive design modification on the aerodynamic loading, it also influences the inertial load on the wing by the weight of the engines. Naturally, one can reason that an engine will get heavier if it needs to produce more power. So, a higher shaft power ratio will consequently lead to a heavier engine on the tip. To quantify this effect, the power loading of each component in the powertrain needs to be re-calculated for the modified designs. For this the assumption of constant total shaft power is applied. In Figure 5.3 a schematic representation of the PTE power train is shown. With P_{s1} and P_{s2} known, the component efficiencies can be used to reversely calculate the power loading of each component.

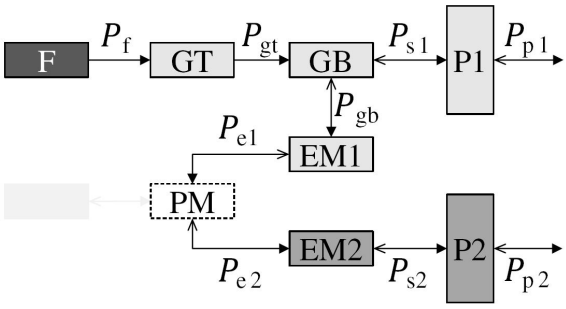

Figure 5.3: Partial turbo-electric power train [28].

With the individual power loading of the system components re-evaluated and the MTOM known, the power of each of the power-train components can be calculated. With these power values obtained, the engines are resized. The turbine size is determined by use of a statistical model by Raymer [24, table 10.4]. The dimensions of the electric engine are roughly based on the Siemens SP260D. Based on the power and size of the engines, the engine weight is determined by a regression method on TCDS (Type Certificate Data Sheets) data from EASA, FAA and CAA, and the assumed power densities.

5.2. CASE STUDY

The wing weight sensitivity study is based on baseline designs that have been modified in terms of propulsive design. The baseline designs used and the design variables are treated in Sections 5.2.1 and 5.2.2 respectively.

5.2.1. BASELINE DESIGNS

In total three different baseline designs have been used and modified for the wing weight sensitivity study. These designs differ in shaft power ratio (φ=0.1, 0.2, 0.3) and are all based on the converged PTE wingtip-mounted propeller configurations presented by Hoogreef et al. [44]. For the designs, a high technology level is assumed yielding an Equivalent Specific Power (ESP) of 9.1 kW/kg for the electrical drivetrain and a Specific Power (SP) of 10.5 kW/kg for the gas turbine. The electrical drivetrain groups all electrical components into a single black box as indicated in Figure 5.4. The technology advancement of the electrical drivetrain is characterised by the ESP, which is a measure for the combined specific power of the electrical drivetrain components and is introduced by de Vries et al. [71]. It represents the combined SP of each component in the electrical drivetrain as formulated

in Equation 5.1. This combined specific power method enables the use of a "black box" approach which is useful for mass estimation in the conceptual sizing phase. It provides a simplified understanding of the potential of the powertrain technology level. It is independent of the specific design of the electrical system, as it does not require information regarding every component in the powertrain. The ESP value of 9.1 kW/kg is deducted from the assumption of a specific power of 22 kW/kg for the electrical machines and 32 kW/kg for the power converters with a 30% weight penalty included to account for additional power distribution and cooling aspects. The specific powers used for the high technology level are expected to be realistic on a long-term basis.

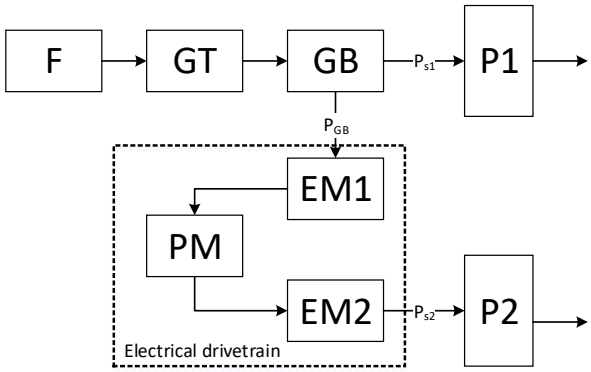

Figure 5.4: Partial turbo-electric power train.

$$ESP \approx \sum_{i=1}^{n} \frac{1}{(1/SP)} \tag{5.1}$$

The top level requirements (TLRs) of the designs presented by Hoogreef et al. are roughly based on the TLRs of the A320. The TLRs used are listed in Table 5.1.

Table 5.1: Top level requirements for reference aircraft.

Specification	Unit	Value
Harmonic range	km	2037
Structural payload	kg	15000
Passengers	-	150
Cruise Mach	-	0.6
Cruise altitude	m	7620
Take-off distance	m	2200
Approach speed	m/s	71

As the developed aero-propulsive model cannot cope with varying wing thicknesses or kinks in the wing planform, the designs have been slightly modified such that the aero-propulsive model could be used. The kink has been removed and in terms of the wing airfoil, the ATR72 Smoothed Airfoil [1] with 18% thickness has been used. An isometric view

[1] http://airfoiltools.com/airfoil/details?airfoil=atr72sm-il [Accessed: 08-07-2020]

of the resulting baseline design for $\varphi = 0.2$ in conventional configuration is shown in Figure 5.5. It is important to mention that these modifications have a substantial influence on the resulting design in terms of performance. It leads to an increase of 5% in MTOM and a reduced PREE of 12%. This is mainly caused by the constant thickness of the airfoil along the span, resulting in a relative high thickness at the tip. Nevertheless, this does not pose an issue for relative comparison between designs although it could influence the effect of the tip-mounted propeller.

The updated base-line designs are obtained by design convergence performed by the Aircraft Design initiator which is treated in more detail in Section 6.1.

Figure 5.5: Isometric view of baseline design with $\varphi = 0.2$.

5.2.2. DESIGN VARIABLES

The sizing and positioning procedures have been used to modify the baseline designs in a number of ways. The designs have been modified in terms of power ratio, main propeller spanwise location and disk area ratio. The definition of the design variables is given in Equation 5.2. The power ratio, φ, is the power of the secondary shaft divided by the total shaft power. The propeller location, η, is given as a fraction of the total wing span. The disk area ratio, DAR is defined as the area of the main propeller divided by the total disk area. The total disk area is kept constant throughout this sensitivity analysis. It seems reasonable that the propellers will need to change in size when the power split is modified. It is expected that a higher shaft power ratio will require a larger propeller at the tip and the main propeller can be down-sized if the total disk area needs to be maintained. For this reason, an additional design variation has been added where the disk area ratio is coupled to the shaft power ratio. An overview of the design modifications implemented and their bounds is shown in Table 5.2 for the different baseline designs.

$$\eta = y/b \qquad \varphi = \frac{P_2}{P_1 + P_2} \qquad DAR = \frac{A_{D1}}{A_{D1} + A_{D2}} \tag{5.2}$$

The designs cannot be varied unlimited as some combinations of parameters will result in an unfeasible design. The modified design is rejected if the main propeller is found to cut through the fuselage for instance. It is also rejected if the required power to drive the propeller is more than the available power or if the propeller tip Mach number is above 0.9. The generation of modified designs are thus limited by physical phenomena.

The propulsive design affects the load on the structure by its aero-propulsive load and

Table 5.2: Design modifications for the wing weight sensitivity study.

Parameter	Range	Baseline		
		$\varphi = 0.2$	$\varphi = 0.1$	$\varphi = 0.3$
Shaft power ratio, φ	0.1-0.35	0.1	0.2	0.3
Main propeller location, η	0.25-0.3	0.25	0.25	0.25
Disk area ratio, A_R	0.764-0.983	0.873	0.873	0.873
Shaft power ratio & Disk area ratio, φ, A_R	0.1-0.35(φ)	-	-	-

by a modified discrete load due to a change in the propulsion system mass. In order to examine the contribution of both, the sensitivity study is performed for an aerodynamically clean wing and full-interaction propeller-wing system. The first approach isolates the effect of the mass of the engines and is depicted in Figure 5.6, whereas the second approach includes both the aero-propulsive and discrete loads as shown in Figure 5.7.

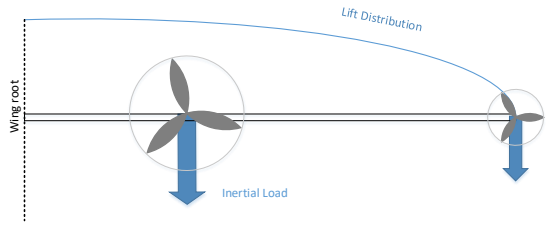

Figure 5.6: Loading for clean aerodynamic wing assumption for structural wing weight analysis.

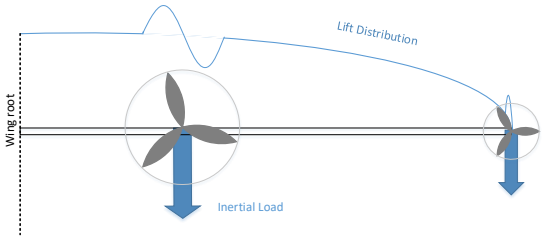

Figure 5.7: Loading for aerodynamic full-interaction for structural wing weight analysis.

5.3. RESULTS

On wing-propulsion level, over 200 design points were evaluated, divided over 3 baseline designs with initial shaft power ratios of 0.1, 0.2 and 0.3. All three baseline studies showed similar results, confirming the sensitivity of the analysis. This chapter discusses the results for the baseline design with φ=0.2. The results of the two other baseline design are presented in Appendix B. It should once more be noted that this approach purely studies the effect of a change in propulsion system design on the wing weight. The wing design is unmodified and there is no feedback to the higher-level aircraft design in terms of mass or (aerodynamic) performance.

The wing weight of all modified designs has been calculated. This has been done with and without the aero-propulsive effects in order to observe the contribution of the discrete and aerodynamic load separately. For the analysis without the aero-propulsive effects, a clean wing is used for the aerodynamic load analysis. Whereas for the analysis with aero-propulsive effects included, a two way (full) interaction model is used as discussed in Chapter 3.

An overview of the results for the variations of the baseline design with a shaft power ratio of 0.2 are presented in Figure 5.8. The marker shades indicate an increase or decrease of the varied parameter compared to the reference value. Results are shown for aero-

propulsive effects included and excluded in order to observe the contribution of the discrete and aerodynamic load separately. It can immediately be seen that the aero-propulsive effects have a minor influence on the wing weight. The maximum difference between the two methods is approximately 1%. This suggests that the aerodynamic load on a clean wing can be used in the structural analysis to get a good first approximation. This is a commonly taken approach and is for instance used by Elham et al. [31]. To study the effects in more detail, Figure 5.9 shows the effect of the varied parameters on the wing mass in separate figures. These figures are discussed in the following subsections, examining the effect of the design parameters individually. Results are shown for aero-propulsive effects included and excluded in order to observe the contribution of the discrete and aerodynamic load separately.

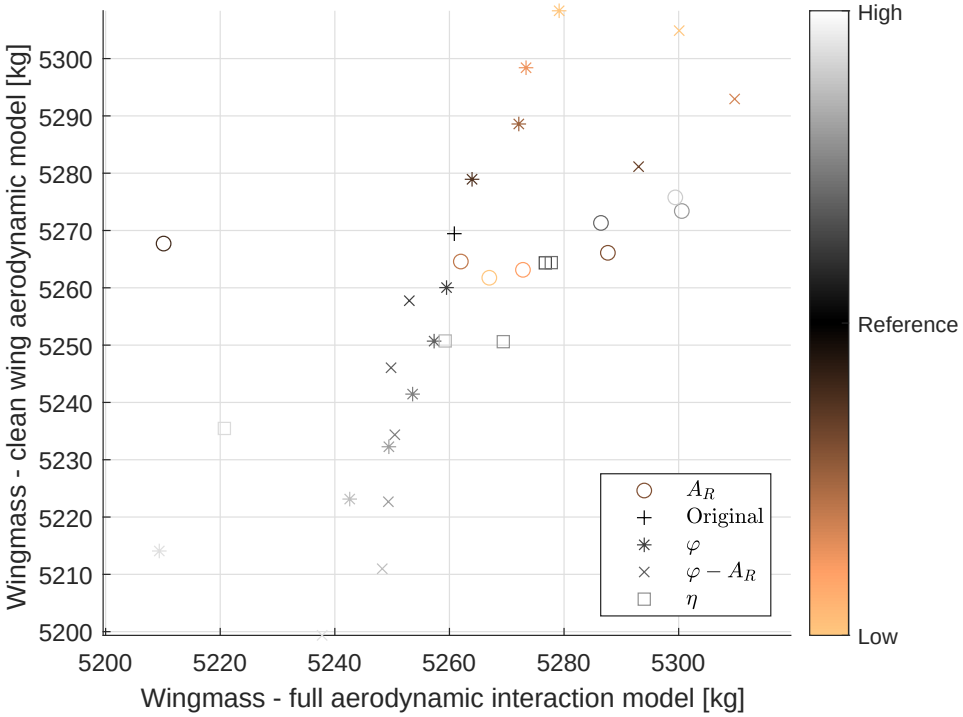

Figure 5.8: Overview of wing mass for variable designs based on φ=0.2. Color shades indicate reduction or increase of modified parameter.

5.3.1. EFFECT OF SHAFT POWER RATIO

Figure 5.9a shows the effect of the shaft power ratio. The full- and clean- aerodynamic method generally show the same trend; a higher shaft power ratio reduces the structural wing weight. With an aerodynamic clean wing, the effect of the shaft power ratio is quite linear and the behaviour shown is expected and can essentially be explained the bending relief phenomena. A higher shaft power ratio means more power is distributed to the tip engine, increasing its mass which attenuates the wing bending relief. The aero-propulsive effects, however, seem to reduce the effect of propulsion system centre of gravity shift. The predicted reduction (or addition) of wing weight compared to the baseline design is less when aero-propulsive effects are included. For shaft power ratios below the reference value ($\varphi = 0.2$), the gain in wing mass is less significant compared to the clean-aerodynamic results. Similarly, for shaft power ratios above the reference value, the decrease in wing mass

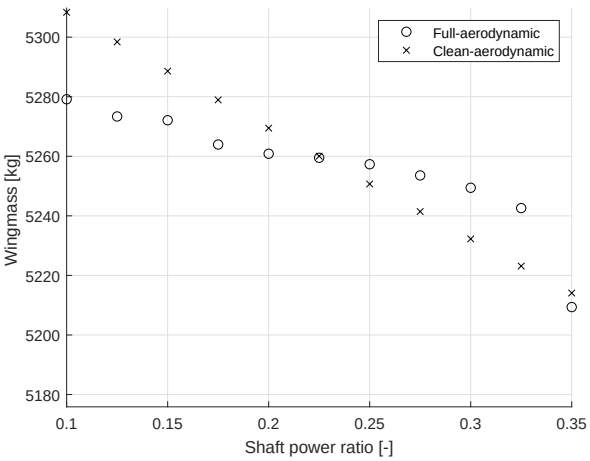

(a) Effect of shaft power ratio.

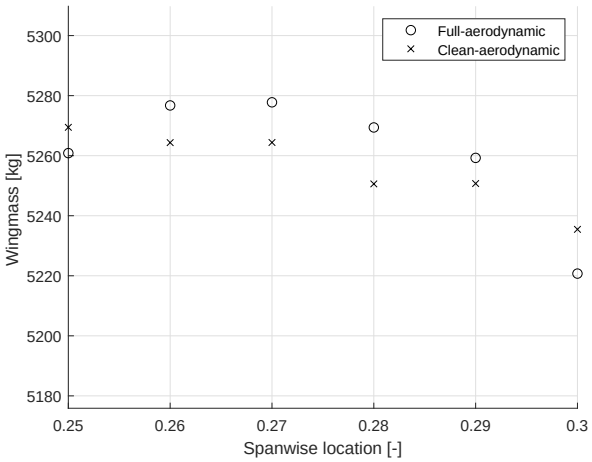

(b) Effect of inboard propeller location.

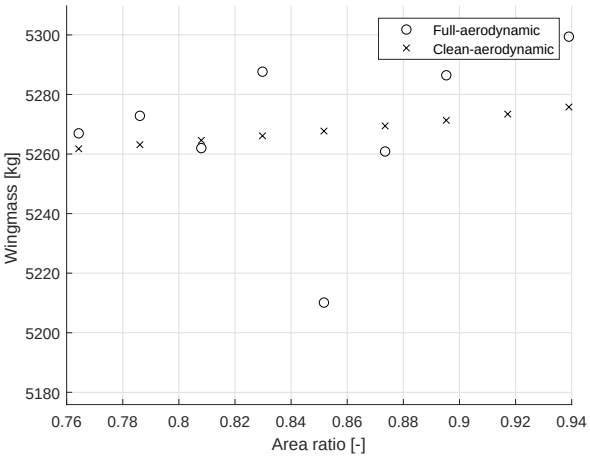

(c) Effect of disk area ratio.

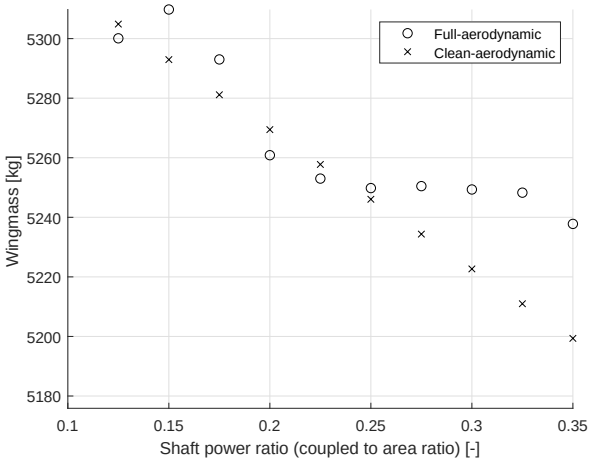

(d) Effect of shaft power ratios with constant individually disk loading.

Figure 5.9: Results of sensitivity study on baseline aircraft with $\varphi = 0.2$

is also less significant. This could reinforce the observation made by Hoogreef et al. [44] about the potential optimum shaft power ratio. It can be argued that the aero-propulsive interference weakens the effects introduced by the shaft power variation in terms of propulsive mass distribution. In short, a higher shaft power ratio results in a beneficial distribution of the propulsive masses but this advantage is weakened by the aero-propulsive effects. A reason for this could be again bending relief; if more power is distributed to the tip propeller, the lift will be shifted outward which will in turn increases the root bending moment.

5.3.2. EFFECT OF MAIN PROPELLER LOCATION

The effect of varying the spanwise location of the main propulsor can be seen in Figure 5.9b. Note that a spanwise location fraction below 0.25 has not been investigated as this would result in an inboard propeller cutting through the fuselage. When only looking at the effect of the weight distribution of the propulsion system, so the clean-aerodynamic results, it is again implied that shifting the centre of gravity of the propulsion system outward will help to decrease the wing mass due to the bending relief effect. This was also observed by Habermann [46]. Shifting the inboard propeller outboard will help to decrease

the wing weight, also when aero-propulsive effects are included. The exact benefit however is expected to be depended on the wing design and taper ratio in particular. When interpreting the results obtained including the aero-propulsive effects, it is important to recall that the relative distance between the inboard propeller and the local leading edge was kept constant. If for a tapered wing the propeller is shifted outboard, this will mean that less wing area is immersed in the propeller slipstream which could influence the aero-propulsive interaction effects.

5.3.3. EFFECT OF COUPLED SHAFT POWER RATIO

The area ratio has been varied independently and coupled to the shaft power ratio. The respective results are shown in Figure 5.9c and Figure 5.9d. For both, the clean-aerodynamic results show expected behaviour which can again be linked to the bending moment alleviation. A higher area ratio equals a larger inboard propeller and a reduced diameter for the wingtip-mounted propeller. This means the tip-mounted propeller will decrease in mass and consequently reduce the bending moment relief causing a heavier wing structure. For the coupled case, a higher shaft power ratio will also result in more disk area for the wingtip-mounted propeller. This means that there will be even more mass on the wingtip and consequently more bending moment relief. When incorporating the aero-propulsive effects, the variation of area ratio suggests a local optimum exists for which the loading distribution causes the wing mass to decrease. This can be seen in Figure 5.9c at an area ratio of approximately 0.85. For the coupled case, the aero-propulsive effects seem to exaggerate the gain in wing mass for low shaft power ratios (φ<0.2). For higher shaft power ratios however, the reduction in wing mass seems to be damped by the aerodynamic effects. In general, a higher shaft power ratio coupled to disk area can be regarded to have a positive effect on the wing weight.

5.3.4. EFFECT ON PROPULSION SYSTEM MASS

Previous results suggest that a wing weight reduction can be obtained by increasing the shaft power ratio. But it should not be disregarded that a change in propulsive design will also influence the weight of the propulsive system itself. In fact, an increase in shaft power ratio significantly influences the weight of the propulsion system in a negative manner as can be seen in Figure 5.10. The increase in propulsion system mass is much more than the respective decrease in wing mass. The mass penalty introduced by the turbo-electric propulsion system cannot be compensated by the reduction in wing weight. Within a design convergence it is expected that with increasing shaft power ratio, the wing mass will eventually increase due a higher weight of the complete wing-propulsive system. Due to the snowball effect in a design convergence study, it is expected that the trend for combined propulsion system - wing mass will even be steeper than projected in Figure 5.11.

5.4. DISCUSSION

This wing weight study investigated the effects of the aero-propulsive loading on the wing weight. Combining the previously presented results a number of remarks can be made. In general, it can be said that clean wing aerodynamics can be used as a good first estimate for the loading distribution used for the wing weight estimation. Not including aero-propulsive effects suggests that a design modification that causes the centre of gravity of

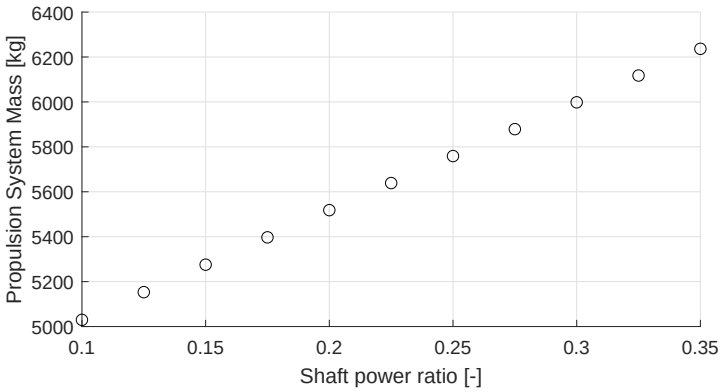

Figure 5.10: Effect of shaft power ratio on propulsion system mass.

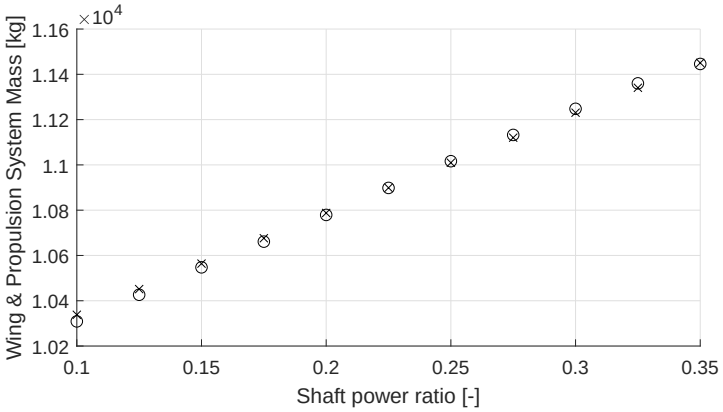

Figure 5.11: Effect of shaft power ratio on wing-propulsion system mass combined based on $\varphi = 0.2$.

the propulsion system to shift outward, will have a positive effect on the wing mass. This was also concluded by Habermann [46]. However, the effect of a design modification of the propulsive system will influence the wing weight by both the discrete and aerodynamic load. If the aero-propulsive effects are included, this observation does not hold anymore for all cases. When the effects of a modification need to be closely studied, or for instance optimised, it is important to include an aero-propulsive model. This is especially relevant because the aero-propulsive interaction has an ambiguous effect on the wing weight. In some cases it weakens the effect of the discrete load while at other times it exaggerates the effect.

When assuming a constant wing design, MTOM,shaft power, and aerodynamic performance it may seem that a reduction of wing mass can be obtained by modifying the PTE propulsive design. But this effect is out-ruled by the increase in propulsion system mass. The mass penalty introduced by the turbo-electric propulsion system modification cannot be compensated by the reduction in wing weight. Within a design convergence it is expected that with increasing shaft power ratio, the wing mass will eventually increase due a higher weight of the complete wing-propulsive system. Due to the snowball effect in a design convergence study, it is expected that the net effect of the wing-propulsion system mass will be more exaggerate than shown is this study. The results presented here might thus be on the conservative side. In other words, if this study predicts an increase of 250 kg in wing-propulsion system mass, it is likely that within a design convergence the actual mass gain will exceed this value. Nevertheless, it is important to keep in mind that the wing

level study focused on the aero-propulsive loading effects on the wing structural weight. It did not consider aero-propulsive benefits throughout the flight mission that could increase the aerodynamic performance of the system which could have a major effect on the overall performance of the design. For this purpose, an aircraft level study is performed that considers both aero-propulsive and aero-structural effects.

6

AIRCRAFT LEVEL SENSITIVITY STUDY

The potential of the wingtip-mounted propeller configuration on aircraft level is evaluated on aircraft level considering the aerodynamic, propulsive and structural effects of such a configuration. To do this, the aero-propulsive and aero-structural modules have been included within an aircraft design convergence study. This study is performed with the *Aircraft Design Initiator*. The integration of the aero-propulsive module within this tool is treated in Section 6.1. The different design variations studied are presented in Section 6.2. Section 6.3 presents the results. The general conclusions and main observations are discussed in Section 6.4.

6.1. AIRCRAFT DESIGN CONVERGENCE INTEGRATION

The design convergence study is performed using the Aircraft Design Initiator (ADI) [44] [72]. This software tool has been developed in-house by the TU Delft. It creates a conceptual aircraft design based on a set of top-level requirements. A design convergence is performed that steps through a number of disciplinary analyses. A detailed description on the foundations of the ADI can be found in [45]. The tool is continuously being extended with new capabilities. It can be used for conventional and less conventional aircraft configurations. With the work of de Vries [28] on preliminary sizing methods for DHEP aircraft integrated, it also became possible to syntheses hybrid configurations. The process flow of the Initiator for a hybrid configuration is presented in Figure 6.1.

The Initiator synthesises an aircraft design based on a list of top-level requirements and the desired configuration. The Initiator starts by collecting data of reference designs from the database. Next, a Class I weight estimation is preformed including a mission analysis followed by a Class II weight estimation. Once convergence of the estimated weights by the two classes has been reached, an aerodynamic analysis is performed and a Class II.V weight estimation is initiated. Here, a FEM is used to estimate the structural wing weight as discussed in Section 4.2. This process continues until a convergence of the aircraft weight has been reached. Originally, the wing structural analysis uses AVL to obtain the aerodynamic loading distribution, assuming a clean aerodynamic wing. This means that the inertial loads of the engines are accounted for but the aero-propulsive effects are neglected.

The baseline version (*revision 2380*) of the Initiator used in this research uses a surrogate model for the aero-propulsive interaction [44]. This surrogate model uses the propeller-wing geometry as input. It is important to note that a number of assumptions were used in

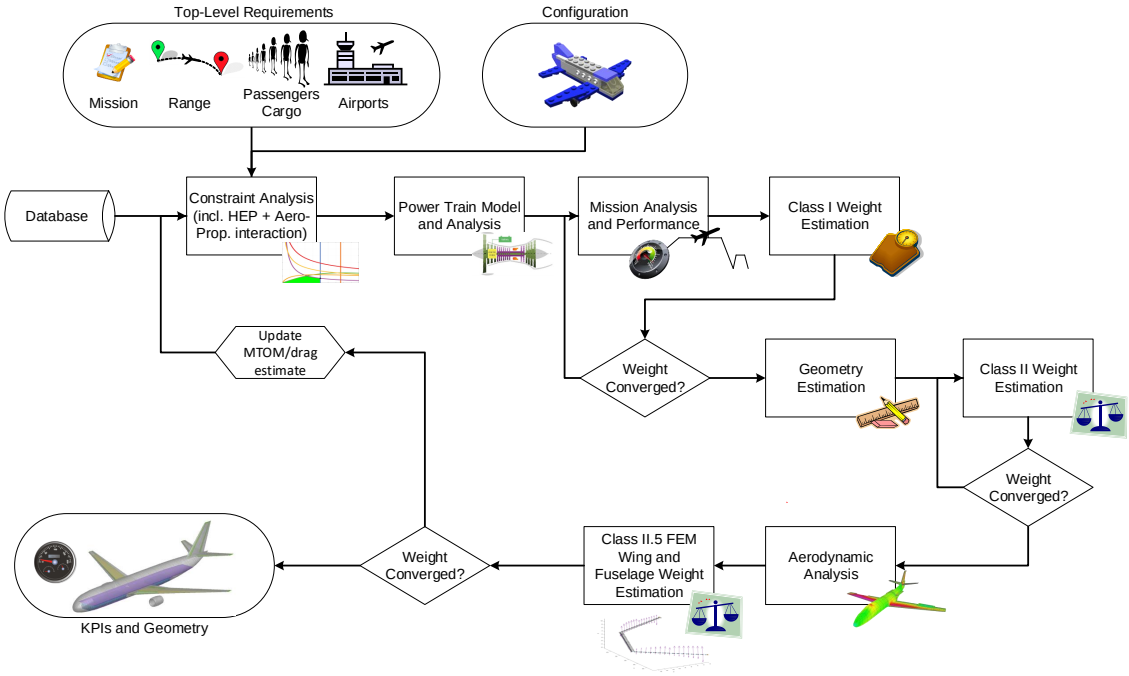

Figure 6.1: Schematic representation of Initiator process flow for DHEP aircraft [44].

the generation of this surrogate model. The wing was assumed to have no taper or sweep and a constant thickness-to-chord ratio of 12%. Moreover, the propellers were placed at one propeller-radius upstream of the wing leading edge and no vertical offset or propeller incidence was present. The parameter used in the surrogate model are presented in Table 6.1. The model is used to quantify the effect of the aero-propulsive interaction on the total lift and drag of the wing. This is applied in the generation of the loading diagrams and the mission analysis within the Class I weight estimation. For the Class II.V wing weight estimation, a clean aerodynamic wing is assumed and the aero-propulsive effects are not taken into account.

Table 6.1: Parameters used in the surrogate model and their bounds.

Parameter	Lower bound	Upper bound
Aspect ratio, AR	8	16
Span fraction occupied by 1 main propeller	0	0.2
Thrust coefficient, T_c	0	1
Advance ratio, J	0.25	2.5
Distance between most outboard DP and wingtip	0	0.5
Clean lift coefficient, CL	-0.075	2.89

It was shown in Chapter 5 that a clean wing assumption for the wing weight estimation can be used as a good first approximation. However, it was also shown that the aero-propulsive effects do influence the wing weight to a certain extent. This effect is expected to be more pronounced in a design convergence loop. This is why the initiator has been adapted to also include the aero-propulsive effects in the wing weight estimation. This

means that instead of the aerodynamic analysis that is performed before the wing weight estimation, an aero-propulsive analysis needs to performed. The aero-propulsive module includes the analysis as presented in Chapter 3 and evaluates the aerodynamics at a 2.5g load.

In addition, the surrogate model used in the Class I weight estimation has been partly replaced by the aero-propulsive module. Because of the limitations and assumptions of the surrogate model discussed previously, the application of the aero-propulsive model would enable more accurate predictions of the aero-propulsive effects. But as the module is time-consuming, it has only been implemented for the cruise phase of the mission analyses. This is the phase that is expected to profit most from the aero-propulsive interaction effects. To estimate the contribution of the aero-propulsive effects on the wing aerodynamics, two analyses for the cruise condition are to be performed. A clean-wing aerodynamic analysis and a full interaction analysis. The difference in lift and drag coefficient between those two cases quantifies the effect of the propulsion system on the aerodynamics. These values are stored and used within the mission analysis module as part of the Class I weight estimation. It was deliberately chosen to run the cruise aero-propulsive analyses in the outer loop of the design convergence. This is because here the 'current' geometry of design is known. Moreover, it will prevent the aero-propulsive module to run in the early stages of the design loop. This is important since the full aero-propulsive analysis is time consuming.

So in short, the Initiator is modified to include the aerodynamic effects of the propulsion system in the estimation of the structural wing weight. For this the aero-structural model discussed in Chapter 4 is used. Moreover, the surrogate model present for the aero-propulsive effects that is used within the Class I weight estimation, is partly replaced by the prediction of the aero-propulsive model presented in Chapter 3. The updated initiator flow process is shown in Figure 6.2. The modifications are shown in bold.

6.2. CASE STUDY

Chapter 5 showed that, when assuming a constant wing design, MTOM, aerodynamic performance and shaft power, it may seem that a reduction of wing mass can be obtained by modifying the PTE propulsive design in terms of shaft power ratio. But this effect is outruled by the increase in the corresponding propulsion system mass. To affirm these observations and study the effect of wingtip-mounted propulsion on aircraft level, a number of design convergence studied were performed. The most important difference with the wing level study is the inclusion of aero-propulsive benefits throughout the different flight phases and the feedback loops present for (aircraft) weight and performance.

As a reference, the wingtip-mounted configurations presented by Hoogreef et all. [44] are used. The configurations use a partial turbo-electric architecture and have a constant shaft power ratio over all mission phases. The top-level requirements of the configurations are the same as presented for the wing weight study and were listed before in Table 5.1. Again, a high technology level is assumed. Similar to the wing weight study, the designs have slightly been modified such that the aero-propulsive module can cope with the generated geometry. The kink has been removed and a constant thickness-to-chord ratio of 18% is used with the ATR72Smoothed airfoil.

The shaft power ratio of the PTE has been varied from 10% to 30%. To see if the potential of wingtip-mounted propulsion is dependent on cruise speed, the study has also been performed for the same top-level requirements but at a slightly lower Mach number of 0.5.

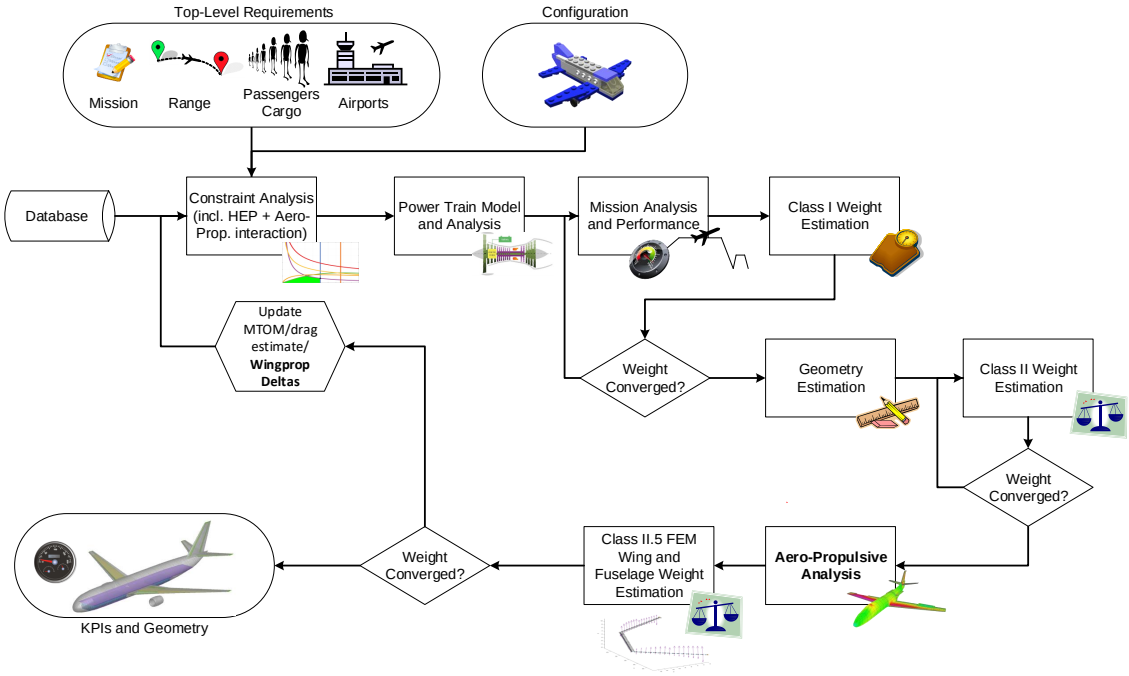

Figure 6.2: Schematic representation of Initiator process flow for DHEP aircraft including the aero-propulsive module. Adapted from [44].

Throughout the study, the propeller diameters were predefined and normalised by the wing span. The inboard propeller was initiated to cover 30% span and the wingtip-mounted propeller 10%. However, it is expected that the effectiveness of the wingtip-mounted propeller as vortex attenuating device is dependent on its size. In addition, Chapter 5 showed that the area distribution between the two propellers could have an effect on the wing weight. To investigate the sensitivity of the overall aircraft design to the wingtip-mounted propeller size, the span fraction ratio of this propeller has been varied as well. Designs are initiated with wingtip propeller span fractions occupied between ΔY=0.1 and 0.3. An overview of the different design modifications studied for the PTE wingtip-mounted propeller configuration on aircraft level are presented in Table 6.2. The span fraction occupied by the wingtip-mounted propellers, ΔY, translates into the propeller diameter as shown in Equation 6.1[32]. N is the number of distributed propulsors, which is equal to 2 for the wingtip-mounted configuration. Extra lateral propulsor clearance is introduced by Δy=0.05.

$$D_P = \frac{\Delta Y}{N\left(1+\Delta y\right)} b \tag{6.1}$$

In addition, a conventional reference design has been analysed. This reference design has the same top-level requirements but has a conventional power train configuration. This means that only a primary power train is present and no DP is used. This configuration can be used to identify the potential benefits of the PTE wingtip-mounted configuration. The reference design is similar to the wing mounted propeller design presented by Hoogreef et all. [44] and Vos and Hoogreef [73] except for the aforementioned modifications. Furthermore, two other variations of the wingtip-mounted propeller configuring

Table 6.2: Different cases studied for PTE wingtip-mounted propeller configuration on aircrfat level.

Case	TLRs	M_{cr}	Shaft power ratio	ΔY
I	See *Table 5.1*	0.6	0.1-0.3	0.1
II	See *Table 5.1*	0.5	0.1-0.3	0.1
III	See *Table 5.1*	0.6	0.2	0.1-0.3
IV	See *Table 5.1*	0.6	0.1	0.1-0.3

have been synthesised using the Initiator. First of all, a conventional twin-engine turboprop configuration but with its engines placed at the wingtip. The second configuration is a conventional turboprop featuring four engines of which two are situated at the wingtip. A summary of the additional configuration initiated are presented in Table 6.3.

Table 6.3: Summary of additional configurations studied compared to reference, APS included.

Parameter	Configuration		
	Reference	Tip-only	Conventional WTMP
			
Power train	Conventional	Conventional	Conventional
Engines	2x turboprop	2x turboprop	4x turboprop
Engine location(s)	0.25	1.0	0.25, 0.1

6.3. RESULTS

As opposed to the study on wing level, the aircraft level sensitivity study does incorporate a feedback loop of the aero-propulsive and aero-structural effects to the overall system as was shown in Figure 6.2. This section discusses the results of the different configurations and variations studied. It starts with addressing the effect of the modifications made to the Initiator.

6.3.1. EFFECT OF AERO-PROPULSIVE MODEL INCLUSION

Originally the design synthesis tool used, the Initiator, did not include aero-propulsive effects in the structural wing weight estimation. Furthermore, the aero-propulsive effects in the different flight phases were predicted by a simplified surrogate model. As discussed in Section 6.1, the aero-propulsive and aero-structural models discussed in Chapter 3 and 4 have been integrated within the design convergence loop. The aero-propulsive model is used to get an approximation for the aerodynamic effects of the propulsion system in cruise, and to get the loading distribution at the critical flight condition of 2.5g. The aero-structural model uses this obtained loading to estimates the structural wing weight in the Class II.V weight estimation. To see the effect of the aero-propulsive and aero-structural models (APS) included within the design convergence, the designs within case study I were evaluated using the original and modified aircraft design initiator.

Overall, the results obtained from the different studies including and excluding the APS model, show similar results. The difference of predicted wing mass is 0.9% at most. For the MTOM this difference is even less (0.4%). The inclusion of the APS effects has a positive influence on the synthesised design in terms of weight. Table 6.4 and 6.5 show the different MTOM and wing mass values obtained for the analysis with and without the APS model with varying shaft power ratio. In all cases, the inclusion of the APS model predicts a decrease in wing weight compared to the original Initiator version. Although this reduction seems insignificant, it translates into a greater overall reduction and can be noticed in the MTOM of the designs. As an example, a reduction of 50 kg leads to a reduction of 140 kg on MTOM. This suggests that the presented wing weight reductions in Section 5.3 might have a more significantly impact on aircraft level than sketched before.

Table 6.4: Effect of shaft power ratio on aircraft mass, APS excluded.

	Shaft power ratio			
Parameter	0.0 (Ref)	0.1	0.2	0.3
MTOM [tons]	55.86	57.70	59.64	61.95
Wing mass [tons]	4.84	5.02	5.21	5.42

Table 6.5: Effect of shaft power ratio on aircraft mass, APS included.

	Shaft power ratio			
Parameter	0.0 (Ref)	0.1	0.2	0.3
MTOM [tons]	55.72	57.55	59.32	61.65
Wing mass [tons]	4.79	4.99	5.16	5.39

So with the inclusion of the APS model, a slightly lighter design is predicted. The weight of the designs is studied in more detail by considering the weight breakdown which is presented in Figure 6.3 and 6.4. It can be seen that the main weight components deliver approximately the same contribution to the total aircraft weight. A slight increase in the percentage made up of payload is seen, which is straightforwardly explained by the fact that the total weight decreases while the payload requirement is unmodified.

Additionally, Table 6.6 shows the sensitivity of the MTOM to a change in shaft power ratio. It can be seen that either with or without the APS model included in the Initiator, the MTOM shows a similar response to an increase in shaft power ratio. The exact sensitivity and trends observed as a function of shaft power ratio in treated in the next subsection.

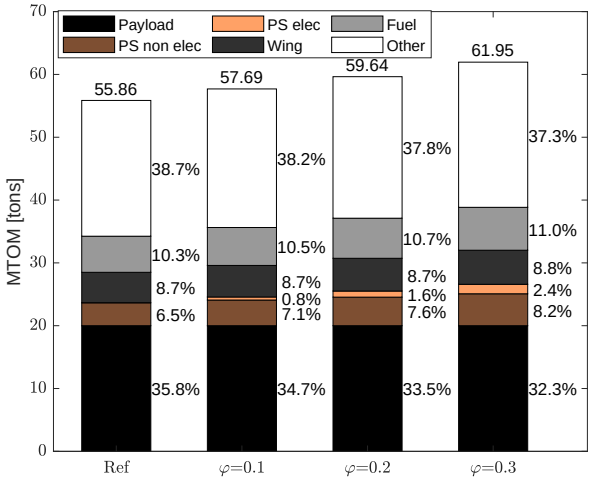

Figure 6.3: Effect of shaft power ratio on aircraft mass breakdown, APS excluded.

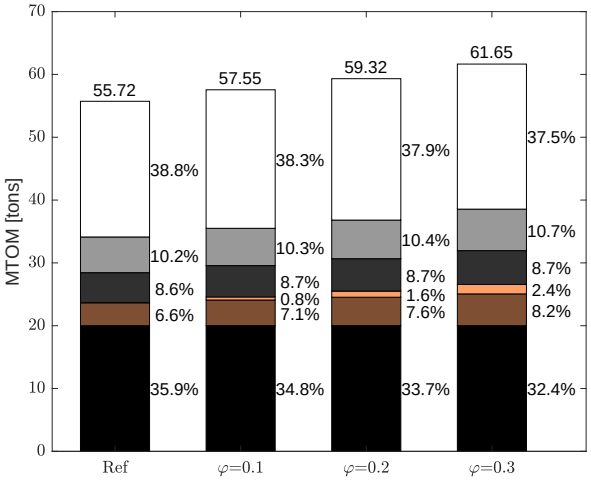

Figure 6.4: Effect of shaft power ratio on aircraft mass breakdown, APS included.

Table 6.6: MTOM increase compared to reference design

Shaft power ratio	MTOM increase compared to reference design, M=0.6.	
	APS excluded	APS included
$\varphi = 0.1$	+3.3%	+3.4%
$\varphi = 0.2$	+6.8%	+6.5%
$\varphi = 0.3$	+10.9%	+10.6%

6.3.2. EFFECT OF SHAFT POWER RATIO

In Figure 6.4 and Table 6.5, already a preview was presented that showed the effect of the shaft power ratio on the MTOM and wing weight of the aircraft. It is clear that both increase significantly with increasing shaft power ratio. The overall weight increase is initiated by the increase in propulsion system weight due to a higher shaft power ratio. Figure 6.4 clearly shows that the relative contribution of the propulsion system to the total weight of the aircraft increases if more power is distributed to the tip.

The weight increase of the propulsion system kick-starts an increase in mass of the complete aircraft. At first, the wing weight may seem to benefit from a higher shaft power ratio. Yet, the increase in propulsion system weight is much more significant, resulting in a weight increase of the complete system as was also found by Habermann [46]. This, in turn, requires a larger wing and propulsion system to deliver the required lift and power. This again increases the mass further and is a typical snowball effect in aircraft design. Indeed as predicted in Chapter 5, the effect of the shaft power ratio on the propulsion system is more pronounced for the aircraft level study. This becomes immediately clear from Figure 6.5.

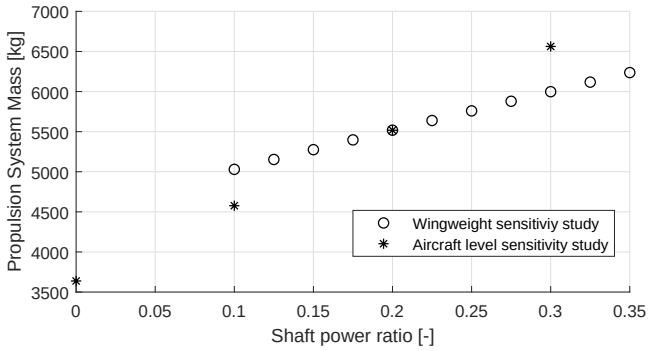

Figure 6.5: Propulsion system mass for different shaft power ratios. Wing weight sensitivity results based on φ=0.2 compared to aircraft level results (case study I).

Besides the weight, other parameters can be used to describe the performance of the different designs. A number of these are listed in Table 6.7. The data is collected from the mission analyses performed in the Class I weight estimation for the cruise phase. The ΔC_L and ΔC_{D_i} indicate the effect of the propulsion on the lift and drag coefficient of the wing compared to a clean configuration as predicted by the aero-propulsive analysis. It can be seen that the induced drag reduces with increasing shaft power ratio at first. At a shaft power ratio of 0.2, both the increase in lift coefficient and reduction in induced drag coefficient are greater than for the conventional reference aircraft. When the shaft power ratio is further increased to 0.3, the lift enhancement and drag reduction both stagnate. This

could indicate the location of a local minimum in terms of optimal shaft power ratio for maximum aero-propulsive benefits. This was also suggested by Hoogreef et al. [44]. The propulsive efficiencies are in the expected range. With increasing shaft power ratio, the inboard propeller efficiency slightly increases while the efficiency of the wingtip-mounted propeller slightly decreases. This is expected when considering the propulsive efficiency formulation as introduced in Chapter 2. Consequently, the weighted average between the two propulsion chains for their respective power share, η_p, decreases. Moreover, an increase of shaft power ratio has a detrimental effect on the wing aerodynamic efficiency and Payload Range Energy Efficiency (PREE) which is defined as the payload weight times the harmonic range of the aircraft divided by the total energy consumed during the nominal mission and is shown in Equation 6.2 [28]. This decrease in performance is caused by the mass increase initiated by a heavier propulsive design which cannot be overcome by the aero-propulsive benefits.

$$PREE = \frac{W_{PL}R}{E_{miss}} \tag{6.2}$$

Table 6.7: Effect of shaft power ratio on different performance parameters at cruise conditions (M=0.6), APS included. One lift count = 0.01 and one drag count = 0.0001.

		Shaft power ratio			
Parameter	Unit	0.0 (Ref)	0.1	0.2	0.3
Lift over drag	-	16.8	16.7	16.9	16.7
ΔC_L	counts	1.4	1.4	2.0	1.8
ΔC_{D_i}	counts	-5.8	-8.9	-10.6	-10.8
η_{ib}	%	85.7	85.9	86.0	86.3
η_{wt}	%	-	86.3	84.8	83.3
η_p	%	85.7	86.3	85.05	84.2
PREE	-	1.65	1.58	1.52	1.42
MTOM	tons	55.7	57.5	59.3	61.6
Wing mass	tons	4.8	5.0	5.2	5.4
Fuel mass	tons	5.7	5.9	6.1	6.6
Span	m	33.4	33.8	34.4	35.1
D_{ib}	m	4.18	4.23	4.29	4.37
D_{wt}	m	-	1.61	1.63	1.67

For the different designs in case study I, the isolated wing has a cruise drag coefficient of about 0.33. With the aero-propulsive effects, this induced drag can be reduced by approximately 2%-3% for the presented designs. This value increases with shaft power ratio so the wingtip-mounted propellers seems to deliver its function as tip vortex attenuating device. Nevertheless, these values are far from the indicated aerodynamic benefits of the application of wingtip-mounted propellers. This could indicate that the chosen design conditions, TLRs or configuration are far from optimal to accomplish the believed aerodynamic benefits of wingtip-mounted propellers. It should also be mentioned once more that the propeller designs could be far from optimal. Either in terms of geometry, or the way they are integrated with the wing. Also the used flight conditions and TLRs might not be the best fit with the wingtip-mounted propeller concept. All of these variables could influence the

potential of wingtip-mounted propeller application that is sketched.

6.3.3. EFFECT OF CRUISE MACH NUMBER

The effect of a lower cruising Mach number on the synthesised design has been investigated. In particular the same study as discussed in Section 6.3.2 has been performed but now for a Mach number of 0.5. All the TLRs remained the same and only the Mach number was changed. Again, the designs have been synthesised for different shaft power ratios by the Initiator. Their converged results have been compared to the previously obtained results for Mach 0.6.

Figure 6.6 shows the mass breakdown of the different designs in case study II with varying shaft power ratios. When this information is compared to Figure 6.4, a number of observations are made. First of all, the decrease of cruise speed leads to lighter designs for all shaft power ratio variations. In general, a mass reduction in the order of 5.6%-7% is obtained. The higher the shaft power ratio, the higher the reduction obtained by the decrease in cruise speed. At the same time, Table 6.8 shows that for the lower cruise Mach number the MTOM seems slightly less sensitive to an increase in shaft power ratio. This could indicate that for a lower cruise Mach number, the effect of the propulsion system mass is less pronounced on aircraft level. From the mass breakdown comparison, it can also be observed that the mass share of the electric propulsion system components is not effected by the lowered cruise speed. Opposing to this, the nonelectric components and wing mass show a small decrease in mass contribution.

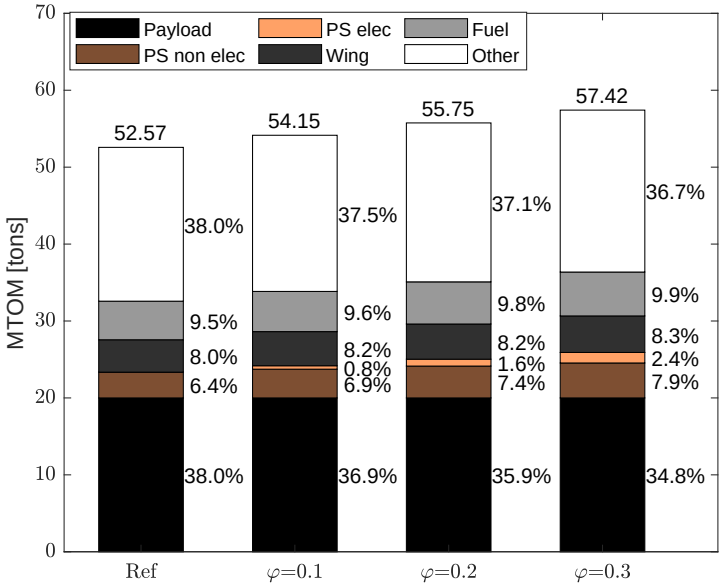

Figure 6.6: Mass breakdown for different shaft power ratios for cruise Mach number of 0.5

In terms of other performance parameters, the value seems to weaken with increasing shaft power ratio just like presented for study case I. The performance parameters are presented in Table 6.9. The aero-propulsive interaction benefits from a lower Mach number as the ΔC_L increases and also the induced drag reduction increases compared to the M=0.6 case. This behaviour was expected due to the higher operating lift coefficient of the system. Willemsen [61] stated that the higher the lift coefficient, the higher the aero-propulsive benefits that can be obtained. Also Hoogreef et al. [44] found that the PREE and

MTOM of a PTE wingtip-mounted propeller configuration both profit from a lower Mach number.

The different designs have an isolated wing cruise drag coefficient of about 0.041. This means that due to the aero-propulsive effects an induced drag reduction of 8%-12% can be obtained. Nevertheless, also a large increase in MTOM is seen of 3%-10%. The combination of the mass gain and aerodynamic benefits results in a decrease of PREE exceeding 11% compared to the conventional reference design.

Table 6.8: Comparison of MTOM increase with respect to reference design for M=0.5 and M=0.6.

	MTOM compared to reference design; φ=0	
Shaft Power Ratio	M=0.5	M=0.6
$\varphi = 0.1$	+3.0%	+3.4%
$\varphi = 0.2$	+6.0%	+6.5%
$\varphi = 0.3$	+9.2%	+10.6%

Table 6.9: Effect of shaft power ratio on different performance parameters at cruise conditions M=0.5, APS included. One lift count = 0.01 and one drag count = 0.0001.

		Shaft power ratio			
Parameter	Unit	0.0 (Ref)	0.1	0.2	0.3
Lift over drag	-	20.75	22.8	22.4	21.9
ΔC_L	counts	2.6	4.5	4.5	4.8
ΔC_{D_i}	counts	-34.3	-59.0	-59.2	-51.0
η_{ib}	%	85.1	85.4	85.6	85.8
η_{wt}	%	-	86.0	84.2	82.6
η_p	%	85.1	85.4	85.3	84.9
PREE	-	1.84	1.80	1.71	1.63
MTOM	tons	52.6	54.1	55.8	57.5
Wing mass	tons	4.2	4.4	4.6	4.7
Fuel mass	tons	5.1	5.2	5.5	5.8
Span	m	32.5	33.0	33.4	33.9
D_{ib}	m	4.00	4.05	4.13	4.15
D_{wt}	m	-	1.57	1.59	1.61

6.3.4. EFFECT OF WINGTIP-MOUNTED PROPELLER SIZE

The importance of the size of the wingtip-mounted propeller has been investigated by varying its dimensions which affects the disk loading. In order to do this, the initiated propeller diameter is varied to cover between 10% and 30% wingspan of a design with 0.2 shaft power ratio. No fixed value is given for the propeller diameter since the wing span and propeller size are interdependent. Figure 6.7 shows that a reduction in MTOM can be obtained by having an increasing wingtip-mounted propeller diameter and consequently a lower disk loading. The results show a generally decreasing trend. Nevertheless, only a minor weight advantage ($\approx$ 1%) can be gained for the specific cases.

Considering the aircraft mass breakdown shown in Figure 6.8, all designs studied show a similar contribution of the different mass components. A slight decreasing contribution of the fuel mass is observed. Combined with the overall decreasing MTOM, a distributed propeller fraction of 0.3 yields a fuel reduction of more than 500 kg for the harmonic mission compared to a span fraction of 0.1, which equals almost 10% of the total fuel mass. In conjunction, an increase in PREE is found with increasing tip-mounted propeller diameter. This is due to the increasing aero-propulsive benefit with increasing propeller size. Both the lift enhancement and induced drag reduction increase. This leads to a increase in lift over drag, which is a measure to indicate the aerodynamic efficiency of the wing. Simultaneously, the propulsive efficiency also benefits from a larger propeller. This was expected based on the propeller efficiency equation from which it is clean that it is more efficient to accelerate a large amount of air by a small proportion compared to a small amount of air by a large proportion. When the propeller size in increased, the disk area increases and the disk loading is decreased. To deliver the approximate same amount of thrust, the propeller will rotate slower. So, it accelerates a larger amount of air by a smaller increment. The increase in propulsive efficiency and wing aerodynamic efficiency result in an increase of the payload range energy efficiency which presents how many joules of useful work, are extracted per joule of energy consumed by the system.

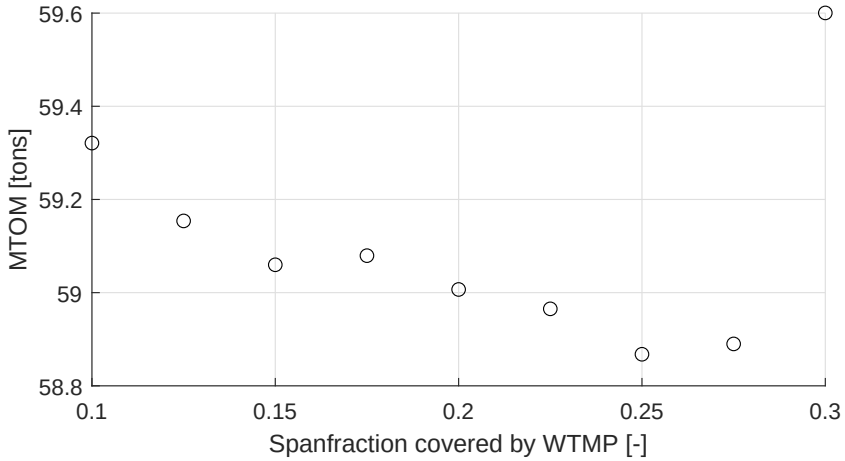

Figure 6.7: MTOM for synthesised designs with φ=0.2 and varying wingtip-mounted propeller size.

Table 6.10 shows promising behaviour of different performance parameters with increasing propeller size. The aerodynamic interaction between the propeller and wing seems to benefit from a larger propeller as both the lift enhancement and induced drag reduction increase. This leads to a increase in lift over drag, which is a measure to indicate the aerodynamic efficiency of the wing. This behaviour was expected based on work by Willemsen [61]. He found that a larger ΔY is beneficial for the drag since a larger ΔY results in a larger wing area with upwash, leading to a decrease in induced drag. The cruise drag coefficient of the isolated wing of the different designs is around 0.033. This means that the induced drag reduction obtained by the aero-propulsive interaction is between 3%-16% for the various designs. Note that a change in sign of the effects could be present around ΔY=0.3. However, this conclusion cannot be drawn based on only two data points and more data points need to be gathered to explain the phenomena. However, an increase of tip-mounted propeller size seems to increase the overall performance of the system. Although an increase in performance is observed with increasing wingtip propeller size, the mass of the aircraft is still

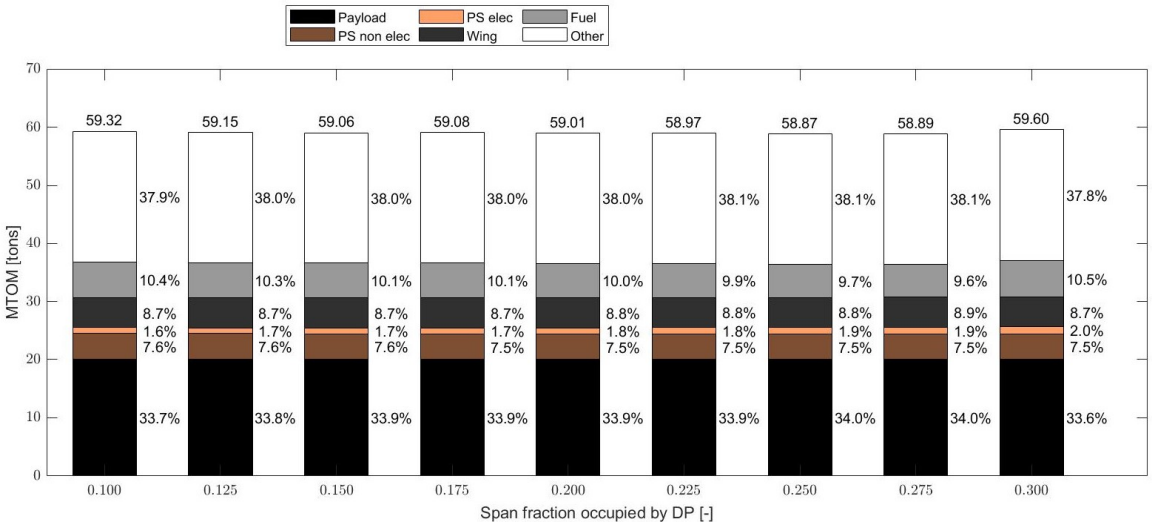

Figure 6.8: Mass breakdown for synthesised designs with φ=0.2 and varying wingtip-mounted propeller size.

significantly higher than the reference design (55.7 tons vs. 58.9 tons). Nevertheless, the design with ΔY=0.275 seems to approach the performance of the conventional reference designin terms of PREE and fuel consumption as highlighted in Table 6.10.

Table 6.10: Effect of propeller size on different performance parameters at cruise conditions for φ=0.2, APS included. One lift count = 0.01 and one drag count = 0.0001.

		WTMP span fraction initiated									
Parameter	Unit	Ref	0.100	0.125	0.150	0.175	0.200	0.250	0.225	0.275	0.3
L/D	-	16.8	16.9	17.1	17.3	17.9	18.0	18.9	18.8	19.7	20.3
ΔC_L	counts	1.4	2.0	2.0	2.4	3.0	3.1	3.8	3.6	4.3	4.9
ΔC_{D_i}	counts	-5.8	-11	-14	-17	-23	-23	-35	-35	-45	-52
η_{ib}	%	85.7	86.1	86.1	86.1	86.1	86.1	86.1	86.1	86.1	86.1
η_{wt}	%	-	84.8	85.9	86.5	86.9	87.1	87.3	87.5	87.5	87.6
η_p	%	85.7	85.8	86.0	86.1	86.2	86.3	86.3	86.3	86.4	86.4
PREE	-	1.65	1.52	1.54	1.56	1.56	1.58	1.61	1.63	1.65	1.5
MTOM	tons	55.7	59.3	59.2	59.1	59.1	59.0	59.0	58.9	58.9	59.6
Wing mass	tons	4.8	5.2	5.2	5.2	5.2	5.2	5.2	5.2	5.2	5.2
Fuel mass	tons	5.7	6.1	6.1	6.0	6.0	5.9	5.8	5.7	5.7	6.2
Span	m	33.4	34.4	34.3	34.3	34.3	34.3	34.3	34.3	34.3	34.3
D_{ib}	m	4.18	4.28	4.27	4.27	4.27	4.27	5.27	4.27	4.27	4.25
D_{wt}	m	-	1.63	2.04	2.45	2.86	3.27	3.67	4.08	4.49	4.92

A larger tip-mounted propeller results in higher aero-propulsive benefits which at a certain point are able to neutralise the mass penalty associated with the PTE configuration. Since this penalty sizes with shaft power ratio, it is expected that the required propeller diameter to cancel out the mass penalty also scales with the shaft power ratio. Or in other words, at a lower shaft power ratio the mass penalty can be compensated with a smaller tip-mounted propeller. To check this hypothesis, case study IV was performed in which the tip-mounted propeller diameter is swept for a design with a shaft power ratio of φ=0.1. The results are summarised in Table 6.11. Similar to case study III, the MTOM slightly decreases

with an increase in propeller diameter. And indeed the reference design performance can already be obtained at a smaller propeller size; ΔY=0.175-0.200 compared to ΔY=0.275 for the higher shaft power case. This is inline with the expectation and confirms that the lower the shaft power ratio, the easier to overcome the PTE weight penalty by use of aero-propulsive interaction benefits. Moreover, case studies III & IV affirm that the tip-mounted propeller size of ΔY=0.1 used in case studies I & II are far from optimal.

Table 6.11: Effect of propeller size on different performance parameters at cruise conditions for φ=0.1, APS included. One lift count = 0.01 and one drag count = 0.0001.

		WTMP span fraction initiated									
Parameter	Unit	Ref	0.100	0.125	0.150	0.175	0.200	0.225	0.250	0.275	0.3
L/D	-	16.8	16.7	17.2	17.3	17.9	18.0	18.3	19.1	19.4	19.7
ΔC_L	counts	1.4	1.4	2.0	2.0	2.7	2.8	3.2	3.8	4.0	4.4
ΔC_{D_i}	counts	-5.8	-8	-15	-15	-21	-23	-28	-37	-39	-43
η_{ib}	%	85.7	85.8	85.8	85.8	85.8	85.8	85.8	85.8	85.8	85.8
η_{wt}	%	-	86.3	86.9	87.2	87.4	87.6	87.7	87.7	87.8	87.8
η_p	%	85.7	85.9	85.9	86.0	86.0	86.0	86.0	86.0	86.1	86.1
PREE	-	1.65	1.57	1.59	1.61	1.63	1.67	1.68	1.69	1.73	1.76
MTOM	tons	55.7	57.6	57.5	57.5	57.4	57.3	57.3	57.2	57.2	57.0
Wing mass	tons	4.8	5.0	5.0	5.0	5.0	5.0	5.0	5.0	5.0	5.0
Fuel mass	tons	5.7	5.9	5.9	5.8	5.7	5.6	5.6	5.5	5.4	5.3
Span	m	33.4	33.8	33.8	33.8	33.8	33.8	33.8	33.8	33.8	33.8
D_{ib}	m	4.18	4.23	4.22	4.22	4.22	4.21	4.21	4.21	4.20	4.19
D_{wt}	m	-	1.61	2.01	2.40	2.82	3.22	3.63	4.03	4.43	4.82

6.3.5. OTHER CONFIGURATIONS

There are also other ways of achieving an aircraft configuration featuring a wingtip-mounted propeller. Previously presented study cases used a PTE configuration with two power trains. However, it is also possible to stick to a conventional powertrain layout. In such a case, a four-engined turboprop aircraft could be used for instance. Alternatively, a twin-engined turboprop could have its engines placed at the tip. These two options of a "conventional" configuration that feature a propeller as a wingtip-vortex attenuating device are synthesised in the same manner as presented before for the same TLRs. The obtained results are again compared to the reference design and are summarised in Table 6.12.

It is clear that the conventional WTMP configuration performs poorly compared to the conventional reference design. An increase in MTOM of 9% is seen due to a heavier propulsion system and wing, initialised by its four engines that introduce a significant weight penalty to the system. Also the PREE shows a significant decrease compared to the reference design. This indicates that more energy and thus fuel is required to fulfil the prescribed mission.

Alternatively, placing all the power at the tip has a positive effect on the design in terms of weight and PREE as seen for the tip-only configuration. This configuration provides an induced drag decrease of 26 drag counts compared to the clean wing. This confirms that more power to the tip is beneficial from an aerodynamic perspective. This configuration can benefit from an induced drag reduction of 8.5 % due to the wingtip-mounted propeller

and an increased bending relief without the penalty of a heavier propulsion system. Such a configuration will however impose new engineering challenges to be solved, such as compliance with regulations at an one-engine-inoperative condition.

These two studies confirm that a larger, and more powerful propeller at the wingtip is beneficial from an aerodynamic perspective whereas the addition of an extra shafts in the power train, has a detrimental effect on the weight.

Table 6.12: Summary of additional configurations studied compared to reference, APS included

Parameter	Configuration		
	Reference	Tip-only	Conventional WTMP
			
Power train	Conventional	Conventional	Conventional
Engines	2x turboprop	2x turboprop	4x turboprop
Engine location(s)	0.25	1.0	0.25, 0.1
Propeller diameter [m]	4.2	4.1	2.2
Shaft power ratio	NA	NA	0.5
MTOM [tons]	55.7	54.5	60.6
Wing mass [tons]	4.76	4.11	5.09
Propulsion system mass [tons]	3.66	3.54	5.06
Fuel mass [tons]	5.7	5.6	8.0
PREE	1.65	1.67	1.17

6.4. DISCUSSION

The different cases studied showed the effect on the synthesised design when shaft power ratio (case study I & II), wingtip-mounted propeller size (case study III & IV) or cruise speed is varied (case study II). An increase in shaft power ratio seems detrimental for the overall aircraft performance if only a small (ΔY=0.1) wingtip-mounted propeller is used. Although the aero-propulsive interaction effects profit from more power distributed to the tip propeller, the increase in associated propulsion system mass out weights this effect. This leads to an increase in MTOM of 10.6% for a shaft power ratio of 0.3 compared to the conventional design (case study I). At the same time, this also means a decrease in PREE and more fuel consumption.

The effects of increasing shaft power ratio can partly be reduced if the cruise Mach number is reduced. If the cruise speed is reduced to M=0.5 instead of M=0.6, the increase in MTOM is slightly reduced to an increase of 9.2% compared to the conventional design. This is because the aero-propulsion effects on the lift and induced drag of the system are more pronounced. An induced drag reduction of 51 drag counts can be obtained while increasing the lift of the system by 5 counts. This is suspected to be caused by the higher lift coefficient that the aircraft is operating at. This higher cruise lift coefficient causes a higher lift-induced drag, meaning more advantage can be gained. Although wingtip-mounted

propellers can be used to offer a positive effect on the aerodynamic performance and loading distribution over the wing, the application of a PTE configuration leads to a significant increase in propulsion system mass. For small size wingtip-mounted propellers these aerodynamic benefits are overshadowed by the substantial increase in mass. The weight penalty of the PTE system implied is simply too large to make a wingtip-mounted propeller beneficial with the partial electric configuration under the current technology levels and configuration assumed.

Advantages can be gained by increasing the size of the wingtip-mounted propeller. Section 6.3.4 showed that increasing the span fraction of the tip-mounted propeller from ΔY=0.1 to 0.275 for a design with a shaft power ratio of 0.2, has a small beneficial effect on the MTOM of the aircraft. More striking is the increase in lift over drag and PREE. A larger tip-mounted propeller generally shows a better performance and a slight decrease in weight for this study. The performance aspects of the design where ΔY=0.275, approach the performance of the reference design quite closely in terms of PREE and fuel mass. This configuration is able to achieve similar performance as the conventional configuration although having a higher MTOM.

If the shaft power ratio is lowered to φ=0.1, this equalisation of performance can already be achieved for a smaller wingtip-propeller size. Case study IV showed that at a distributed propulsion span fraction around ΔY=0.175 results in a similar performance as the reference design. The fact that this performance is achieved at a smaller propeller diameter can be explained by earlier observations. The higher the shaft power ratio, the higher the mass penalty introduced by the propulsion system. This means that the aero-propulsive effects need to compensate by a larger quantity. The aero-propulsive benefits generally increase with wingtip-mounted propeller size. Since at a lower shaft power ratio the aerodynamic compensation required is less, the required propeller diameter can also be reduced to achieve the reference performance. When the tip-mounted propeller size is further increased, the performance of the system can even exceed the performance of the reference design; the PREE is increased and the harmonic fuel mass reduced.

Based on the study on the effect of the tip-mounted propeller size, it can be said that the potential of wingtip-mounted propeller lay in the configuration with a small shaft power ratio combined with a relatively large tip-mounted propeller. Case studies I & II were performed for a small tip propeller span fraction (ΔY=0.1) and sketched a quite unpromising outlook. Case studies III & IV proved that the disk loading of the wingtip-mounted propeller is an important parameter to keep in mind when studying wingtip-mounted propulsion. The resulting aero-propulsive benefits have a major influence on the outcome in terms of performance.

The results from case studies III & IV put the potential of the wingtip-mounted propeller configuration in a much brighter perspective compared to case studies I & II. This stresses that the exact layout of the wingtip-mounted propeller design has a huge influence on the predicted performance. To be able to quantify the highest achievable potential of a wingtip-mounted propeller configuration, a multidisciplinary design optimisation (MDO) should be performed. Design variables that are proven to be important to consider are the disk loading and shaft power ratio.

This aircraft level study together with the aero-propulsive model could be used as a baseline for a MDO on wingtip-mounted propeller configurations. Nevertheless, there are a number of improvements that can be made. To start with, the aero-propulsive model is

applicable to limited wing geometry. It is unable to cope with varying thickness and airfoils along the span, as well as dihedral or a kink in the wing planform. This idealisation of the wing planform is often used in the aerodynamic study on wingtip-mounted propellers. These limitations obstruct the aerodynamic analyses of realistic wing planforms, which is highly desirable.

Furthermore, for the integration with the Initiator, the generation of the (wing) loading diagrams within the Class I weight estimation still largely rely on the surrogate model. This is also the case for the mission analysis for the flight phases other than the cruise phase. It is expected that a more accurate prediction of the aero-propulsive interaction effects for the different flight phases would modify the design point because the designs are not cruise-limited as shown in the design diamgrams in Appendix C. To use a full interaction aero-propulsive model in all of these analyses would be very time consuming and would violate the purpose of the Initiator; to rapidly synthesis designs. So, it is inevitable to use an aero-propulsive surrogate model within the design convergence loop. However, the performance of the currently implemented surrogate model is inadequate. When the aero-propulsive effects estimated by the aero-propulsive and surrogate model are compared, large discrepancies are seen. Figure 6.9 and 6.10 show the comparison for lift and induced drag respectively. It is clear that for both lift and drag, the surrogate predicted aero-propulsive effects show large deviations from the aero-propulsive model predicted effects. This could have a large influence on the predicted performance of the synthesised designs. The surrogate predicted effects are much more conservative and could result in a pessimistic representation of the potential of the configuration. Recalling the assumptions and limitations of the surrogate model discussed in Section 6.1, the idealised geometry assumption could have a large share in the origin of the discrepancies. To get a more realistic prediction of the aero-propulsive effects, the surrogate model should be updated to better relate to the considered design. It is expected that this will have an influence on the synthesised design. Based on the comparison with the aero-propulsive model, it is reasonable to say that it will modify the designs in a positive manner, resulting in a brighter perspective for wingtip-mounted propulsion. Nevertheless, the comparison presented in Figure 6.9 and 6.10 only presents the discrepancies for the cruise phase. It is not a given that are these drastic differences are also the case for the other flight phases.

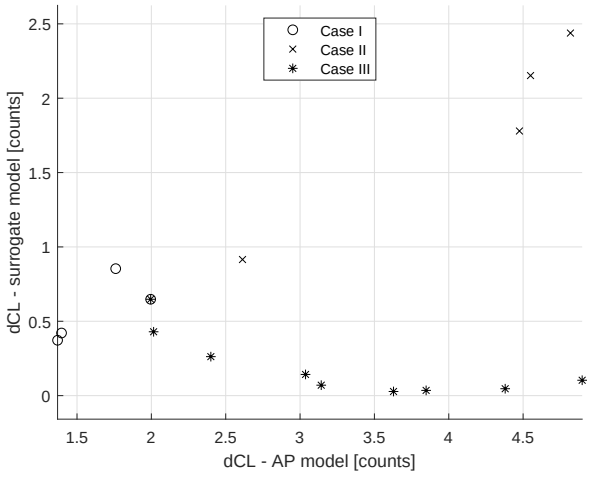

Figure 6.9: Predicted aero-propulsive effect on clean wing lift coefficient for cruise conditions

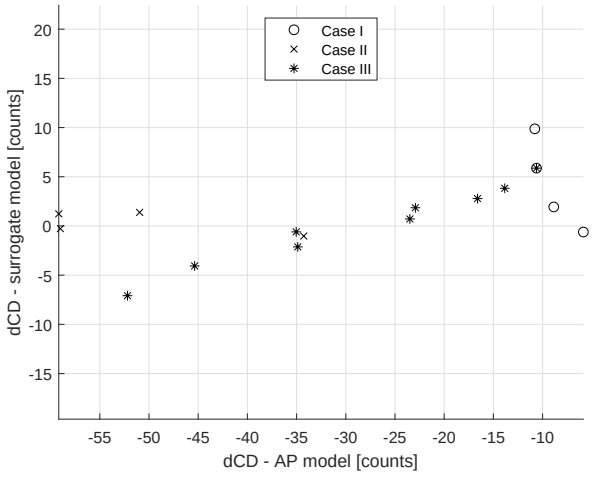

Figure 6.10: Predicted aero-propulsive effect on clean wing induced drag coefficient for cruise conditions

In terms of the optimally of the design, there are also a number of other design parameters that could be considered. For instance, the propeller design has been taken as a priori. Possible advantage can be gained if also the (wingtip) propeller design is optimised for propeller-wing interaction and weight. In addition, the relative positioning with respect to the wing can be examined. The vertical and axial position of the propellers will also influence the interaction effects.

All in all, the potential of the wingtip-mounted propeller configuration seems to be largely influenced by the exact configuration. Multiple design were generated which clearly have an adherent performance compared to the conventional reference design. These were mainly cases with a high-shaft power ratio and a small tip-mounted propeller. Nonetheless, certain design have also showed to have a similar (or even better) predicted performance, although having to face a slight mass penalty. In short, the different case studies suggest that most benefits can be gained from a wingtip-mounted propeller configuration if a low shaft power is combined with a large tip-mounted propeller size.

7

CONCLUSION AND RECOMMENDATIONS

This chapter presents the conclusions of the performed research in Section 7.1. Section 7.2 provides recommendations for future research.

7.1. CONCLUSIONS

This thesis presented a methodology of combining aerodynamic, structural and propulsive effects of a wingtip-mounted propeller configuration. These disciplines have been coupled in order to assess the potential of such a configuration and to identify the major design variables influencing the weight and performance of the system. The researched focused on a regional turboprop aircraft with top level requirements similar to that of the A320. Moreover, it features a Partial Turbo Electric power train. The concept comprises two turboprops on the primary shaft and two elektroprops on the secondary shaft. The shaft power ratio, a measure of the power share between the shafts, is constant throughout the different flight phases.

A numerical model has been developed to study the combined propeller-wing aerodynamics. The building blocks of the numerical model consist of a Vortex Lattice Method, Blade Element method, slipstream model and jet correction method. The major assumption that has been used in the model is that the individual propellers do not interfere with each other and their induced velocity fields can simply be superimposed. Since the aerodynamic behaviour of the propeller and wing are dependent on each other, this model uses an iterative approach to capture the two-way interaction. This numerical model to evaluate the propeller-wing aerodynamics was validated using experimental data. It was found that the numerical model predicts the experimentally observed trends well. Nevertheless, a number of discrepancies were seen which are believed to be caused mainly by not modelling the effects of the nacelle.

Furthermore, an aero-structural model has been developed. This model estimates the wing weight based on physical phenomena rather than statistics. It uses the wing geometry, aerodynamic loading and inertial loads to estimate the minimal structural wing weight required. Typically, a clean aerodynamic wing loading is used for such an approach. However, by including the aero-propulsive model in the structural weight estimation, an aero-structural model is obtained that is sensitive to a change in aero-propulsive load. If the propulsive design is changed, this does affect the structural weight estimation by both a change in aerodynamic and inertia load.

To study the potential of the wingtip-mounted propeller configuration, two sensitivity studies on different levels were performed. First, the effect of (propulsive) design modifications were studied on wing level. For this case, the wing geometry was based on a reference design and only the propulsive design was changed in terms of shaft power ratio, propeller size and inboard propeller location. No feedback loop was included on aircraft mass or aerodynamic performance. This means that the drag and weight of the system were assumed to equal that of the reference design. This study purely focused on the effect of the propulsive design on the estimated structural wing weight without looking at the potential aerodynamic benefits throughout the mission.

It was found that the response of the wing weight to a change in propulsive design can easily be explained by the principle of bending moment relief in case of a clean aerodynamic wing assumption. Placing the centre of gravity of the propulsion system further outboard reduces the wing root bending moment, which results in less structure required and consequently a lower wing weight. The effect of the inclusion of the aero-propulsive interaction is less straight-forward than the effect of the discrete loads. The aero-propulsive effects have an ambiguous effect on the wing weight. Nevertheless, a general trend can be seen for the shaft power ratio. An increase in shaft power ratio seems to have a positive influence on the wing mass although the gain is only minor (1%). However, this effect cannot compensate for the mass increase of the propulsion system itself which is far more significant. An increase in shaft power ratio from 0.1 to 0.2 increases the mass of the propulsion system by approximately 10%. Combining the weight of the wing and propulsion system, a clear increase in mass is seen with increasing shaft power ratio. The mass penalty introduced by the propulsion system mass overshadows the reduction in wing mass. However, due to the assumptions made and the scope used, the wingtip-mounted propeller configuration seems more disadvantageous than it could potentially be. Partly by not considering the full iterative design loop, and because the aero-propulsive performance benefits are not included in the evaluation.

Moreover, the wing level study showed that the aerodynamic interaction between the the propeller and wing has a limited effect on the predicted wing weight. The maximum deviation between the clean aerodynamic wing and full aerodynamic wing studied was in the order of 1%. This confirms that the commonly used assumption of a clean-aerodynamic wing within a wing weight estimation method, is also acceptable in the conceptual design phase of a wingtip-mounted propeller configuration.

Nevertheless, a change of this order in wing weight, is exaggerate in the MTOM when a design convergence study is performed. That is why in the aircraft level study, the aero-structural model is used to estimate the wing weight including the aero-propulsive effects. The sensitivity study on this level greatly differs from the wing level study as a full conceptual design convergence study is performed by using the TU Delft in-house build Aircraft Design Initiator. Moreover, it updates the aerodynamic performance of the aircraft by including the aero-propulsive benefits. The aero-propulsive benefits are mainly estimated by use of an already build-in simplified surrogate model. Only for the cruise phase, the aero-propulsive model is evaluated to get the propeller-wing interaction effects on the wing lift and drag.

Modifications in shaft power ratio showed that wing weight and MTOM both increase with increasing the distributed power to the tip when the distributed propulsion span fraction in unmodified. This is initiated by the increase in propulsion system mass due to

a higher shaft power ratio. This trend was also expected from the wing level study. Although the aero-propulsive benefits also increase with shaft power ratio, this does not weigh against the increase in propulsion system mass it comprehends for designs with only a small wingtip-mounted propeller (ΔY=0.1). An almost linear relationship between shaft power ratio and MTOM was observed. For the design with M_{cr} = 0.6, an increase of 10 percent points for the secondary shaft power split leads to an increase in MTOM of approximately 3.5% compared to the conventional reference design without wingtip-mounted propulsion. For the design with M_{cr} = 0.5, this increment is slightly less; approximately 3%. This suggests that the mass penalty introduced by the increase in shaft power ratio shrinks with a lower cruise speed. Besides a gain in MTOM, an increase in shaft power ratio, while maintaining the other design variables, also results in a substantial decrease in Payload Range Energy Efficiency which translates into more fuel required for the mission. For both cruise speed cases, a shaft power ratio of 0.3 results in a PREE decrease of >10% compared to the conventional reference design.

The shaft power studies were performed for wingtip-mounted propellers with a size of ΔY=0.1. With the study on the effect of propeller size conducted, it was found that these dimensions were far from optimal. Significant advantages can be gained by increasing the size of the wingtip-mounted propeller. The aero-propulsive interaction effects benefit from the larger dimensions both enhancing lift and reducing the induced drag. In terms of mass, the increase in propeller size is relatively penalty free when compared to an increase in shaft power ratio while still stimulating the aero-propulsive benefits. Contrary, the weight of the aircraft even slightly profits from a larger wing-mounted propeller. When the wingtip-mounted propeller size is increased, it is eventually possible to attain an equal performance as the conventional reference design in terms of energy efficiency, although facing a mass penalty caused and depend on the shaft power ratio chosen. For a shaft power ratio of 0.1, the reference performance is attained for a tip-mounted propeller size of ΔY=0.175 with an increase in MTOM of 2.8%. For a shaft power ratio of 0.2, this performance is attained at a larger tip-mounted propeller size (ΔY=0.275) and an increase in MTOM of 5% compared to the reference design. If larger wingtip-mounted propellers are used, the performance could be increased beyond the reference performance.

All in all, it is obvious that the potential performance benefits of the wingtip-mounted propeller greatly depend on the (propulsive) design parameters used. However, based on the conducted studies in this research, the wingtip-mounted propeller configuration with a low shaft power ratio and large tip-mounted propeller seems most assuring. The lower the shaft power ratio, the easier to overcome the PTE weight penalty by use of aero-propulsive interaction benefits.

7.2. DIRECTIONS FOR FUTURE RESEARCH

Although this research has given some new insides on the potential of the wingtip-mounted propeller configuration, there is still a lot to be investigated. This section provides recommendations to improve and/or extend the currently presented research.

- The aero-propulsive model is limited to simple geometry planforms. Its application can be extended such that more realistic designs can be studied. Room for improvement is found in the addition of a kink, dihedral angle and airfoil thickness variations.
- The most promising wingtip-mounted propeller configurations likely features a rel-

ative large tip-mounted propeller. The aero-propulsive model assumes that there is no mutual interference between the propellers. This assumption was deemed valid if the propellers are separated by a large distance ($\gg 1R$). However, if larger propellers are used the distance between the blade tips become smaller and mutual interaction might become important.

- The simplified surrogate model used within the Initiator shows large discrepancies when compared to the aero-propulsive model predictions. Variations as large as 55 drag counts and 4 lift counts were seen. This is likely caused by the idealised wing geometry used in the generation of the surrogate model. To get a more realistic prediction of the aero-propulsive effects in the different flight phases, the surrogate model should be updated to better relate to the considered design.
- A multidisciplinary design optimisation study could be conducted to quantify the maximum potential of the wingtip-mounted propeller configuration. Possible advantage can be gained if the propeller designs are considered for optimal propeller-wing interaction, weight and inertia loads introduced on the wing. In addition, the relative positioning of the propellers with respect to the wing can be examined. The vertical and axial position of the propellers will also influence the interaction effects. Additionally, it would be valuable to identify for which type of mission this configuration could be most suitable.
- Attention should also be given to different disciplines as they could strengthen (or weaker) the benefits of a wingtip-mounted propeller. As an example, a wingtip-mounted propeller could also be used for stability and control of the aircraft. If the propellers are used to enhance directional stability and control, the size of the vertical tailplane could be reduced. On the other hand, an one-engine-inoperative situation might result in a yawing moment that is to large to be correct by the rudder. Furthermore, noise and aero-elastic phenomena might also pose new challenges similar to ground clearance issues.

A

Overview of Integration Studies on Wingtip-Mounted Propellers

Table A.1: Summary of PEGASUS studies

Study	Configuration	Methodology	Results
A [36]	• Two hybrid electric wingtip-mounted tractor propellers delivering thrust majority • Two electric foldable inboard tractor propellers assisting during takeoff • One electric rear mounted BLI pusher propeller • Based on ATR-42-500	• Optimized for takeoff gross weight • Design parameters: wing area, thrust scaling parameter, power provided by gas turbine • Use of two different methodologies (FLOPS, SUAVE) that agree on results	• Wingtip mounted propellers is approximated to offer a 18% increase in effective propulsive efficiency for the PEGASUS concept • Estimated 31% increase in gross weight for the hybrid mission compared to conventional • Concept has potential to decrease gross weight and energy required compared to other hybrid electric regional aircraft • Constraint on rate of climb in cruise has great effect on propulsion size • Vehicle weight is found to be strongly dependent on reserve mission requirements

B [38]	• PEGASUS (= configuration of study A) • Inboard propulsor fixed at ATR-42 position	• One way interaction effects (Propeller on wing) • Only considers wing and propeller • Wing must maintain target C_L • Thrust = Drag • Propeller modelled as actuator disk • Uses FlightStream	• Wingtip-mounted propeller effectively decreases viscous and induced drag • Increased propeller diameter increases viscous drag • Increased propeller diameter increases induced drag, but is still less than the situation without propeller • Little effect of tip Mach number • Decreased disk loading (e.g. larger propeller) results in a higher propeller efficiency requiring less shaft power • Operating only the tip-mounted propeller results in a 5% decrease in required thrust • Required power is reduced by 5% when both propeller classes are operating in comparison to only tip-mounted • Tip propulsion decreases induced drag by 9 % compared to a clean wing

C. [39]	• Updated PEGASUS configuration: Planform modified to roughly match wing loading of ATR 42-500 • Scaled version of ATR 72-500	• Uses LEAPS analyses tool • Assumed 10% decrease in induced drag thanks to wingtip-mounted propellers compared to clean wing • Estimated drag penalty of 4.4% when inboard propellers are operating • Assumed no propulsive benefit of BLI	• A higher supplied power ratio results in a lower energy required and larger ramp and battery weight • The PEGASUS concept uses 19% less energy than the conventional version but is heavier by 49% • Between 0-10% induced drag decrease, the ramp weight, battery weight, and energy required show linear decreasing behaviour

Table A.2: Summary of wingtip-mounted propeller studies

Study	Configuration	Methodology	Results
D [40]	• Based on Tecnam P2006T • A dozen of smaller high lift propellers distributed over the wings leading edge • Two large main propulsors mounted at the wingtip	• Simplified AVL-XROTOR modelling • Fast design space exploration by low-order tools to quickly analyses thousands of combinations of design variables	• Higher span loading, smaller propeller diameter-to-wingspan ratio and higher velocity-to-propeller tip speed ratio all result in a drag reduction • Higher subsonic propeller tip speeds and larger propeller diameter increase propulsive efficiency • Aerodynamic efficiency is increased with lower span loading • Estimated 5-10% increase in L/D due to wingtip-mounted propeller, CFD studies indicate under prediction of this value

E [41]	• X-57 cruise configuration from [40]	• Studied influence of location, number, rotational direction and diameter of propeller and wing chord distribution • Objective: maximise aerodynamic efficiency • High-order free-wake potential flow method for aerodynamic analysis • Additional profile drag estimation to account for viscous drag	• Inboard-up rotating propellers with a high diameter (low loading) are more aerodynamic efficient • Optimiser placed wingtip-mounted propeller slightly inboard to a 95% span position, slightly below the vertical • Drag reduction was driven by reduced profile drag • The total trimmed power requirement was reduced by 1.5% • Surprising local minimum were found with outboard-up rotating propellers located more inboard if the propeller was forced to have a small radius (heavily loaded)

F [42]	• TLARs comparable to current turboprops (e.g. ATR72) • HEP architecture • Conventional fuel as main energy source, batteries used to cover peak power • High aspect ratio • Four electrically driven wingtip-mounted propellers, two for tip vortex reduction, two for directional control • Two conventional positioned propellers	• Fuel remains main energy source • All propellers have the same size and deliver the same thrust	• Mission fuel reduction of 5.5% compared to non HEP • Reduced mission fuel of 1.5% due to aerodynamic effects • Reduction of 3% due to reduced size of vertical tail plane because of powered directional control

G [44]	• Baseline designed using Initiator tool [45] • TLARs based on Airbus A320 • Two inboard propellers • Two wingtip-mounted propellers • Partial turbo-electric architecture	• LLM with propeller represented by actuator disk • One way aerodynamic interaction • Ten design variables describing propeller distribution, sizing, operating conditions and wing area • Payload Range Energy Efficiency (PREE) as figure of merit • Resulting concepts are feasible but not optimal • Sensitivity to different technology scenarios and shaft power ratio • Skin-friction drag approximated • Surrogate model created for $\Delta C_L, \Delta C_D$	• Technology scenario mainly affects the mass of the aircraft, or more directly the power trains • Shaft power ratio affects both MTOW and PREE • Improved technology level has more influence on large shaft power ratio's • An improved specific power of the powertrain will not mean an as-large improvement on aircraft level • Lower shaft power ratios yield better results especially between 10%-20% • Wingtip-mounted propeller configuration performed worse than expected due to the advance ratio that was limited by the tip speed Mach number • A larger aircraft range generally improves the PREE as the aeropropulsive benefits act over a larger time span to overcome the mass penalties

H [46]	• Turbo-electric version based on ATR 72-500 • Distributed propulsion with at least two wingtip-mounted propeller, if more than two propellers are used • Propellers are distributed equidistantly between tip and inboard propeller	• Design variables: aspect ratio, propeller size, number, thrust split and span-wise location, power to weight ratio • Evaluates wing and stabilizer structural masses • Uses Aeroelastic Aircraft Design and Simulation Tool (dAEDalusNXT), based on coupled (Unsteady) Vortex Lattice and beam element theory • Structural sizing uses Beam Element Theory • Constant disk loading assumed • Effect on fuselage weight not considered • Aerodynamic interference effects between propeller and wing are not considered • The induced drag reduction effect of the tip-mounted propeller is quantified using an empirical relationship	• Moving the centre of gravity of the propulsion unit further outboard results in root bending moment relieve and decreases the wing weight • A higher wing aspect ratio increases the wing weight • Disk loading and power to weight ratio of the electric motor showed to have little effect • For the objective of reducing block fuel it is suggested to use a high aspect ratio wing with tip-mounted propellers and (number of) inboard propellers shifted as far outboard as possible within the constraints

B

Additional Wing Weight Sensitivity Results

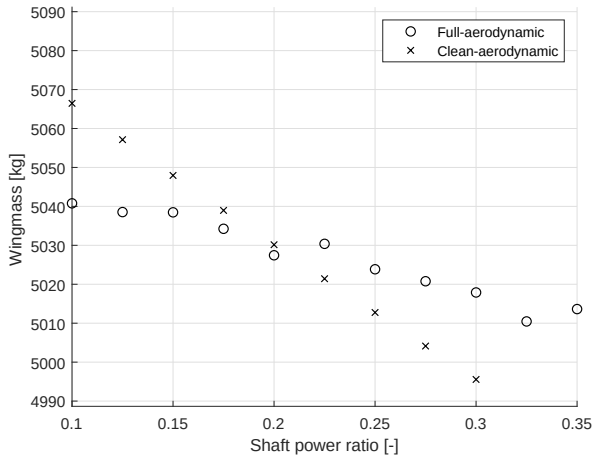

(a) Effect of shaft power ratios.

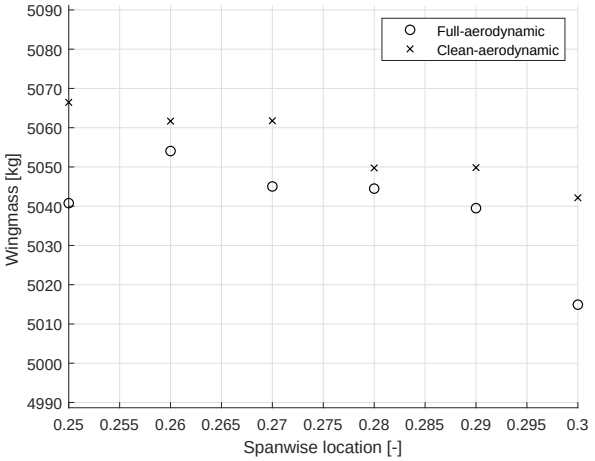

(b) Effect of inboard propeller locations.

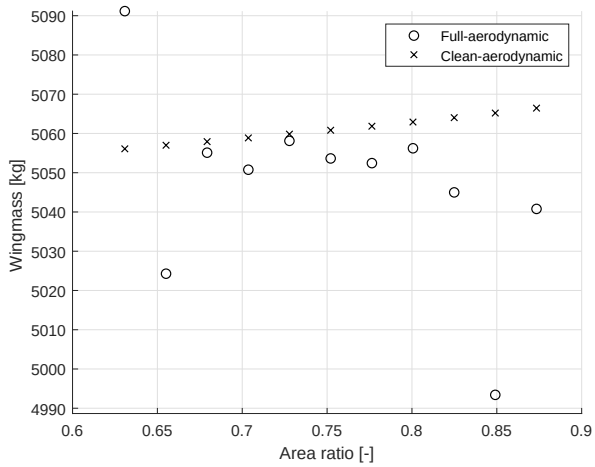

(c) Effect of disk area ratios.

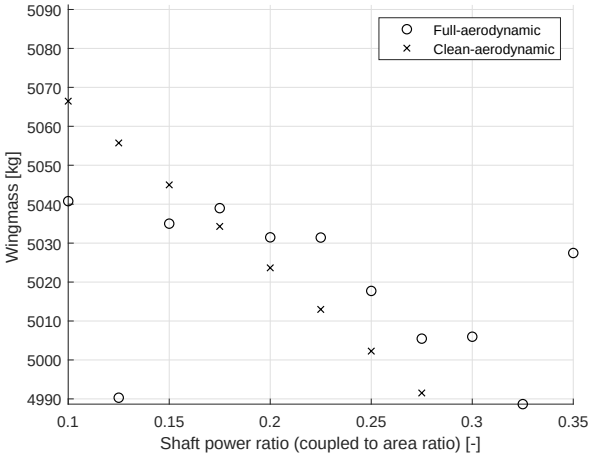

(d) Effect of shaft power ratios with constant individually disk loading.

Figure B.1: Results of sensitivity study on baseline aircraft with $\varphi = 0.1$

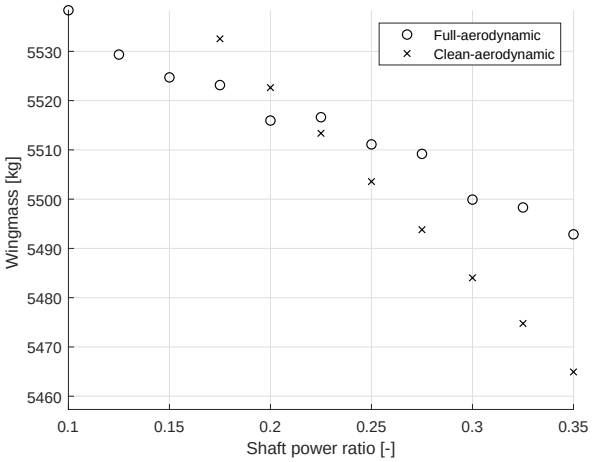

(a) Effect of shaft power ratios.

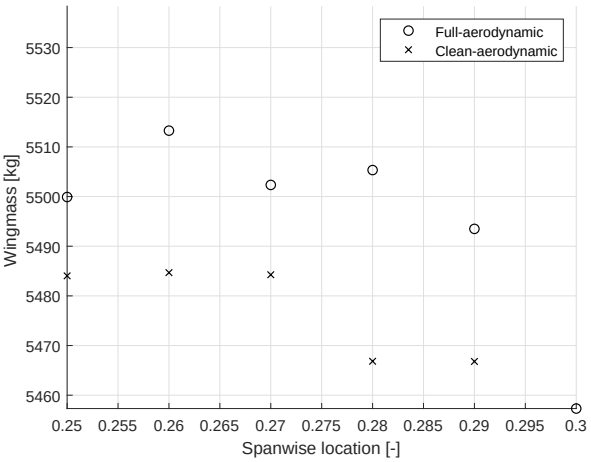

(b) Effect of inboard propeller locations.

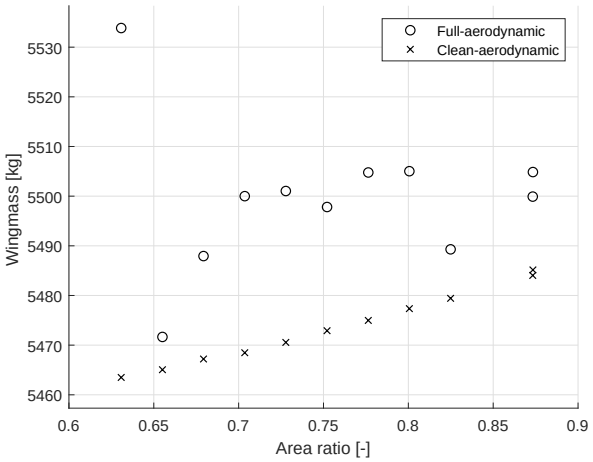

(c) Effect of disk area ratios.

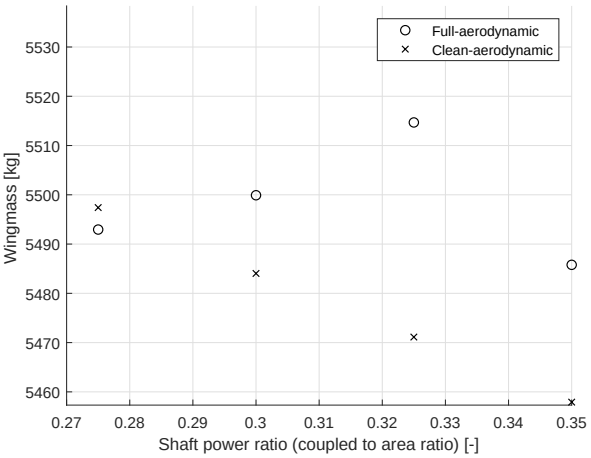

(d) Effect of shaft power ratios with constant individually disk loading.

Figure B.2: Results of sensitivity study on baseline aircraft with $\varphi = 0.3$

C

DESIGN POINT DIAGRAM

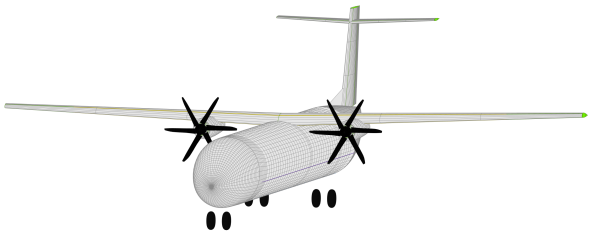

Figure C.1: Isometric view of reference aircraft. $M_{cr} = 0.6$

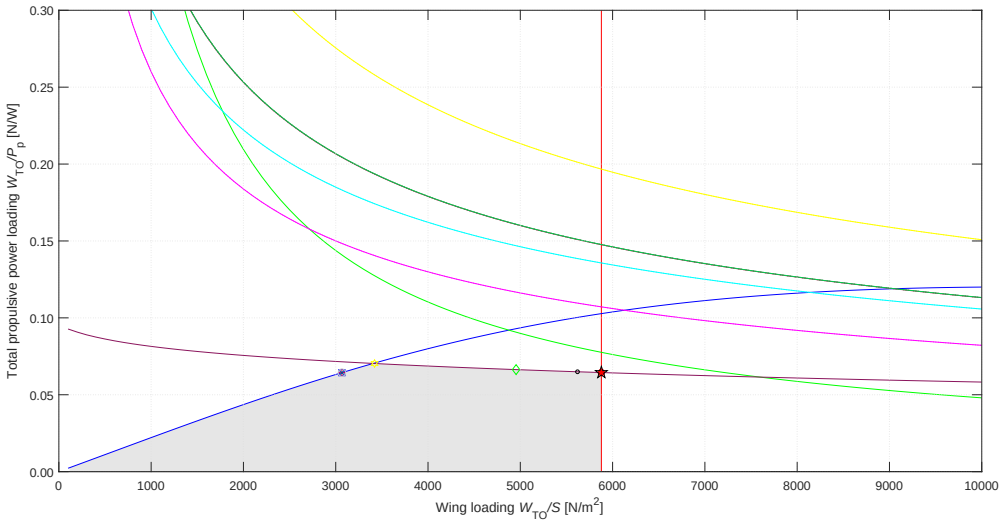

Figure C.2: Design point diagram for reference aircraft. $M_{cr} = 0.6$

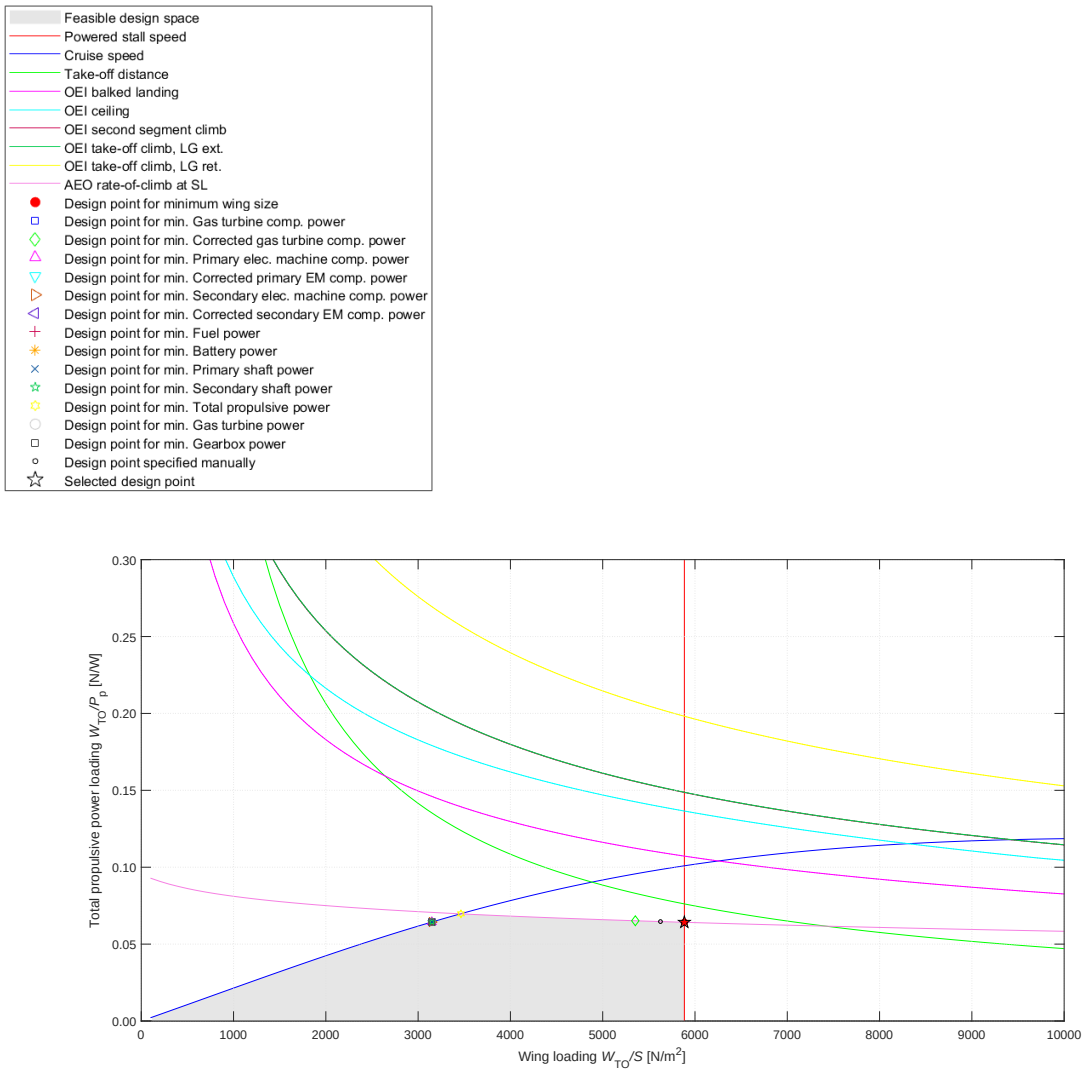

Figure C.3: Design point diagram for design with φ=0.1 ΔY= 0.2

BIBLIOGRAPHY

[1] Joseph R. Chambers, *Cave of the Winds: The Remarkable History of the Langley Full-Scale Wind Tunnel* (NASA, 2014).

[2] M. H. Snyder and G. W. Zumwalt, *Eects of wingtip-mounted propellers on wing lift and induced drag,* Journal of Aircraft **6**, 392 (1969).

[3] L. R. Miranda and J. E. Brennan, *Aerodynamic effects of wingtip-mounted propellers and turbines, 4th Applied Aerodynamics Conference,* (1986), 10.2514/6.1986-1802.

[4] L. J. and L. F., *Induced drag reduction with wing tip mounted propellers,* in *2nd Applied Aerodynamics Conference* (American Institute of Aeronautics and Astronautics, 1964).

[5] J. Patterson and G. Barlett, *Effect of a wing-tip mounted pusher turboprop on the aerodynamic characteristics of a semi-span wing,* (1985), 10.2514/6.1985-1286.

[6] Mark D. Moore, *Misconceptions of electric aircraft and their emerging aviation markets,* 52nd Aerospace Sciences Meeting (2014), 10.2514/6.2014-0535.

[7] T. Sinnige, N. van Arnhem, T. C. A. Stokkermans, G. Eitelberg, and L. L. M. Veldhuis, *Wingtip-Mounted Propellers: Aerodynamic Analysis of Interaction Effects and Comparison with Conventional Layout,* Journal of Aircraft **56**, 295 (2019).

[8] Veldhuis, L.L.M., *Propeller Wing Aerodynamic Interference,* Ph.D. thesis, Delft University of Technology (2005).

[9] T. Stokkermans, N. Van Arnhem, T. Sinnige, and L. Veldhuis, *Validation and comparison of rans propeller modeling methods for tip-mounted applications,* in *AIAA Aerospace Sciences Meeting* (2018).

[10] J. Fischer, *Simulation & Analysis of the Aerodynamic Interactions between Distributed Propellers and Wings,* Master's thesis, Delft University of Technology (2017).

[11] M. Patterson and B. German, *Simplified aerodynamics models to predict the effects of upstream propellers on wing lift,* in *53rd AIAA Aerospace Sciences Meeting* (Kissimmee, Florida, 2015) pp. 10–2514.

[12] J. Conway, *Analytical solutions for the actuator disk with variable radial distribution of load,* Fluid Mechanics **297** (1995), 10.1017/s0022112095003120.

[13] C. Alba, A. Elham, B. German, and L. L. Veldhuis, *A Surrogate-Based Multi-Disciplinary Design Optimization Framework Exploiting Wing-Propeller Interaction, 18th AIAA/ISSMO Multidisciplinary Analysis and Optimization Conference,* (2017), 10.2514/6.2017-4329.

[14] J. De Young, *Propeller at high incidence,* Journal of Aircraft **2**, 241 (1965).

[15] C. Alba, *A surrogate-based multi-disciplinary design optimization framework exploiting wing-propeller interaction*, Master's thesis (2017).

[16] K. Epema, *Wing Optimisation for Tractor Propeller Configurations*, Master's thesis, TU Delft Aerospace Engineering (2017).

[17] TING, L. and LIU, C. H., *Thin airfoil in nonuniform parallel streams.* Journal of Aircraft **6**, 173 (1969).

[18] F. Chow, E. Krause, C. Liu, and J. Mao, *Numerical investigations of an airfoil in a nonuniform stream,* Journal of Aircraft **7**, 531 (1970).

[19] L. Ting, C. Liu, and G. Kleinstein, *Interference of wing and multipropellers,* AIAA Journal **10**, 906 (1972).

[20] R. Nederlof, *Improved modeling of propeller-wing interactions with a lifting-line approach: Investigation of a suitable correction method to account for the finite slipstream height*, Master's thesis, Delft University of Technology (2020).

[21] S. Rethorst, *Aerodynamic of nonuniform flows as related to an airfoil extending through a circular jet,* Journal of the Aerospace Sciences **25**, 11 (1958).

[22] E. Torenbeek, *Synthesis of Subsonic Airplane Design* (Delft Univ. Press, Delft, The Netherlands, 1982).

[23] J. Roskam, *Airplane Design* (DARcorporation, Lawrence, KS, 1985).

[24] D. Raymer, *Aircraft design: A conceptual approach,* AIAA Education Series (2002), 10.2514/4.869112.

[25] M. Voskuijl, J. Van Bogaert, and A. Rao, *Analysis and design of hybrid electric regional turboprop aircraft,* CEAS Aeronautical Journal **9**, 15 (2018).

[26] G. Wroblewski and P. J. Ansell, *Mission analysis and emissions for conventional and hybrid-electric commercial transport aircraft,* in *AIAA Aerospace Sciences Meeting* (AIAA, 2018).

[27] C. Pornet and A. Isikveren, *Conceptual design of hybrid-electric transport aircraft,* Progress in Aerospace Sciences **79**, 114 (2015).

[28] R. de Vries, M. Brown, and R. Vos, *Preliminary Sizing Method for Hybrid-Electric Distributed-Propulsion Aircraft,* Journal of Aircraft **56**, 2172 (2019).

[29] M. Droegkamp, *Finite element model weight estimation,* SAWE Paper No. 2089, 51st Annual Conference (1992).

[30] G. Bindolino, G. Ghiringhelli, S. Ricci, and M. Terraneo, *Multilevel structural optimization for preliminary wing-box weight estimation,* Journal of Aircraft **47**, 475 (2010).

[31] A. Elham, G. La Rocca, and M. J. L. van Tooren, *Development and implementation of an advanced, design-sensitive method for wing weight estimation,* Aerospace Science and Technology **29**, 100 (2013).

[32] R. Elmendorp and G. La Rocca, *Comparative design & sensitivity studies on box-wing airplanes,* Italian Association of Aeronautics and Astronautics XXV International Congress 9-12 September 2019 (2019).

[33] V. Liu Xu, *Propeller-wing whirl flutter: an analytical approach*, Master's thesis, Delft University of Technology (2020).

[34] T. Sinnige, *Aerodynamic and Aeroacoustic Interaction Effects for Tip-Mounted Propellers: An Experimental Study*, Ph.D. thesis, Delft University of Technology (2018).

[35] S. Van Der Meer, *Numerical Assessment of Directional Stability and Control with Tip-mounted Propellers*, Master's thesis, Delft University of Technology (2020).

[36] K. R. Antcliff and F. M. Capristan, *Conceptual design of the parallel electric-gas architecture with synergistic utilization scheme (PEGASUS) concept,* in *18th AIAA/ISSMO Multidisciplinary Analysis and Optimization Conference* (American Institute of Aeronautics and Astronautics, 2017).

[37] J. Welstead and J. L. Felder, *Conceptual design of a single-aisle turboelectric commercial transport with fuselage boundary layer ingestion,* in *54th AIAA Aerospace Sciences Meeting* (American Institute of Aeronautics and Astronautics, 2016).

[38] N. J. Blaesser, *Propeller-Wing Integration on the Parallel Electric-Gas Architecture with Synergistic Utilization Scheme (PEGASUS) Aircraft,* in *2019 AIAA SciTech Forum and Exposition;* (San Diego, CA, United States, 2019).

[39] Capristan, F. M., Blaesser, and N. J., *Analysis of the parallel electric-gas architecture with synergistic utilization scheme (pegasus) concept,* NASA/TM2019220396, L-21042, NF1676-33672 (2019).

[40] N. K. Borer, M. D. Patterson, J. K. Viken, M. D. Moore, J. Bevirt, A. M. Stoll, and A. R. Gibson, *Design and performance of the NASA SCEPTOR distributed electric propulsion flight demonstrator,* in *16th AIAA Aviation Technology, Integration, and Operations Conference* (American Institute of Aeronautics and Astronautics, 2016).

[41] J. A. Cole, T. Krebs, D. Barcelos, A. Yeung, and G. Bramesfel, *On the integrated aerodynamic design of apropeller-wing system,* AIAA Scitech 2019 Forum (2019), 10.2514/6.2019-2300.

[42] M. Strack, G. P. Chiozzotto, M. Iwanizki, M. Plohr, and M. Kuhn, *Conceptual Design Assessment of Advanced Hybrid Electric Turboprop Aircraft Configurations,* in *17th AIAA Aviation Technology, Integration, and Operations Conference* (American Institute of Aeronautics and Astronautics, 2017).

[43] N. K. Borer, J. M. Derlaga, K. A. Deere, M. B. Carter, S. A. Viken, M. D.Patterson, B. L. Litherland, and A. M. Stoll, *Comparison of aero-propulsive performance predictions fordistributed propulsion configurations,* (2017).

[44] M. F. M. Hoogreef, R. de Vries, T. Sinnige, and R. Vos, *Synthesis of Aero-Propulsive Interaction Studies Applied to Conceptual Hybrid-Electric Aircraft Design,* AIAA Scitech 2020 Forum (2020), 10.2514/6.2020-0503.

[45] R. J. M. Elmendorp, R. Vos, and G. La Rocca, *A Conceptual Design and Analysis Method for Conventional and Unconventional Airplanes,* ICAS 2014: Proceedings of the 29th Congress of the International Council of the Aeronautical Sciences, St. Petersburg, Russia, 7-12 September 2014 (2014).

[46] A. L. Habermann, *Eects of distributed propulsion on wing mass in aircraft conceptual design,* AIAA AVIATION 2020 FORUM (2020), 10.2514/6.2020-2625.

[47] J. D. Anderson Jr, *Introduction to flight*, eighth ed. (McGraw-Hill Education, 2017).

[48] J. D. Anderson Jr, *Fundamentals of aerodynamics*, 6th ed., edited by 6 (McGraw-Hill Education, 2016).

[49] L. Prandtl, *Applications ofmodern hydrodynamics to aeronautics,* NASA Technical Report (1923) .

[50] J. Katz and A. Plotkin, *Low-Speed Aerodynamics* (Cambridge University Press, 2001).

[51] E. J. t. Dijksterhuis, *Archimedes*, Princeton legacy library (Princeton University Press, Princeton, New Jersey, 1987).

[52] W. J. M. Rankine, *On the mechanical principles of the action of propellers,* Transaction of the Institute of Naval Architects **6**, 13 (1865).

[53] W. Froude, *On the Elementary Relation Between Pitch, Slip, and Propulsive Efficiency,* Transaction of the Institute of Naval Architects **19**, 22 (1878).

[54] Q. R. Wald, *The aerodynamics of propellers,* Progress in Aerospace Sciences **42**, 85 (2006).

[55] A. El-Sayed, *Fundamentals of Aircraft and Rocket Propulsion* (2016).

[56] T. Theodorsen, *The theory of propellers iii : the slipstream contraction with numerical values for two-blade and four-blade propellers,* NACA report 777 (1944).

[57] P. L, *Mutual influence of wings and propeller,* NACA TN-74 (1921).

[58] D. P. Witkowski, A. K. H. Lee, and J. P. Sullivan, *Aerodynamic interaction between propellers and wings,* Journal of Aircraft **26**, 829 (1989).

[59] I. Kroo, *Propeller-wing integration for minimum induced loss,* Journal of Aircraft **23**, 561 (1986).

[60] R. T. Johnston and J. P. Sullivan, *Unsteady wing surface pressures in the wake of a propeller,* Journal of Aircraft **30**, 644 (1993).

[61] R. Willemsen, *A sensitivity studyon the aerodynamicperformance of awingtip-mounted tractorpropeller-wing system*, Master's thesis, Delft University of Technology (2020).

[62] M. Drela, *Qprop formulation,* MIT Aero & Astro (2006).

[63] B. Nootebos, *Aerodynamic Analysis and Optimisation of WingtipMountedPusher Propellers*, Master's thesis, Delft University of Technology (2018).

[64] N. van Arnhem., *Design and Analysis of an Installed Pusher Propeller with Boundary Layer Inflow.*, Master's thesis, Delft University of Technology (2015).

[65] B. Chandrasekaran, *Method for the prediction of the installation aerodynamics of a propfan at subsonic speeds*, Tech. Rep. (Hampton, VA, United States, Apr 1985).

[66] N. van Arnhem, R. de Vries, T. Sinnige, R. Vos, G. Eitelberg, and L. L. M. Veldhuis, *Engineering method to estimate the blade loading of propellers in nonuniform flow,* AIAA Journal , 1 (2020).

[67] L. Veldhuis and P. Heyma, *Aerodynamic optimisation of wings in multi-engined tractor propeller arrangements,* Aircraft Design **3**, 129 (2000).

[68] T. Melin, A. T. Isikveren, and M. I. Friswell, *Induced-drag compressibility correction for three-dimensional vortex-lattice methods,* Journal of Aircraft **47**, 1458 (2010).

[69] T. H. G. Megson, *Aircraft Structures for Engineering Students.* (Elsevier, 2007).

[70] N. L. en Ruimtevaartlaboratorium, *N250 propeller Shoptest.*, Tech. Rep. (NLR, 1993).

[71] R. de Vries, M. Hoogreef, and R. Vos, *Aero-propulsive efficiency requirements for turboelectric transport aircraft,* in *AIAA Scitech 2020 Forum* (American Institute of Aeronautics and Astronautics, 2020).

[72] G. L. Rocca, T. Langen, , and Y. Brouwers, *The design and engineering engine. towards a modular system for collaborative aircraft design,* in *Proceedings of ICAS 2012* (2012).

[73] R. Vos and M. F. M. Hoogreef, *System-level assessment of tail-mounted propellers for regional aircraft,* Proceedings of the 31st Congress of the International Council of the Aeronautical Sciences (2018).